The Pennsylvania State University

The Graduate School

Department of Energy and Mineral Engineering

ALTERNATE REPRESENTATIONS FOR NUMERICAL MODELING OF MULTI-STAGE HYDRAULICALLY FRACTURED HORIZONTAL WELLS IN SHALE GAS RESERVOIRS

A Thesis in

Energy and Mineral Engineering

by

Nithiwat Siripatrachai

Submitted in Partial Fulfillment
of the Requirements
for the Degree of

Master of Science

August 2011

The thesis of Nithiwat Siripatrachai was reviewed and approved* by the following:

Turgay Ertekin
Professor of Petroleum and Natural Gas Engineering
Thesis Advisor

John Yilin Wang
Assistant Professor of Petroleum and Natural Gas Engineering

Luis Ayala
Associate Professor of Petroleum and Natural Gas Engineering

R. Larry Grayson
Professor of Energy and Mineral Engineering
Graduate Program Officer of Energy and Mineral Engineering

*Signatures are on file in the Graduate School

ABSTRACT

Increasing demand of oil and natural gas and depletion of production from conventional resources accelerate the advancement of technology to economically produce oil and natural gas from unconventional resources. Various sources of unconventional gas such as coalbed methane, shale gas, and gas hydrate have been exploited. This work primarily focuses on shale gas reservoirs which are source rocks for conventional reservoirs. Like other unconventional reservoirs, shale has extremely low permeability in nanodarcy range.

Horizontal well is widely used in the production of shale gas due to its higher wellbore length exposed to the formation resulting in higher gas production rates and ultimate recovery. Hydraulic fracturing which is commonly used in tight formations is a process of pumping high pressured fluid mainly composed of water into the formation. Hydraulic fracturing creates fractures serving as high-permeability pathways that allow gas that is stored further away to flow into the wellbore. To produce natural gas at economic rate, hydraulic fracturing technique is implemented to increase production and, therefore, ultimate recovery.

Reservoir simulation is one of the most important techniques in exploration and production. Reservoir simulator can be used in history matching, production forecast, and field optimization. Unfortunately, utilizing numerical reservoir simulator in field optimization can be time-consuming as reservoir modeling and computation could take several hours for each scenario and the optimal cases could be overlooked. In reservoir simulation, shale gas reservoirs can be represented with dual-porosity, single-permeability model with adsorbed gas on shale surface.

Conventional representation in reservoir simulation and design of hydraulic fracturing is transverse fracture planes. Each transverse plane represents a single-stage hydraulic fracturing. For horizontal wells, multi-stage hydraulic fracturing is implemented to create multiple transverse

vertical planes perpendicular to the wellbore length. This transverse hydraulic fracture representation is widely used in the design of hydraulic fracturing and reservoir modeling. However, microseismic field data show that high pressured fluid creates a hydraulically fractured zone instead of transverse fracture planes. Therefore, in reservoir simulation, an alternative representation for hydraulic fracturing called "crushed zone" hydraulic fracture representation is proposed. This crushed zone can be represented by an elliptical zone of high fracture permeability and smaller fracture spacing instead of high-permeability transverse fracture planes. Difficulty lies in the characterization of hydraulic fracturing whether which model is more representative and what are their equivalent representations.

Artificial neural network (ANN) is a widely used technology in science and engineering because of its capability of computing highly non-linear relationships. Due to its ability to provide simulation results in seconds, ANN can serve as a powerful tool in reservoir simulation. Several studies at The Pennsylvania State University involving hydrocarbon recovery have been completed using ANNs. In this study, two ANNs based models are developed. The first ANN called "Performance Prediction ANN" can instantly predict production profile of a hydraulically fractured horizontal well completed in shale gas reservoirs with an error less than 10% from numerical reservoir simulation. The second ANN called "Equivalency ANN" is developed to establish equivalent hydraulic fracture representations between transverse hydraulic fracture representation and crushed zone representation. The equivalent representation from ANN when run with numerical reservoir simulator yields cumulative gas production within ±15% error compared to results obtained via conventional simulation.

Table of Contents

List of Figures

List of Tables

Acknowledgements

First and foremost I would like to express my sincere appreciation towards my academic advisor Dr. Turgay Ertekin for his invaluable guidance, steady support, patience, and assistance throughout the development of this work. Without his key suggestions, this work would not have been successful. Special thanks also go to Dr. John Yilin Wang and Dr. Luis Ayala for their contributions as committee members. Their recommendations and contributions to this work are greatly appreciated.

I would also like to express my gratitude to my family, my father Tawatchai Siripatrachai, my mother Rungsima Siripatrachai, and my sister Tanisa Siripatrachai who have given their constant support and guidance in my study and career.

In addition, many of my friends and colleagues have been very supportive. I am fortunate to have the opportunity to engage in technical discussions during our weekly meetings with my research group members, Kanin Bodipat and Sachin Rana. My thanks also extend to Ihsan Burak Kulga for his help and suggestions in the development of this work and Amir Mohammad Nejad for his help in the development of the Graphical User Interface. Finally, I would like to thank Pichit Vardcharragosad for his academic and career guidance and suggestions throughout my study at The Pennsylvania State University.

Chapter 1

Introduction

Increasing demands of natural gas and depletion of conventional resources accelerates the exploration and production of unconventional resources. Unconventional reservoir is defined as reservoir where advanced technology is required in order to produce the resources at economic rates. Examples of unconventional gas are coalbed methane, shale gas, and gas hydrate. This work focuses on shale gas.

Shale is a type of clay and a source rock for conventional hydrocarbon reservoirs. Shale is considered as double-porosity, single-permeability system having extremely low permeability and porosity compared to conventional formation. In shale gas reservoirs, gas can be stored in three forms: free gas in matrix pores, free gas in fractures, and adsorbed gas on the surface of shale. Adsorbed gas can be primarily characterized by two parameters: Langmuir Volume (V_L) and Langmuir Pressure (P_L).

To economically produce gas from shale, a technology called hydraulic fracturing is implemented in the production of shale gas. Hydraulic fracturing is the process of pumping large amount of fluid, mainly composed of water, into the wellbore at high pressure and rate creating fractures in the formation. To prevent the fractures from closure, proppant is also pumped into the formation along with the fracturing fluid. The fractures created by hydraulic fracturing serve as high-permeability pathways that allow gas that is stored further away to flow into the wellbore. A successful fracture treatment can significantly increase gas production rates and ultimate recovery.

In optimization of the field, numerical reservoir simulation is utilized. Reservoir modeling and simulation can be time-consuming and the most-optimized approach might be overlooked. Furthermore, determination of equivalent hydraulic fracture representations can be laborious as several reservoir modeling and simulations may be required before an equivalent system can be established. Artificial neural network (ANN), which is an experience-based learning system, is introduced to overcome these challenges. The highlight of ANN is its ability to compute highly non-linear relationships. The trained ANN can instantly provide production profile of the field as well as an equivalent hydraulic fracture representation in seconds.

In the development of ANNs, CMG[1] GEM[2] is used to simulate the production profile of a hydraulically fractured horizontal well in shale gas reservoirs. The inputs and outputs from the numerical model are used in training and testing of ANNs. MATLAB[3] neural network toolbox is employed in training of the ANNs. Two ANNs are developed in this work. The first ANN which is called "Performance Prediction ANN" is developed for prediction of gas production rates over 50 years from multi-stage hydraulically fractured horizontal wells in shale gas reservoirs. The second ANN called "Equivalency ANN" is developed to provide an alternative equivalent representation of hydraulic fracturing. This equivalent representation is called "crushed zone" representation. Chapter 5 discussed the two hydraulically fracture representations in more details.

Chapter 2 reviews information of unconventional gas reservoirs, horizontal wells, and hydraulic fracturing technology. The problem statement of this work is stated in Chapter 3. Chapter 4 provides an overview of ANNs, its algorithms, training process. In Chapter 5, the two hydraulic fracture representations and the generation of training and testing sets are covered. The

[1] CMG: **C**omputer **M**odeling **G**roup, A numerical reservoir simulator by Computer Modeling Group Ltd.
[2] GEM: **G**eneralized **E**quation-of-State **M**odel Compositional Reservoir Simulator
[3] MATLAB: **MAT**rix **LAB**oratory, A tool for numerical computation by The MathWorks™

previously-generated input and output sets are used in the development of ANNs which is discussed in Chapter 6. The results (e.g. performance) obtained from the ANNs are discussed in Chapter 7. Chapter 8 provides the summary and conclusion of this work. Finally, a graphical user interface (GUI) is built to provide an ease of use of the developed ANNs, and the user manual is included in Appendix A.

Chapter 2

Literature Review

This chapter briefly explains unconventional reservoirs, horizontal wells, and hydraulic fracturing technology.

2.1 Unconventional Gas Reservoirs

Conventional gas reservoir is a gas reservoir which can be produced economically under current technology. Because of rapid depletion of conventional gas reservoirs and an increase in natural gas demand, the focus in oil and gas industry has been on unconventional gas reservoirs. Coalbed methane, gas hydrates, shale gas, and tight sand gas reservoirs are called as unconventional gas reservoirs. According to National Petroleum Council, these unconventional reservoirs have an estimated gas in place of 32,400 Tcf worldwide. As new technology becomes available, unconventional reservoirs become more attractive. Production from unconventional reservoirs requires advanced technology in order to produce natural gas at economic rates. The following are common characteristics of unconventional gas reservoirs as they:

- are difficult to develop due to its low permeability relative to conventional reservoirs
- have large volumes of hydrocarbons in place
- require advanced stimulation technologies
- are more expensive in well drilling and completion compared to conventional gas reservoirs

Unconventional gas resources are increasing importance worldwide, especially in the United States. According to U.S. Energy Information Administration (EIA), production from unconventional gas reservoirs sums up to approximately 11,670 Bcf[1] in 2009. This production provides approximately 55.6 percent of current natural gas consumption in the United States. Furthermore, production from unconventional gas reservoirs is projected to reach approximately 19,840 Bcf in year 2035.

2.1.1 Shale Gas Reservoirs

Shale is a type of clay or mud that can easily split into layers. These layers were compressed by formation pressure or other geological circumstances and turned into a fine-grained sedimentary rock. Shale formations function as source rocks and seals for conventional reservoirs. Gas migrates from source rock to sandstone or carbonate reservoirs. There, gas is accumulated and trapped in the sandstone resulting in a gas reservoir. Shale gas reservoir is defined as highly organic formation having permeability ranging from 0.1 mD to 10^{-7} mD. Figure 2-1 shows a sample of sandstone and shale reservoirs.

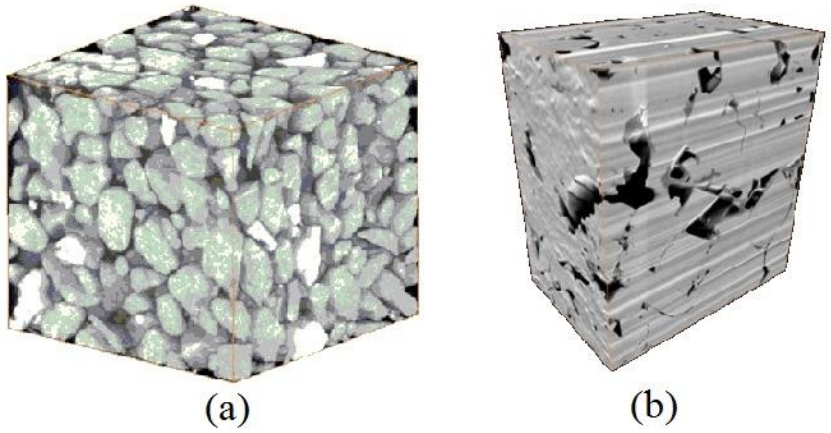

Figure 2-1: (a) High porosity sandstone, (b) Naturally fracture shale (Ingrain Digital Rock Physics Lab)

[1] Bcf stands for **b**illion **c**ubic **f**eet or 10^9 cubic feet.

As can be seen in Figure 2-1(a), sandstone has relatively higher porosity and the formation is less compressed. In Figure 2-1(b), shale, on the other hand, is a very tight porous medium. In nature, shale is a dual-porosity, single-permeability system exhibiting matrix porosity and fracture porosity. Natural gas is stored in shale in three forms: free gas in matrix pores, free gas in natural fractures, and adsorbed gas on shale surface. Gas produced from shale is mostly methane, but some are wet gas. The adsorption / desorption mechanism is governed by Langmuir isotherm where two properties are associated with: Langmuir volume or gas content (V_L) and Langmuir pressure (P_L). An example of desorption is shown in Figure 2-2. As the production continues, reservoir pressure decreases from point 1 to point 2. Gas then starts to desorb from shale surface. The amount of gas released per ton of shale is equal to the difference in gas adsorption capacity (V_L) between point 1 and 2. It can be seen that the amount of desorbed gas is larger at low pressure.

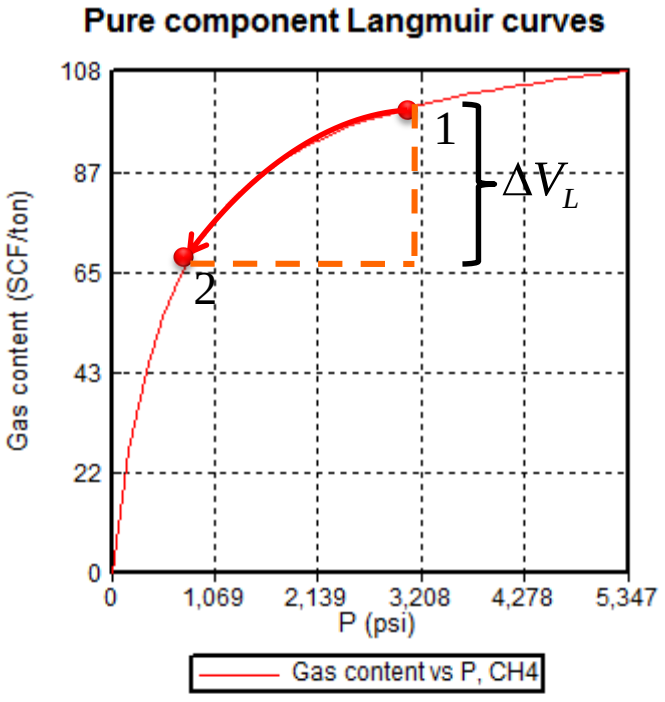

Figure 2-2: Langmuir Isotherm

The overall flowing mechanism of gas from shale matrix through the wellbore is similar to the coalbed methane reservoirs as explained in Figure 2-3.

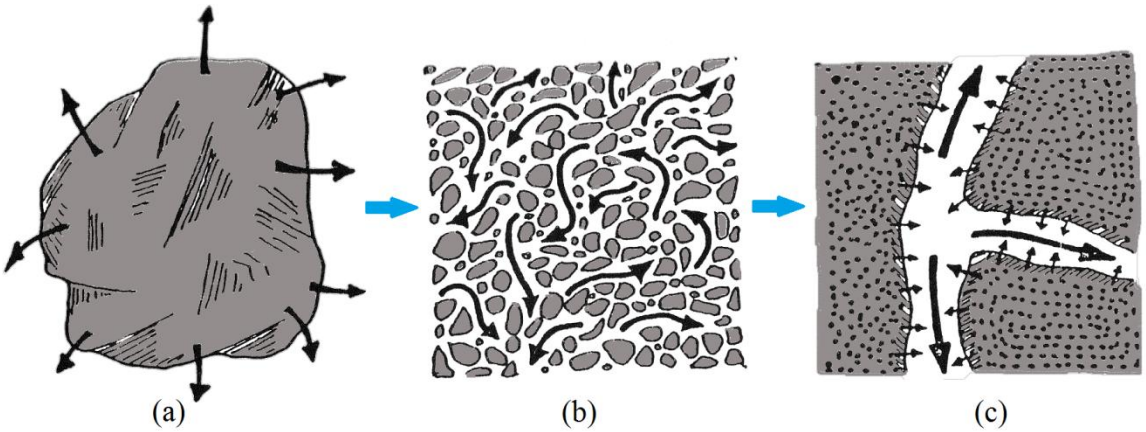

Figure 2-3: Flow Mechanism of Coalbed Methane and Shale Gas (Remner, 1986)

Although shale gas reservoirs and coalbed methane reservoirs share similar flow mechanism, contribution of adsorbed gas to gas produced is not as dominant as in coalbed methane reservoirs. Once the well is put on production, gas is desorbed from shale surface through matrix pores as depicted in Figure 2-3(a). In Figure 2-3(b), gas flows from shale matrix to fracture. The flowing mechanism in ultra low permeability system is governed by diffusion. Gas then subsequently flows through fractures which have relatively higher permeability to the wellbore as shown in Figure 2-3(c). Due to shale's ultra low permeability, in order to produce gas at commercial rate and volume from shale, horizontal drilling and stimulation technique called hydraulic fracturing is required.

According to U.S. Energy Information Administration, natural gas production from shale formations in the U.S. in 2009 is 3,280 Bcf. This number accounts for about 15.64% of the gas production in the U.S that year[2]. It is projected to increase to 12,250 Bcf in 2035. According to Sumi (2008), U.S. natural gas production from shale mainly comes from the following four basins:

[2] According to EIA, natural gas production in 2009 is approximately 20,960 Bcf.

- San Juan Basin in New Mexico/Colorado
- Antrim Shale in Michigan
- Devonian shales
- Barnett Shale in Texas

2.2 Horizontal Wells

According to U.S. Energy Information Administration, horizontal well is a well that is drilled vertically or slightly inclined extending from the surface to the location slightly above the target oil or gas pay zone. Then the well begins building up angle and continue horizontally (or near-horizontal) parallel to the reservoir's pay zone. Horizontal wells are drilled so that the lateral section stays within the formation of interest. Horizontal wells are classified into several categories based on lateral well length. With advanced drilling technology, a horizontal well can extend up to 8,000 feet of lateral section length. The advantage of horizontal wells over that of vertical wells is its higher wellbore surface area exposed to the formation allowing more gas to flow into the wellbore as shown in Figure 2-4. The cost of drilling a horizontal well could reach several million dollars.

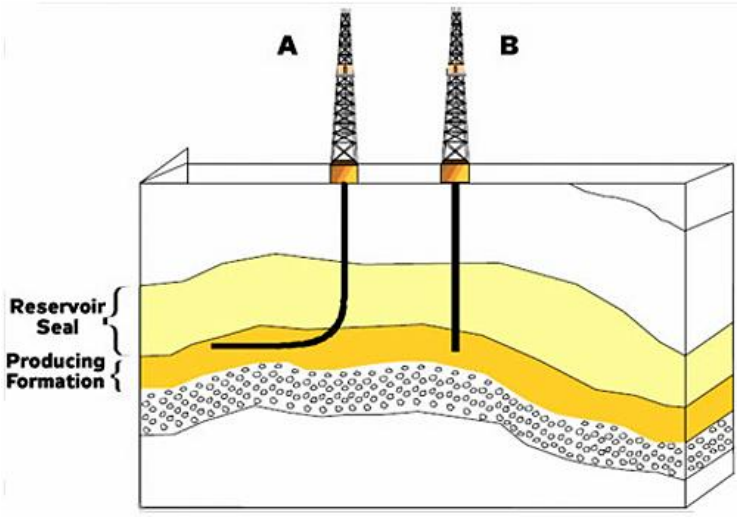

Figure 2-4: Comparison of Vertical Well and Horizontal Well (U.S. Energy Information Administration)

2.3 Hydraulic Fracturing

Hydraulic fracturing is a well stimulation technique used to increase production and ultimate recovery of hydrocarbon by pumping high pressured fluid into the wellbore creating fractures in the formation. The fractures can extend several hundred feet further away from the wellbore. These fractures having higher permeability serve as pathways for hydrocarbon to flow to the wellbore. Hydraulic fracturing is universally used in exploitation of shale gas reservoirs to produce natural gas at economic rate. The benefit of hydraulic fracturing is extended when coupled with horizontal drilling as several stages of hydraulic fracturing can be implemented.

2.3.1 Process

Hydraulic fracturing involves 2 simplified main steps. The first step is fracturing fluid preparation. Fracturing fluid is mainly 99.5% comprised of water and proppants which can be sand or ceramic beads and 0.5% of other chemical additives such as acid and anti-bacterial

agents. Proppants prevent created fractures from closure after the hydraulic fracturing has stopped. After the fracturing fluid has been prepared, the second step is to pump high-pressurized fracturing fluid at high rate to the perforated section of the wellbore creating fractures around the wellbore. After pumping stops, the fracturing fluid (water and chemical additives) returns to the surface leaving proppants in the formation. Hydraulic fracturing process can be repeated multiple times for maximum performance and maximum recovery. Each time this process is repeated is called a "stage". Implementing hydraulic fracturing multiple times is called multi-stage hydraulic fracturing.

2.3.2 Types of Hydraulic Fracturing

There are two types of hydraulic fracturing categorized based on fracture orientation and proppant propagation. Figure 2-5 shows graphical representation of the two types.

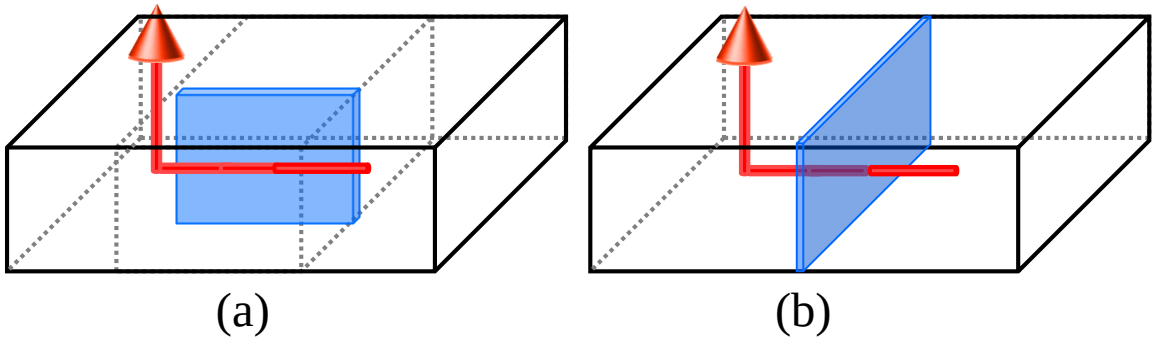

Figure 2-5: (a) Longitudinal Hydraulic Fracturing (b) Transverse Hydraulic Fracturing

The first type shown in Figure 2-5(a) is longitudinal hydraulic fracturing. The fracture plane of this type is oriented along the length of a horizontal section of the well where fracture height is confined within the pay zone. This type of hydraulic fracturing could create fracture planes with nearly infinite conductivity. However, due to limited horizontal penetration, gas stored further away from the wellbore might not be effectively recovered. On the other hand, with

the second type, called transverse hydraulic fracturing, fractures may extend several hundred feet into the formation but at lower proppant concentration. This work focuses on multi-stage transverse hydraulic fracturing. (Warpinski et al., 2008)

Chapter 3

Problem Statement

Reservoir simulation and reservoir engineering techniques play crucial roles in oil and gas exploration and production such as field optimizations of single or multiple wells in the field. However, optimization process can be time consuming and the optimal approach might not be achieved. Moreover, reservoirs with insufficient known or accurate parameters are frequently encountered. The first part of this study focuses on a development of an artificial neural network (ANN) for prediction of gas production rates from hydraulically fractured horizontal wells in shale gas reservoirs. The developed ANN can be used as a tool to assist reservoir engineers to overcome these challenges.

Hydraulic fracturing is implemented to produce gas at economic rates. Microseismic field data show that hydraulic fracturing creates a "crushed zone" around the wellbore. Accordingly, "crushed zone" hydraulic fracture representation is an elliptical zone of high fracture permeability and small fracture spacing around the wellbore due to hydraulic fracturing, and it can be used as an alternative representation of the stimulated zone. Difficulty lies in the characterization of hydraulic fracturing whether which model is more representative and what are their equivalent representations. The determination of equivalent systems can be laborious. Therefore, the second part of this study primarily focuses on the development of an ANN for establishing equivalencies between transverse hydraulic fracture representations and "crushed zone" hydraulic fracture representations.

ANN is capable of modeling and computing highly non-linear relationships with large number of variables. Due to high simulation speed of ANN, ANN is increasing popularity in

petroleum industry. ANN learns the structure of the model of interest by finding relationships between inputs and outputs and assigning weights and biases to the connections of the network. Several studies have been done using ANN as a tool in the application of reservoir simulation and achieve reasonable good results (Fausett, 1994).

In this study, the first ANN tool called "Performance Prediction ANN" is developed to model and simulate a hydraulically fractured horizontal well in shale gas reservoirs. The ANN will be able to predict the production profile over a 50-year period for given reservoir parameters and completion design characteristics. The reservoir parameters include reservoir thickness (h), compressibility of formation (c_f), matrix permeability (k_m), fracture permeability (k_f), matrix porosity (ϕ_m), fracture porosity (ϕ_f), natural fracture spacing (nf_{sp}), reservoir temperature (T_i), initial reservoir pressure (P_i), Langmuir volume (V_L), and Langmuir pressure (P_L). The other part of inputs in this study is design characteristics of horizontal wells and hydraulic fracturing. Characteristics associated with the two are drainage area per horizontal well (A), lateral length of a horizontal well (HW_l), number of transverse hydraulic fracture planes (N_{HF}), hydraulic fracture spacing (HF_{sp}), hydraulic fracture half length (xf), hydraulic fracture permeability (k_{hf}), and specified pressure at the well (P_{sf}). The reservoir parameters and design characteristics are inputs to a numerical model to obtain the production profile and cumulative production after 50 years of production. Once the ANN is developed, it can predict the production profile of any data sets in seconds with less than 10% error from actual numerical reservoir simulator without using any reservoir simulator.

The second ANN tool called "Equivalency ANN" is developed to establish equivalency between two different hydraulic fracture representations. The design characteristics of crushed zone hydraulic fracture representation parameters are minor axis length of the crushed zone (a_{minor}), major axis length of the crushed zone (a_{major}), crushed zone fracture permeability ($k_{f,cz}$), and crushed zone fracture spacing ($nf_{sp,cz}$). For a given reservoir, the trained network will be able

to accurately provide an equivalent "crushed zone" hydraulic fracture representation which can generate production profile within 15% error when compared with production profile generated from transverse hydraulic fracture representation.

Figure below illustrates the development protocol of the ANNs.

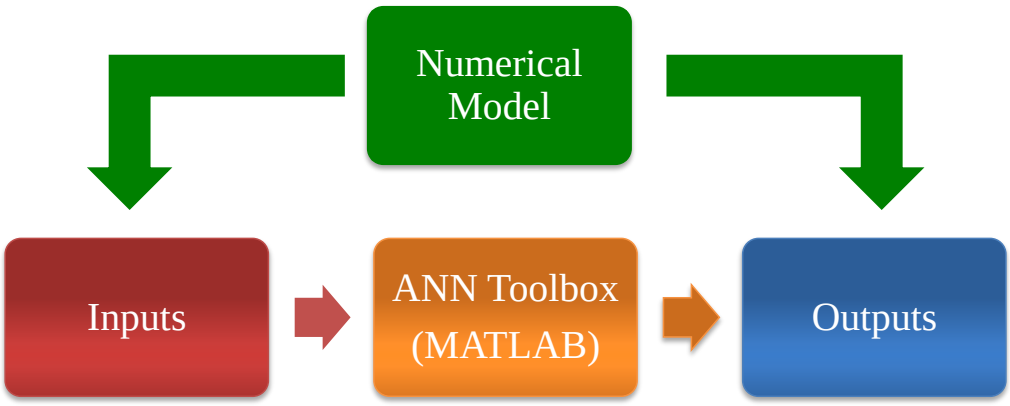

Figure 3-1: ANN Toolbox Protocol

As shown in Figure 3-1, a commercial numerical model is employed to generate production data from wide ranges of reservoir parameters and design characteristics. Reservoir parameters and design characteristics are used as inputs; the production data are used as outputs in the training of the network. To obtain the ANN tools, MATLAB is employed in various steps which are explained in greater details in Chapter 5 and Chapter 6. More information about ANNs, its algorithms, transfer functions, and training techniques are presented in Chapter 4.

Chapter 4

Artificial Neural Networks

This section provides some background about Artificial Neural Network and its associated key concepts.

4.1 Introduction

Artificial Neural Network (ANN) is an information-processing system inspired from biological network. ANN is widely accepted for its ability to handle non-linear systems. ANNs, also known as expert systems, have been widely implemented in a number of applications in several areas such as science, engineering, and finance. For example, ANNs have been utilized in weather forecast, robotics, and financial markets. The application of artificial neural networks also extends to oil and gas industry. For oil and gas industry, a number of studies have been done for various types of formations, completion designs, applications such as history matching and field optimization (Hagan et al., 1996; Fausett, 1994).

The origin of ANNs comes from neurons of human brain. ANN mimics mainly 3 components from biological neuron – axon, soma, and dendrite. Dendrites receive signals from other neurons. Soma then processes the scaled signals by summing them. The processed signals then are transmitted to other neurons through connecting axons. The artificial neurons mimic the architecture of the biological neuron. Each input is represented by a neuron, and the connections between neurons are characterized by their respective weights.

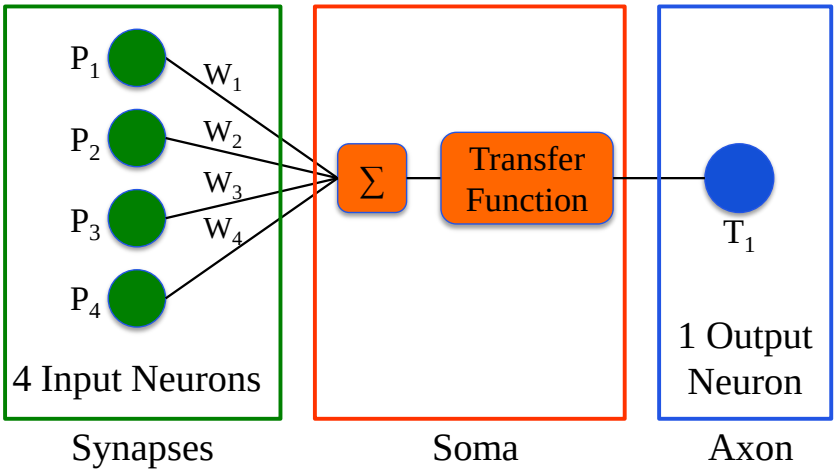

Figure 4-1: Simple Network (reproduced from Parada, 2008)

For a simple artificial neural network shown in Figure 4-1, signal from each neuron is multiplied by weight connecting the input neuron and output neuron. The weighted signal is summed and activated by transfer function before it is sent to other neurons. Training of ANNs is the process of determining the optimal weights for the problem of interest. Once the network is trained, the connecting weights between neurons are established, and it is said the network has "learned" and become an expert in the area of study.

4.2 Transfer Functions

An important part of ANN is transfer function or activation function. It transforms input signals into output signals by scaling using the user specified transfer function. Once the weighted input is activated using transfer function, it is sent to other neurons. In MATLAB's Neural Network Toolbox, there are 14 transfer functions; however, an observation from previous studies in petroleum engineering found that 4 transfer functions are applicable in the purpose of this study. The four transfer functions utilized in the training process of ANNs in this work will be discussed below.

- Hard Limit Function (*hardlims*)

  This transfer function gives only two outputs: 1 if signal is greater than zero and -1 if signal is less than zero. Hard limit function is not differentiable at transition point, and for this reason, hard limit function has limited usage for more complicated applications (Marren, 1990). Hard limit function can be described by the following equation:

$$f(y) = \begin{cases} 1 \; if \; y > 0 \\ -1 \; if \; y < 0 \end{cases}$$

- Linear Function (*purelin*)

  One of the most simple transfer functions other than hard limit function is linear transfer function. The output from linear function is multiplication of input and a constant. Linear transfer function is commonly used in the output layer of a network because outputs from networks with linear transfer function in the output layer do not need to be denormalized (Parada, 2008).

$$f(y) = K \cdot y \; where \; K \; is \; constant$$

- Log-Sigmoid Function (*logsig*)

  Log-sigmoid function is a continuous non-linear transfer function considered as one of the most frequently used in petroleum engineering applications. Log-sigmoid function takes the input and activates the neurons and gives the scaled outputs in the range between 0 and 1. Log-sigmoid function is described in the equation below.

$$f(y) = \frac{1}{1 + e^{-y}}$$

- Hyperbolic Tangent Sigmoid (*tansig*)

  Similar to log-sigmoid function, hyperbolic tangent sigmoid transfer function is a non-linear transfer function frequently used in the training of ANNs. The difference from

log-sigmoid function is that the output from this function is in the ranges of -1 and 1. Hyperbolic tangent sigmoid function is differentiable anywhere.

$$f(y) = \frac{e^{y} - e^{-y}}{e^{y} + e^{-y}}$$

4.3 Backpropagation Networks

Backpropagation network (BPN) is a supervised learning feed-forward network. Inputs are processed in forward direction through layers. The errors are calculated from the difference between the target and predicted output. The errors are used to update weights and biases and propagated back through the network. BPN is the most well-known and widely used in many applications. The inputs and outputs are introduced into the training process. Backpropagation is a learning method which requires continuous transfer functions as derivatives are used in the training. Two types of networks are utilized in this work. They will be briefly discussed below (Marren, 1990).

4.3.1 Feed-Forward Backpropagation Network

Feed-forward backpropagation network is a network in which inputs are sent in forward direction through layers. Once it reaches the output layer, the weights and biases are adjusted as the error is propagated backward. Feed-forward backpropagation network is commonly used in a static problem i.e. not a time-related problem. The training of the second network, Equivalency ANN, predominantly focuses on this type of networks as the outputs of the network are crushed zone parameters which are not time-related.

4.3.2 Cascade Feed-Forward Backpropagation Network

This type of network is simply a feed-forward network with an additional weight connection from the input to each layer. Cascade feed-forward backpropagation network is frequently used in the applications which inputs and outputs are time-related. An example of this network is the prediction of gas rates or cumulative production. Since outputs of the Performance Prediction ANN are gas rates at various times, this type of network is implemented in the training of the Performance Prediction ANN.

4.4 Training the Network

Training an ANN is a heuristic process. The objective of training an ANN is to determine the optimal weights of connections between neurons that yield satisfactory network performance i.e. low error. The proper network architecture for a given problem depends on several factors. The followings are the list of architecture of network that a designer can vary in the training process.

- Number of hidden layers
- Number of neurons in each layer
- Transfer function
- Training algorithm
- Connection between layers (fully or partially connected)

Apart from the previously mentioned network configuration, number of training sets and functional links are influential to the training and performance of the network. Since training an ANN is a heuristic process, a good starting point for training a network is proposed by Neuroshell (1998). The formula is presented below:

$$Number\ of\ Hidden\ Neurons = \frac{N_{input} + N_{output}}{2} + \sqrt{N_{set}}$$

where N_{input} is the number of inputs, N_{output} is the number of output, and N_{set} is the number of training sets. Using this formula as a starting point for the training of the network, network architecture is adjusted accordingly as training continues. Typically, one can select a feed-forward BPN with one hidden layer and specified the number of hidden neurons as described previously. After selecting type of network and initial network architecture, the step-by-step training process implemented in this work is listed below:

1. Train and test the network
2. If necessary, adjust type of network
3. If necessary, adjust training and learning algorithm
4. Adjust number of hidden layers
5. Adjust number of neurons in each hidden layer
6. Add or remove functional links as appropriate

Increasing number of hidden layers as well as number of neurons increases the complexity of the network. This allows the network to handle more complicated problems. To successfully train the network, functional links are frequently added to input and / or output layers. Functional links are additional inputs and outputs added to the network to provide additional relationships between original inputs and outputs. Functional links can be product, quotient, and eigenvalue (λ) of parameters where eigenvalue is an alternative way to represent parameters in matrix form with a single number. Implementing eigenvalue may improve the performance of the network as shown by Ramgulam et al. (2006). As an important remark, adding functional links created from outputs in the input layer is strictly prohibited. The mentioned training process is a general guideline. Depending on the complexity of the problem, more number of neurons, hidden layers, and functional links may be required.

4.5 Overlearning, Underlearning, and Generalization

As the training of the network continues, one may encounter overlearning which is one of the most common problems in training of artificial neural networks. Overlearning, i.e. memorization, occurs when the network starts to memorize the given data set instead of generalizing. The results from memorized network initially appear to be in good agreement with the actual outputs. However, when the network is tested with the new data sets, the network does not produce the proper results to new data sets. Having a complex network and longer training for a simple problem may result in network's overlearning. On the other hand, underlearning may occur from lack of training due to too short training period or the architecture of the network is not sophisticated enough to handle the complexity of the problem. Underlearned network usually results in a poor performance. To obtain a generalized network, the data sets are randomly divided into 3 parts: 1) Training sets, 2) Validation sets, and 3) Testing sets. Both validation sets and testing sets are excluded from training. During training, error in validation sets is monitored. As the training continues, validation error should decrease as well as the training error. At some point, the validation error typically begins to increase. This is an indication that the network start to memorize the relationships between inputs and outputs of the training sets. As stated earlier, memorized network could lead to a false impression or misleading that the network is properly trained. When overlearning occurs, the training must be stopped. Figure 4-2 shows the training performance of a network. It can be seen that at approximately 4,800 epochs (shown in red circle), the validation error starts to increase indicating that the network has started memorizing.

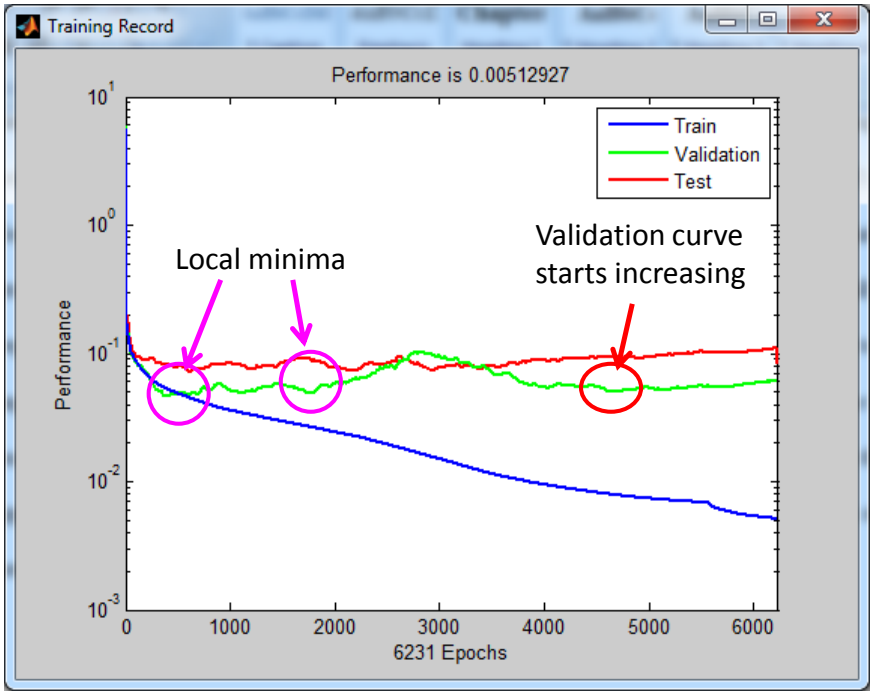

Figure 4-2: Network Overlearning and Local Minima

Another challenge in training the artificial neural network is finding the global optimal solution. As the training continues network errors decrease and approaches global optimal solution. It is important to avoid the local minima which are not the solution to the problem and make sure that the network's global optimal solution is reached. Illustrated in Figure 4-2 is a plot of error as a function of training epochs. The pink circles are locations of the local minima. At those locations, the network thinks that the training should be stopped as the validation error starts to increase. However, after a number of epochs, the validation error starts decreasing again. This indicates that the network has just passed a local minimum. It can be seen that there are many local minima before the global solution is obtained. For the system of interest, hundreds of dimensions with many local valleys can be expected (Beale et al.,2010).

Chapter 5

Generation of Training and Testing Sets

This section covers two stimulated zone representations: transverse hydraulic fracture model and crushed zone hydraulic fracture model. A MATLAB code is written to automatically generate input files for the numerical model. The compositional model is utilized to generate production profiles for transverse hydraulic fracture model and establish equivalency between the two representations. The following reservoir conditions are assumed:

- 2-dimensional model
- Homogeneous, isotropic square reservoir with non-uniform grid distribution
- Reservoir contains mainly methane and negligible residual water
- One horizontal well is placed at the center of the reservoir along the X direction
- The well is produced with constant specified pressure (P_{sf})

In addition, shale gas reservoirs can be modeled with dual-porosity, single-permeability system. Since shale is a tight system, and mainly fracture contributes to the flow, it is logical to establish the following two constraints.

- Fracture permeability (k_f) > Matrix permeability (k_m)
- Fracture porosity (ϕ_f) < Matrix porosity (ϕ_m)

The total simulation period is 50 years. Since the ANNs in this study are developed for shale gas reservoirs, wide ranges of shale gas reservoir properties and well completion design characteristics are selected for the development of the ANNs. The input data used in generating production profile for training the ANNs must be uniformly distributed in the desired ranges of interest in order to obtain ANNs which can handle a wide range of inputs. In this work,

parameters of small values such as matrix and fracture permeability are generated on a logarithmic scale and taken the anti-logarithmic back to its normal scale to avoid misleading of "uniformly distributed data". The distributions of parameters are listed in Appendix C. Figure 5-1 shows an overall workflow in the generation of training and testing sets. After obtaining the uniformly distributed data, data sets for numerical model are generated. Numerical model is implemented to generate production profile. The data sets are cleaned up before they are used in the training of ANNs. After obtaining the ANNs with the desired performance, distribution of parameters and network's prediction are plotted.

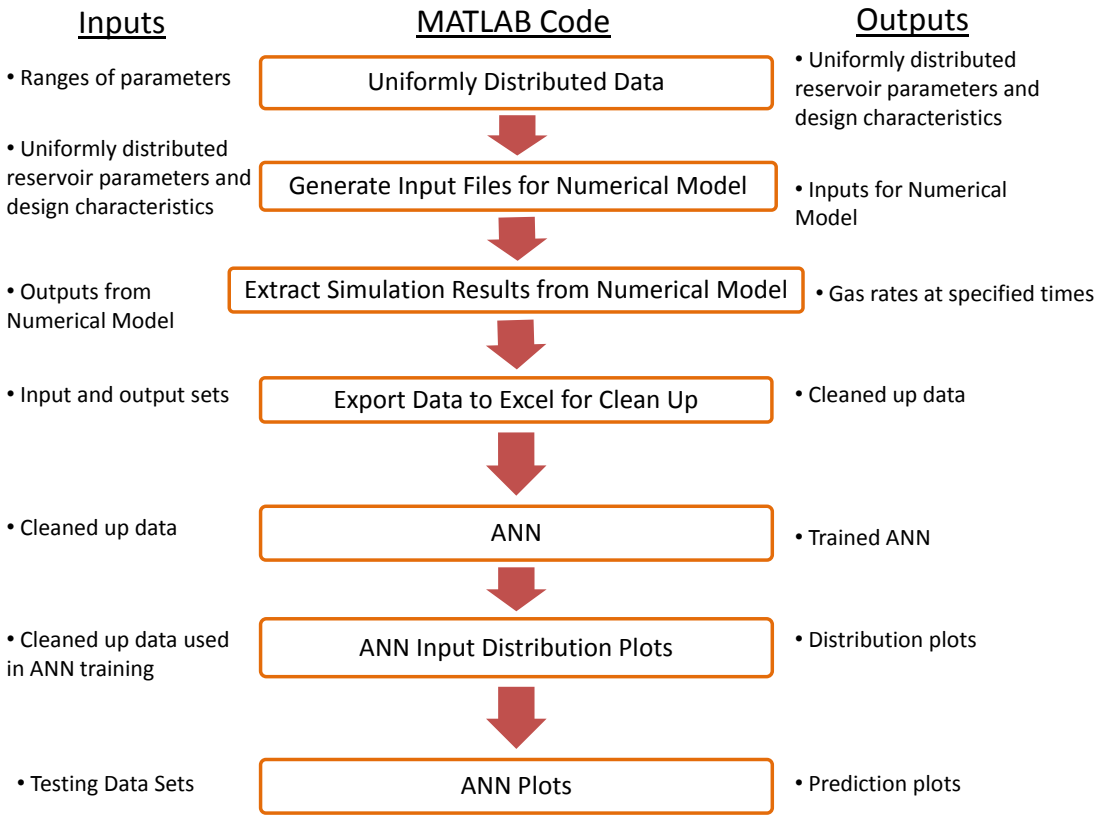

Figure 5-1: Overall Workflow in Generation of Training and Testing Sets

5.1 Hydraulic Fracture Models

Two hydraulic fracture representations associated with the development of the two ANNs will be discussed in this section. The first representation is the transverse hydraulic fracture representation. The second representation is crushed zone hydraulic fracture representation.

5.1.1 Transverse Hydraulic Fracture Representation

The conventional hydraulic fracture representation is the transverse fracture planes. Service companies design hydraulic fracturing in "stages", and each stage is represented by a very thin fracture plane. Figure 5-2 shows a sample of microseismic field data for a multi-stage hydraulically fractured horizontal well. Different colored dots indicate different hydraulic fracture stages.

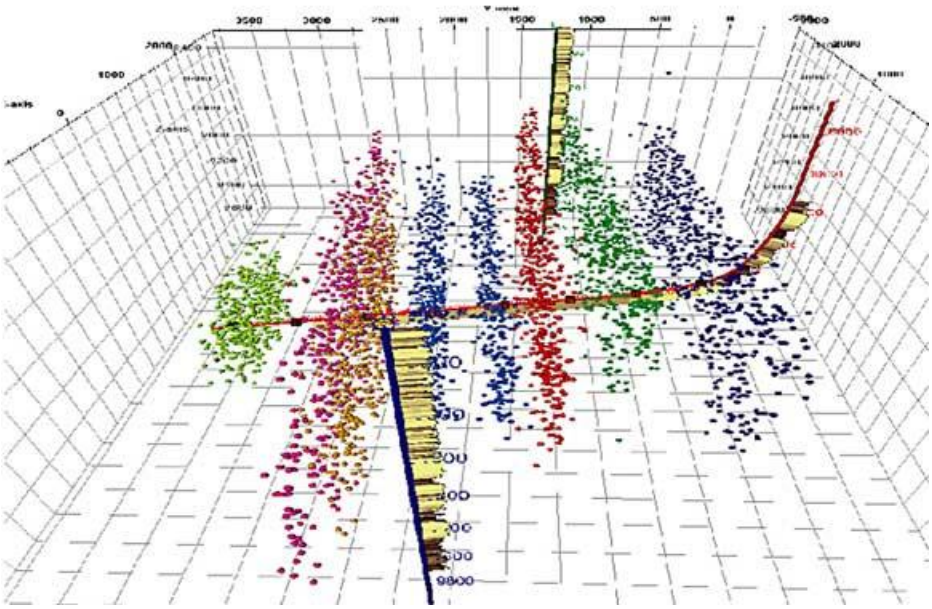

Figure 5-2: Transverse Fracture Planes Microseismic Field Data Resulting from Multi-stage Hydraulic Fracturing (National Energy Board)

How far the fracture penetrates the formation depends on how massively high pressured fluid is pumped into the formation. This representation is designed based on how each hydraulic fracture stage is created. In reservoir simulation, transverse hydraulic fracture plane is modeled by a very thin blocks (roughly 0.5 inch or smaller) with high fracture permeability. Depending on fracture width, hydraulic fracture permeability can vary from 10 mD to 10^6 mD.

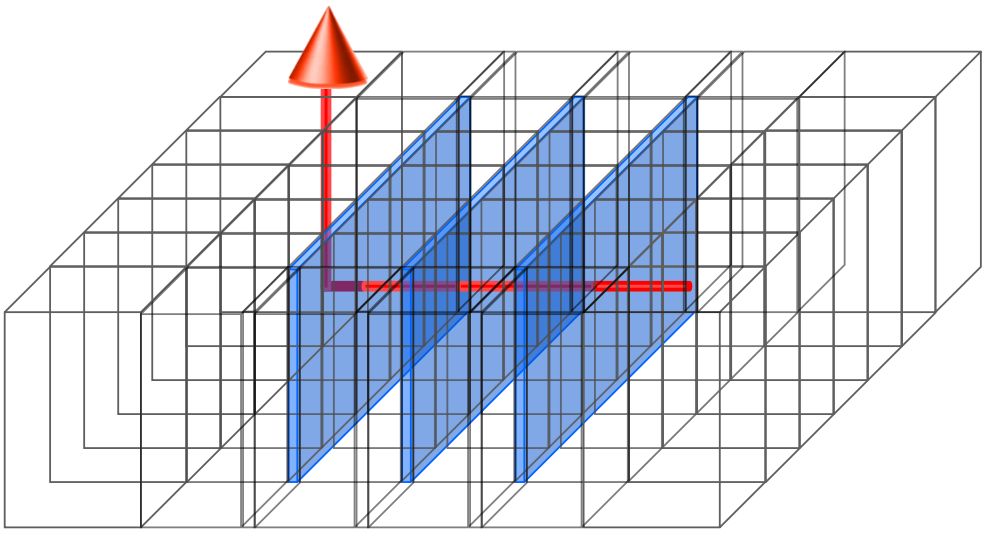

Figure 5-3: A Sample 3D View for Transverse Hydraulic Fracture Model

A sample of 3D model for transverse hydraulic fracture representation is shown in Figure 5-3. A horizontal well is drilled so that the lateral section is placed in the middle of the reservoir. Three hydraulic fracturing stages have been implemented in this reservoir. In this work, hydraulic fracture planes are assumed to span and reach the entire thickness of the reservoir. Each side of the hydraulic fracture is called a “wing”, and both wings can span up to 50% of the length of the drainage area.

Grid sensitivity is influential on gas production rates, especially initial gas rate. This has been taken into consideration in reservoir modeling of this work. Figure 5-4 shows a production comparison of the same reservoir completed with the same transverse hydraulic fracture design characteristics but different grid refinement i.e. different number of grid blocks in x- and y-

direction. In this figure, models with different refinements are plotted in different colors. Production profiles plotted in blue, red, pink, and green are from the model with 24×22, 12×11, 9×5, and 9×3 blocks, respectively. Red curves show the actual model used in this work. It can be seen that production profile from the highest refined model (blue curves) overlaps the one obtained from actual model used in this work (red curves). As the refinement increases, the production profile is accurately captured. However, insignificant improvement in gas production rates is achieved as refinement increases beyond 12×11 blocks. The initial gas rates from the actual model and the highest refined model are 13.94 and 19.4 MMscf/day, respectively. This is approximately 28.13% difference. Even though the difference in initial gas rate is large, overall production profiles are in good agreement. With this number of grid blocks and refinement for hydraulic fracturing, the simulation time is reasonable, and gas production rates have been accurately captured.

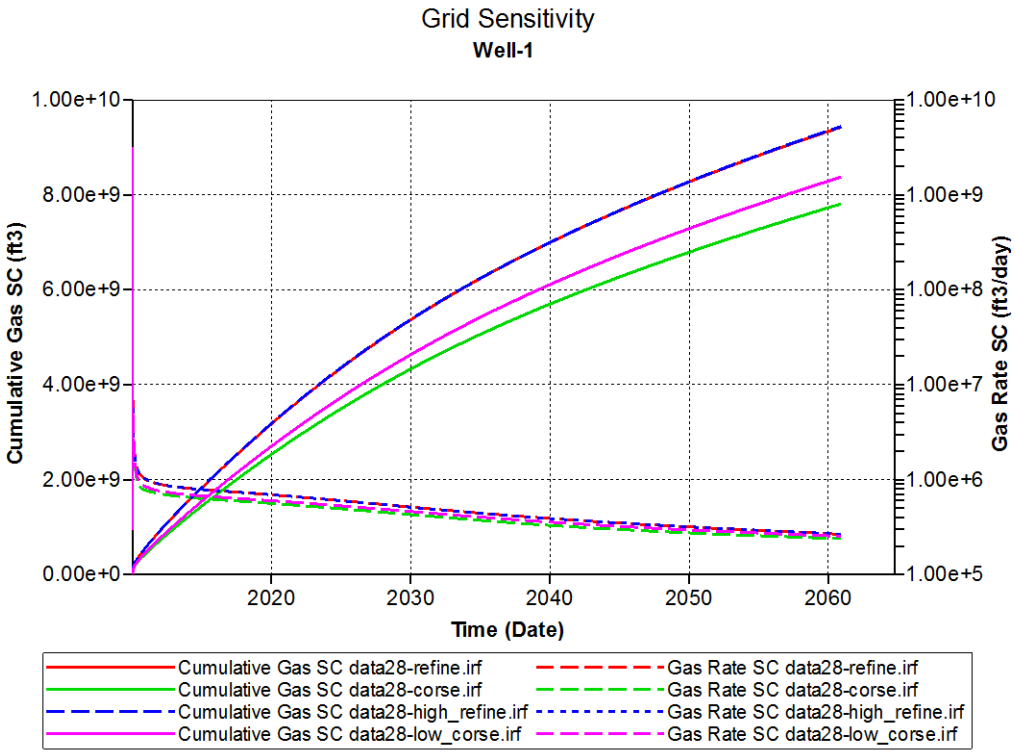

Figure 5-4: Grid Sensitivity on Gas Production Rates

5.1.2 Crushed Zone Hydraulic Fracture Representation

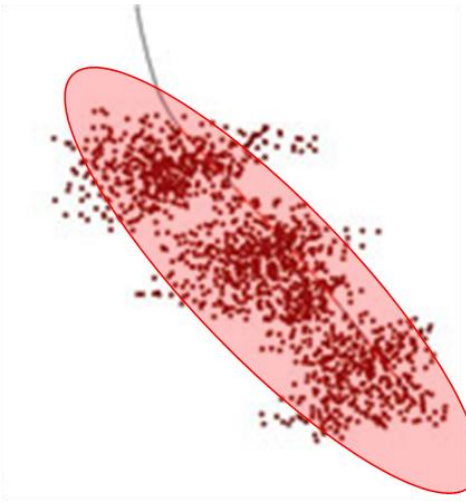

Figure 5-5: Elliptical Shape Microseismic Field Data Resulting from Multi-stage Hydraulic Fracturing (modified from Hart Energy Exploration and Production)

An alternative representation of the transverse hydraulic fracture model is the crushed zone hydraulic fracture model. Figure 5-5 shows a microseismic field data of a multi-staged hydraulically fractured horizontal well. Hydraulic fracturing creates a fractured area around the wellbore. In this work, this massively fractured area is called “crushed zone”. The “crushed zone” has an elliptical shape. This homogeneous isotropic zone has relatively higher fracture permeability than the original fracture permeability and smaller fracture spacing than the original fracture spacing. In reservoir modeling, instead of representing the multi-stage hydraulic fractures with long skinny high permeability planes as depicted in Figure 5-3, we represent multi-stage hydraulic fractures with an elliptical zone of higher fracture permeability and smaller natural fracture spacing. An example of 3D view of the crushed zone hydraulic fracture model is shown in Figure 5-6 where the crushed zone is represented by blue area around the wellbore.

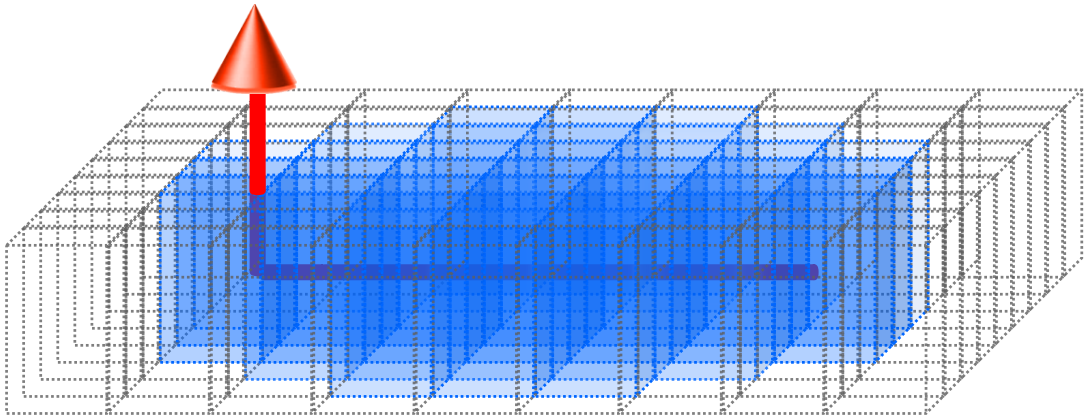

Figure 5-6: A Sample 3D View for the Crushed Zone Hydraulic Fracture Model

This work focuses on establishing equivalency between the two representations (Figure 5-3 and Figure 5-6), and "equivalent representation" is defined as a crushed zone hydraulic fracture representation that can generate the production profile within 10% cumulative production error from the transverse hydraulic fracture representation for the same reservoir properties, horizontal well length, and specified pressure at the well. The elliptical area around the horizontal well in the crushed zone hydraulic fracture model can be described by an elliptic equation.

$$\frac{x^2}{{a_{major}}^2} + \frac{y^2}{{a_{minor}}^2} = 1$$

where a_{major} and a_{minor} are the major axis and minor axis length of the ellipse, respectively. Since the area around the wellbore is massively hydraulic fractured, the reservoir properties in that region are altered. In this work, two properties are modified – fracture permeability (k_f) and natural fracture spacing (nf_{sp}). The two "crushed zone" properties are called "crushed zone permeability ($k_{f,cz}$)" and "crushed zone fracture spacing ($nf_{sp,cz}$)", respectively. The subscript "cz" which stands for crushed zone is added to distinguish the altered properties from the original properties. Therefore, this work will describe crushed zone hydraulic fracture representation with 4 parameters: major axis length of the crushed zone (a_{major}), minor axis length of the crushed zone (a_{minor}), crushed zone permeability ($k_{f,cz}$), and crushed zone fracture spacing ($nf_{sp,cz}$).

The methodology for establishing equivalent crushed zone representations is illustrated in Figure 5-7.

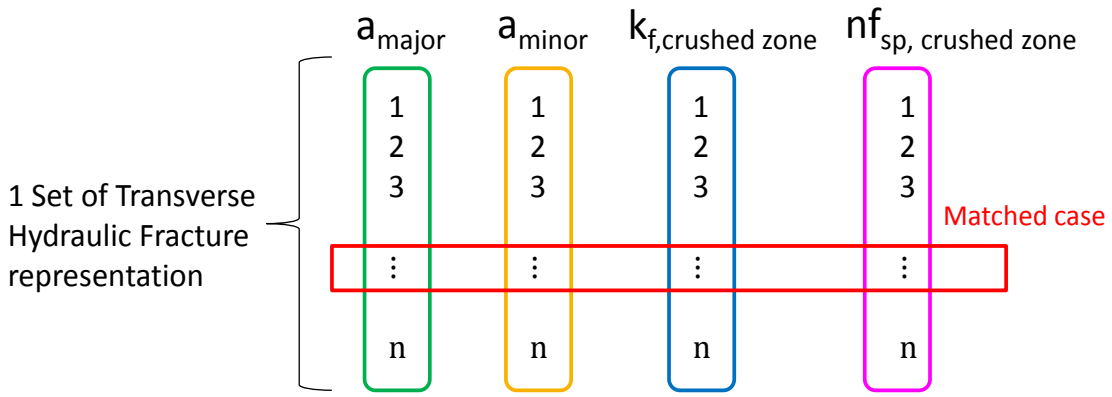

Figure 5-7: Methodology for Establishing Equivalent Representations

For a data set with transverse hydraulic fracture representation, several matching sets ("n" in this case) are generated with the crushed zone hydraulic fracture representation to match the gas rates and cumulative production. The production profiles are then compared with the production profile of the transverse hydraulic fracture representation. Once the production profiles agree within 10% error, the equivalency has been established, and the crushed zone parameters for the case with the least error are recorded. The process is repeated several times until enough data sets are obtained for the training of the Equivalency ANN.

5.2 Output Selection Process

Two techniques are attempted to describe the production profiles: curve fitting and gas rate selection. Both techniques and their advantages and disadvantages are discussed in the following section.

5.2.1 Curve Fitting

This technique attempts to represent the production profile with a mathematical representation. Previous studies have been done using this technique and proved to be effective. Three mathematical equations have been tested: hyperbolic equation, exponential equation, and logarithmic equation. The advantage of this method is smaller number of parameters introduced to ANN. With smaller number of parameters, training ANN is easier when compared with training with larger number of parameters as network has fewer parameters to learn. However, this technique might not be able to represent production profiles, especially during the first 10 years of production, for every scenario.

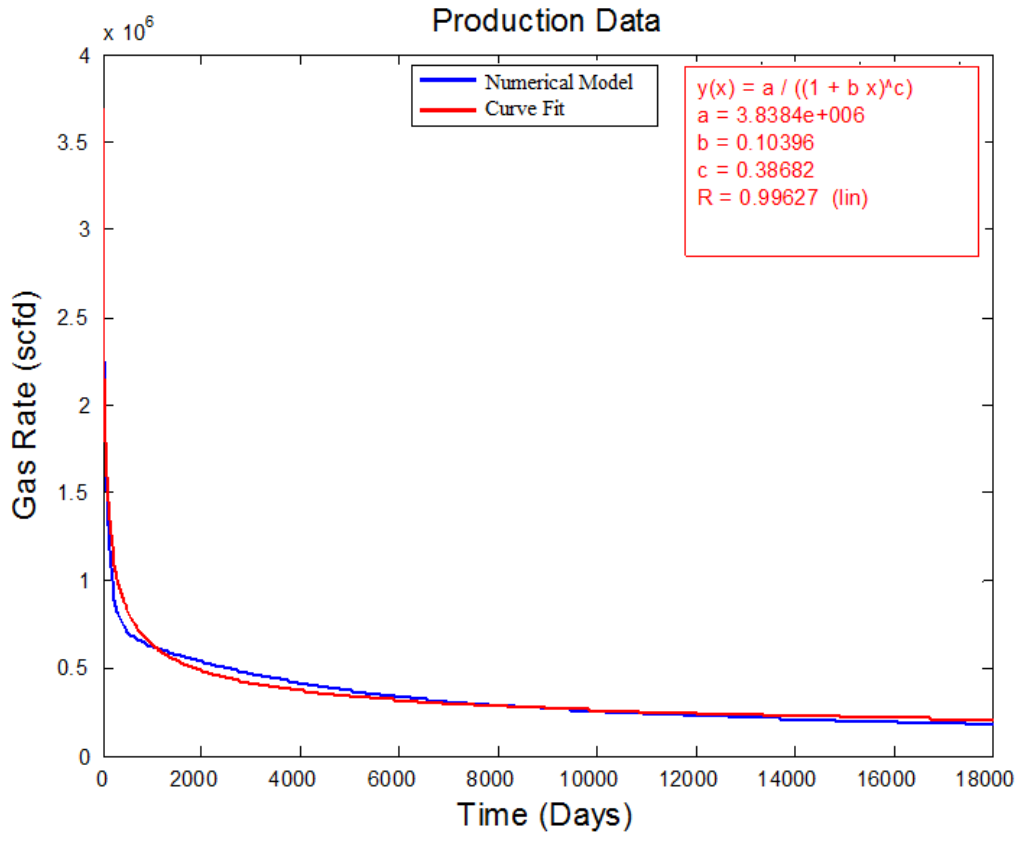

Figure 5-8: Production Profile Compared with Hyperbolic Curve Fit

Figure 5-8 shows the comparison between the actual production profile and curve-fitted production profile. The blue line is the actual production profile from numerical model; the red line is curve-fitted production profile. Even though the curve fit has a regression coefficient of 0.99627, the curve generated by hyperbolic coefficients does not agree with the actual production profile during the first 6,000 days. For example, the error on day 3,000 is approximately 11.67%. For the development of this work, it is not recommended to introduce the network with curve-fitted coefficients that are not able to capture the actual production profile. Therefore, gas rate selection is used in the development of this work. This technique is discussed in the following section.

5.2.2 Gas Rate Selection

Gas rates at specified times (q_t) from the production profile are selected and are listed as follow: q_1, q_{180}, q_{360}, q_{540}, q_{720}, q_{900}, q_{1080}, q_{1440}, q_{1800}, q_{2160}, q_{2520}, q_{2880}, q_{3240}, q_{3600}, q_{5400}, q_{7200}, q_{10800}, q_{14400}, and q_{18000} where the subscripted numbers refer to the number of days the well has been on production. More frequent gas rates are selected at the beginning of the production because there is a significant change during the early life of the reservoir. Figure 5-9 shows a comparison between specified gas rates and production profiles from the same data set as shown in Figure 5-8. Gas rate selection technique can capture the significant change in gas rate at the beginning of the production while the curve fitting technique yields an error of 11.67%. It can be seen that there's a significant change in production rate during the first 10 years. Therefore, more frequent gas rates are extracted during this period. After approximately 4,000 days, production reaches stabilized stage where gas rates change slightly over a long period. Thus, a smaller number of data points is required.

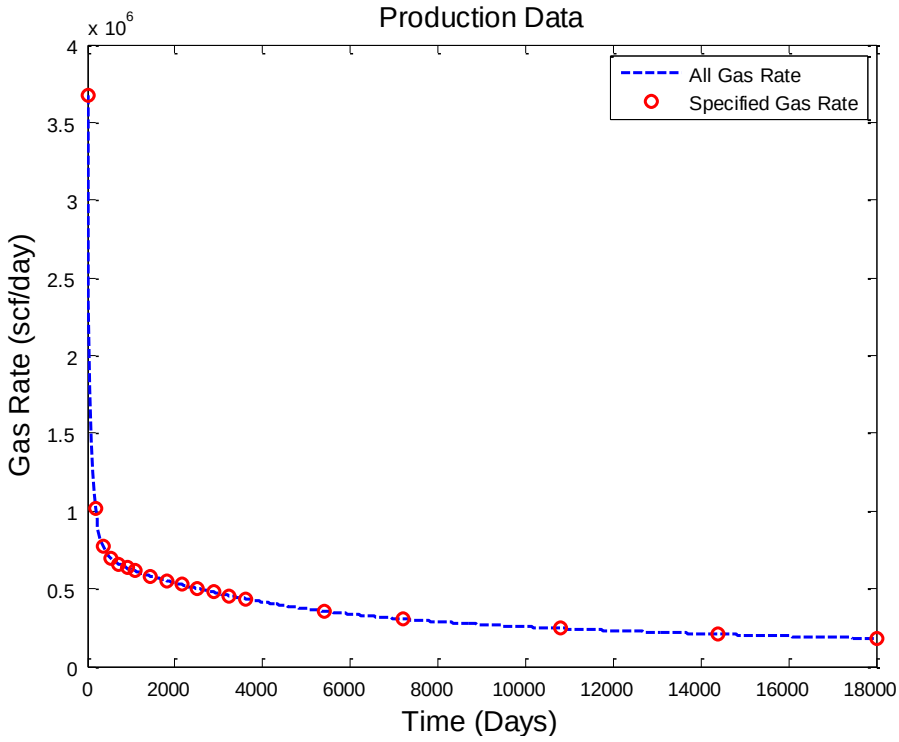

Figure 5-9: Representing Production Profile with Specified Gas Rates at Various Times

5.2.3 Data Clean Up

Several hundreds of data sets have been simulated. These results may not be realistic e.g. initial gas rate of 100 MMscf/day or cumulative production of 120 Bcf. To obtain realistic results from ANN, the data used to train the network must also be realistic. This means the following constraints are applied to remove the unrealistic results.

- Maximum gas rate at 1 day < 15 MMscf/day
- Cumulative gas production < 15 Bcf
- Maximum gas rate after 20 years of production < 1 MMscf/day

After applying the constraints, the ranges of data used in training the network are updated. They are listed in Table 5-1 below.

Table 5-1: Range of Reservoir Parameters and Design Characteristics for Transverse Hydraulic Fracture Representation

Parameter	Minimum Value	Maximum Value	Unit
Thickness (h)	50	300	ft
Compressibility of Formation (c_f)	5×10^{-6}	8×10^{-6}	1/psi
Matrix Permeability (k_m)	10^{-7}	0.01	md
Fracture Permeability (k_f)	0.0001	0.2	md
Matrix Porosity (ϕ_m)	2	16	%
Fracture Porosity (ϕ_f)	0.1	3	%
Natural Fracture Spacing (nf_{sp})	1	40	ft
Reservoir Temperature (T_i)	130	300	˚F
Initial Reservoir Pressure (P_i)	3,000	8,000	psi
Langmuir Pressure (P_L)	200	800	psi
Langmuir Volume (V_L)	50	200	scf/ton
Area (A)	50	300	acres
Horizontal Wellbore Length (HW_l)	900	2,168	ft
Number of Hydraulic Fracture (N_{HF})	2	19	-
Hydraulic Fracture Spacing (HF_{sp})	100	300	ft
Fracture Half Length (xf)	100	850	ft
Hydraulic Fracture Permeability (k_{hf})	10	10^6	md
Specified Pressure (P_{sf})	14.7	3,920	psi

Chapter 6

ANN Model Development

In this chapter, development of both Performance Prediction ANN and Equivalency ANN will be discussed. Using the data sets as discussed in Chapter 5, MATLAB neural network toolbox is utilized in the training of both networks. Observations from previous studies (Thararoop et al, 2008; Kulga, 2010) found that backpropagation networks with conjugate gradient algorithms yield better results than other algorithms. Furthermore, *tansig* and *logsig* transfer function are more applicable in this field than other transfer functions like *hardlims*. Linear transfer function (*purelin*) is used in the output layer of both ANNs.

6.1 Performance Prediction ANN

Initial inputs and outputs of this network are listed in Table 6-1. Inputs are categorized into two groups based on their natures. The first group of inputs is reservoir parameters. Inputs in this group include reservoir thickness (h), compressibility of formation (c_f), matrix permeability (k_m), fracture permeability (k_f), matrix porosity (ϕ_m), fracture porosity (ϕ_f), natural fracture spacing (nf_{sp}), reservoir temperature (T_i), initial reservoir pressure (P_i), Langmuir pressure (P_L), and Langmuir volume (V_L). The second group of inputs is transverse fracture design characteristics. Drainage area per horizontal well (A), horizontal well length (HW_l), number of hydraulic fractures (N_{HF}), hydraulic fracture spacing (HF_{sp}), fracture half length (xf), hydraulic fracture permeability (k_{hf}), and specified pressure (P_{sf}) fall into this group. As discussed in Chapter 5, the outputs from this network are specified gas rates at various times starting on the

first day to approximately 50th year of production. The day the gas rate is extracted from the numerical model is specified by subscripted number.

Table 6-1: Initial Inputs and Outputs for the Performance Prediction ANN

Inputs	Reservoir Parameters	h, c_f, k_m, k_f, ϕ_m, ϕ_f, nf_{sp}, T_i, P_i, P_L, V_L,
	Transverse Fracture Design Characteristics	A, HW_l, N_{HF}, HF_{sp}, xf, k_{hf}, P_{sf}
Outputs	Production Profile	q_1, q_{180}, q_{360}, q_{540}, q_{720}, q_{900}, q_{1080}, q_{1440}, q_{1800}, q_{2160}, q_{2520}, q_{2880}, q_{3240}, q_{3600}, q_{5400}, q_{7200}, q_{10800}, q_{14400}, and q_{18000}

The training starts with the simplest network which is a three-layer cascade feed-forward backpropagation network. However, this network cannot handle the complexity of the problem. Number of hidden layers, number of neurons in each hidden layer, and functional links are adjusted as appropriate to determine the network architecture that yields the desired performance.

After iteratively conducting a number of retraining, the proposed architecture of this network is shown in Figure 6-1. The network yields overall gas rate error within 10% of numerical simulated results. More detailed discussion on performance of this network is given in Chapter 7. The architecture of the Performance Prediction network is a 4 hidden layer cascade feed-forward backpropagation network with 20 neurons in each hidden layer. Three and seven functional links are added in the input and output layer of the network, respectively. Hyperbolic tangent sigmoid transfer function (*tansig*) is attached to all hidden layers. Linear transfer function (*purelin*) is used in the output layer. Functional links for this network are products, quotients, and eigenvalues of parameters which are influential to the gas production. Adding functional links that are physically meaningful is equivalent to forcing the network to learn the relationships between inputs and outputs in the correct direction. For example, eigenvalue λ_2 is calculated from fracture permeability, number of hydraulic fracturing, hydraulic fracture spacing, and fracture half length. These parameters are influential to the gas production rates. The network is trained

with 600 data sets. Sample of training sets are listed in Appendix D. Given reservoir parameters and design characteristics with transverse hydraulic fracture representation within the range listed in Table 5-1, this network predicts gas rates within 10% average error.

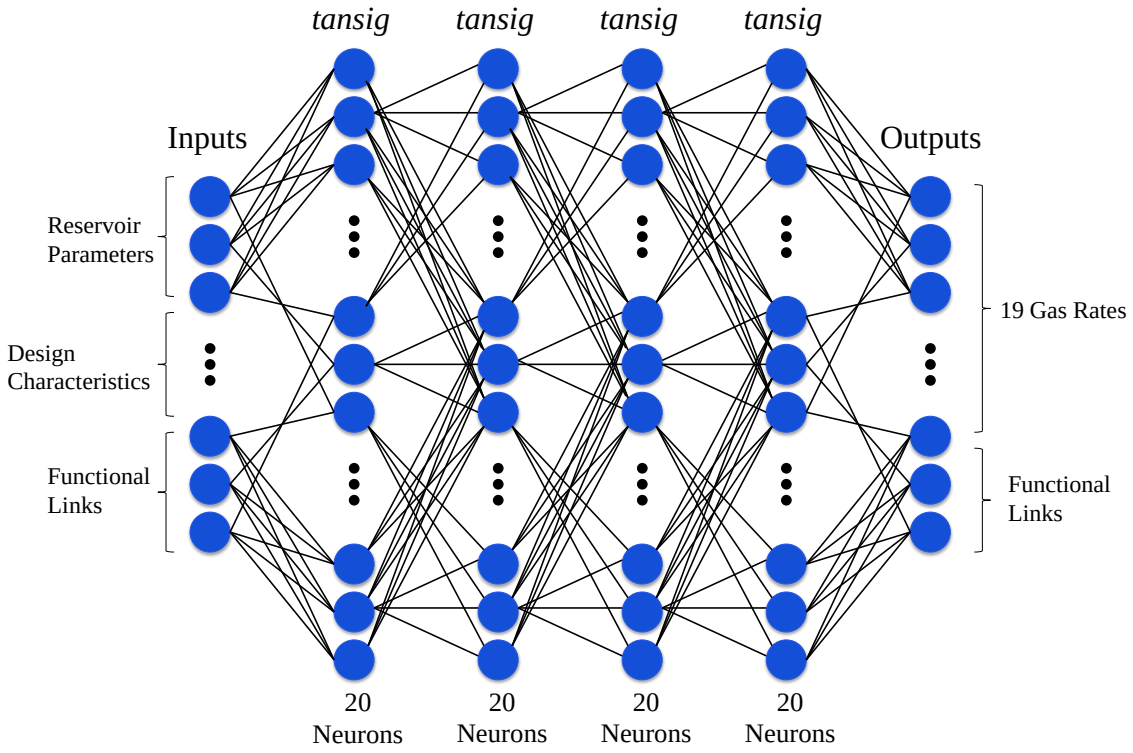

Figure 6-1: Performance Prediction Network Architecture

Inputs and outputs including functional links are listed in Table 6-2.

Table 6-2: Inputs and Outputs for the Proposed Performance Prediction ANN

Inputs	Reservoir Parameters	h, c_f, $\log_{10}(k_m)$, $\log_{10}(k_f)$, ϕ_m, ϕ_f, nf_{sp}, T_i, P_i, P_L, V_L,
	Transverse Fracture Design Characteristics	A, HW_l, N_{HF}, HF_{sp}, xf, $\log_{10}(k_{hf})$ P_{sf}
	Functional Links	λ_1*, $\phi_m \cdot h$, $\phi_m \cdot \log_{10}(k_m)$
Outputs	Production Profile	q_1, q_{180}, q_{360}, q_{540}, q_{720}, q_{900}, q_{1080}, q_{1440}, q_{1800}, q_{2160}, q_{2520}, q_{2880}, q_{3240}, q_{3600}, q_{5400}, q_{7200}, q_{10800}, q_{14400}, and q_{18000}
	Functional Links	CGP[6], λ_2**, λ_3***, λ_4****, P_i/P_{sf} $0.05 \cdot \log_{10}(k_{hf})/\log_{10}(k_m)/xf$, $HW_l \cdot xf$

[6] CGP stands for **C**umulative **G**as **P**roduction

Note:

* λ_1 is an eigenvalue calculated from the following equation: $\lambda_1 = eig\begin{bmatrix} log_{10}(k_f) & N_{HF} \\ HF_{sp} & xf \end{bmatrix}$

** λ_2 is an eigenvalue calculated from the following equation: $\lambda_2 = eig\begin{bmatrix} q_1 & GPC \\ P_i & log_{10}(k_f) \end{bmatrix}$

*** λ_3 is an eigenvalue calculated from the following equation: $\lambda_3 = eig\begin{bmatrix} q_1 & xf \\ log_{10}(k_{hf}) & GPC \end{bmatrix}$

**** λ_4 is an eigenvalue calculated from the following equation: $\lambda_4 = eig\begin{bmatrix} T_i & P_i \\ P_L & V_L \end{bmatrix}$

6.2 Equivalency ANN

Training procedure for the Equivalency ANN is similar to the procedure that was done for the Performance Prediction ANN. The initial inputs and outputs of the network are listed in Table 6-3.

Table 6-3: Initial Inputs and Outputs for the Equivalency ANN

Inputs	Reservoir Parameters	h, c_f, k_m, k_f, ϕ_m, ϕ_f, nf_{sp}, T_i, P_i, P_L, V_L,
	Transverse Fracture Design Characteristics	A, HW_l, N_{HF}, HF_{sp}, xf, k_{hf} P_{sf}
Outputs	Equivalent Crushed Zone Representation	a_{minor}, a_{major}, $k_{f,cz}$, $nf_{sp,cz}$

The architecture of the Equivalency ANN is shown in Figure 6-2. This feed-forward backpropagation network has 6 hidden layers with 40, 35, 30, 25, 20, 15 neurons in each layer. The first and last hidden layers are connected with log-sigmoid transfer function (*logsig*) while other layers are attached with hyperbolic tangent sigmoid transfer function (*tansig*). The architecture of this network has a funnel shape i.e. number of neurons in hidden layers is decreasing as inputs are propagated toward outputs. This may be due in part of large difference in the number of inputs (23) and outputs (13). The network is trained with 400 data sets and tested with additional 124 data sets.

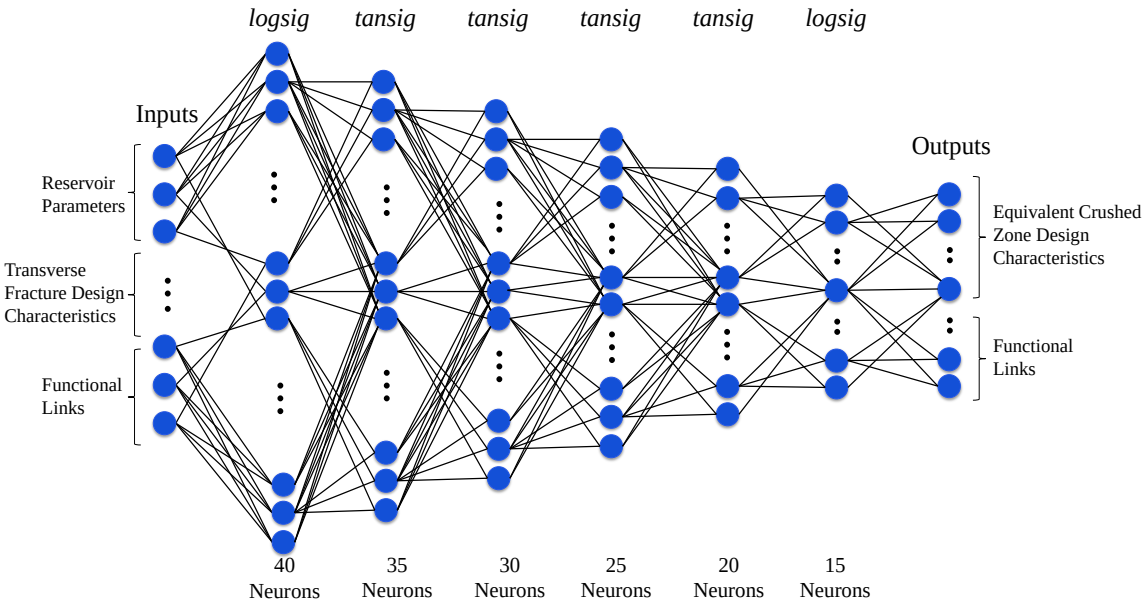

Figure 6-2: Equivalency Network Architecture

The inputs, outputs, and functional links for the Equivalency ANN are listed in Table 6-4.

Table 6-4: Inputs and Outputs for the Proposed Equivalency ANN

Inputs	Reservoir Parameters	h, c_f, $\log_{10}(k_m)$, $\log_{10}(k_f)$, ϕ_m, ϕ_f, nf_{sp}, T_i, P_i, P_L, V_L,
	Transverse Fracture Design Characteristics	A, HW_l, N_{HF}, HF_{sp}, xf, $\log_{10}(k_{hf})$ P_{sf}
	Functional Links	$c_f \cdot nf_{sp}$, P_i/P_{sf}, $HW_l \cdot HF_{sp}$, $A \cdot h \cdot \phi_m$, $V_L \cdot xf$
Outputs	Equivalent Crushed Zone Representation	a_{minor}, a_{major}, $k_{f,cz}$, $nf_{sp,cz}$
	Functional Links	$\sqrt{\left(\frac{a_{minor}}{2}\right)^2 + \left(\frac{a_{major}}{2}\right)^2}$, $a_{minor} \cdot xf$, $nf_{sp,cz} \cdot nf_{sp}$, $k_{f,cz} \cdot HF_{sp}$, $h \cdot HW_l$, $a_{major} \cdot N_{HF}$, $k_{f,cz} \cdot xf/\log_{10}(k_m)$, $N_{HF} \cdot HF_{sp}$, $k_{f,cz}/k_f$

After training the network, the errors for crushed zone parameters are analyzed. The percentage errors are used as indicators to determine whether an equivalent representation has been established.

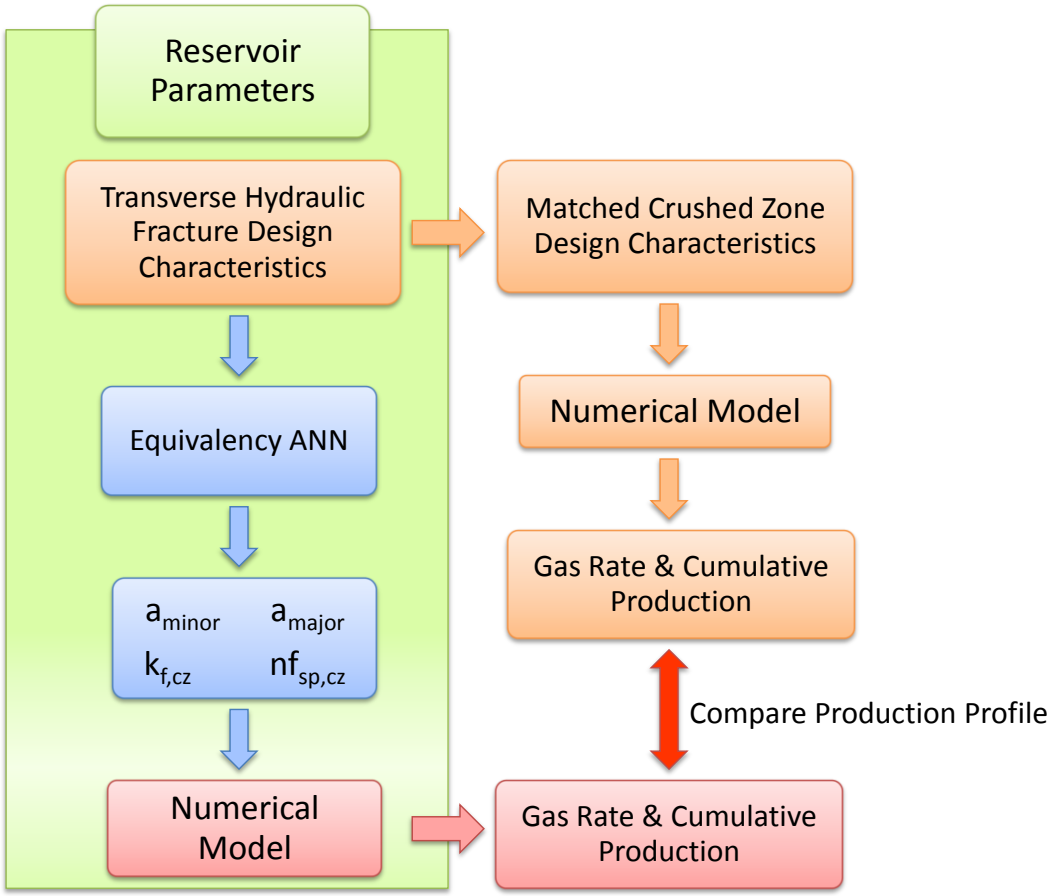

Figure 6-3: Testing Protocol for the Equivalency ANN

Figure 6-3 shows the testing protocol for the Equivalency ANN. The production profiles for a certain set of reservoir parameters and transverse hydraulic fracture design characteristics have been determined during the generation of training and testing sets for Performance Prediction ANN. The same reservoir parameters along with transverse hydraulic fracture design characteristics are sent to the Equivalency ANN. The Equivalency ANN returns the four crushed zone parameters (a_{minor}, a_{major}, $k_{f,cz}$, and $nf_{sp,cz}$). MATLAB code is employed to create inputs for numerical model for the equivalent crushed zone hydraulic fracture representation using the reservoir parameters and crushed zone design characteristics. Production profile of the equivalent representation from ANN is then compared with that of actual crushed zone representation. The performance of the ANN in establishing equivalency will be discussed in Chapter 7.

Chapter 7

Results & Discussions

This chapter discusses the results of both Performance Prediction ANN and Equivalency ANN. First, the gas rate prediction of the Performance Prediction ANN and cumulative gas production calculated from the gas rates will be analyzed. The next subsection discusses the performance of the Equivalency ANN. The utilization of ANNs can be explained as follows. Once the inputs are specified, the required functional links are calculated. Both inputs and functional links are normalized between -1 and 1 before they are sent to the network. Each input is multiplied by its connecting weight. The weighted inputs are summed and activated by a transfer function before they are sent to the next hidden layer. The process is repeated until it reaches the output layer. The outputs are displayed to the user.

7.1 Performance Prediction ANN

7.1.1 Prediction Performance Analysis

Error analysis for the Performance Prediction ANN can be done using the following equation:

$$q_{t,error} = \frac{\left|q_t - q_{t,ANN}\right|}{q_t} \times 100$$

where $q_{t,error}$ is gas rate error from actual value at time t, q_t is gas rate at time t from numerical model, and $q_{t,ANN}$ is gas rate at time t from ANN. The specified time "t" has been discussed in Chapter 5. Gas rates at specified times from numerical model are compared with the predicted gas

rates from ANN. Overall error for gas rates can be calculated by taking the average of the gas rate errors at each time as described by the following equation:

$$q_{ave,error} = \frac{\sum q_{t,error}}{N}$$

where N is the number of gas rates. In this work, 19 gas rates are extracted from numerical reservoir simulator for each run. Thus, the average gas rate error can be described as the sum of all the gas rate errors divided by 19. The overall error is used as an indicator for determination of network performance.

The proposed ANN is tested with additional 520 data sets. Plots of testing sets with various reservoir parameters and design characteristics for the Performance Prediction ANN are shown in Figure 7-1 through Figure 7-5. Gas rates follow a typical hyperbolic decline curve. Depending on reservoir parameters and design characteristics, initial gas rate can be as high as 15 MMscf/day and as low as 0.2 MMscf/day for the case of very tight systems, and it can be several times larger than the second specified gas rate (q_{180}). Gas rates for typical systems become stabilized after approximately 2,000 days i.e. no significant changes in gas rates between consecutive data points. After 20 years of production (roughly 7,300 days), gas rates usually fall below 1 MMscf/day.

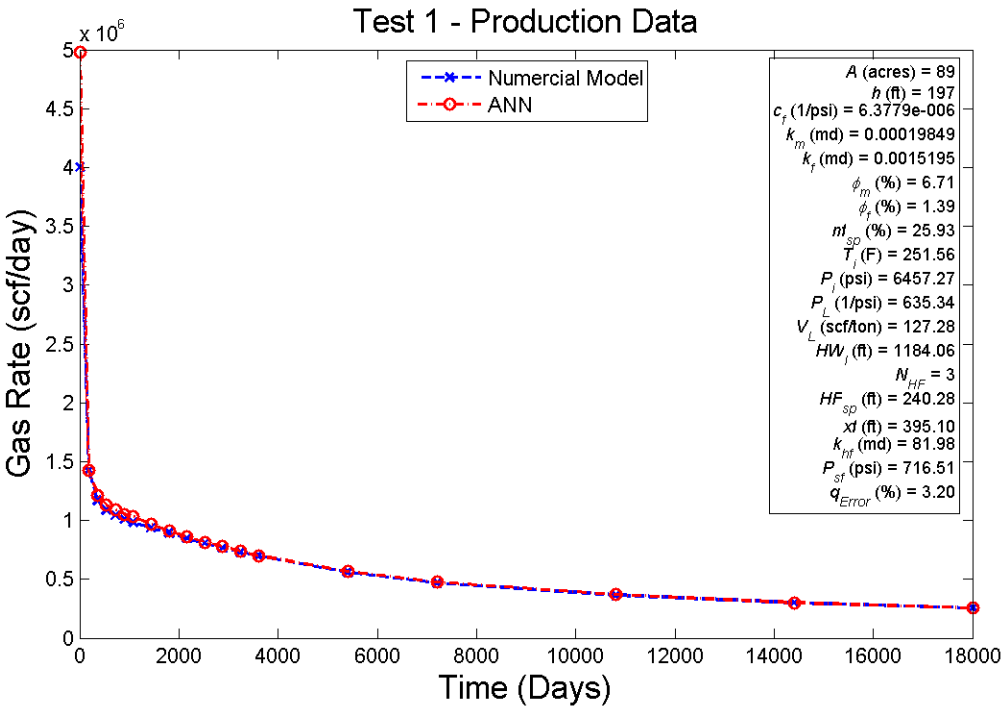

Figure 7-1: Prediction of Production Performance for Data Set 1

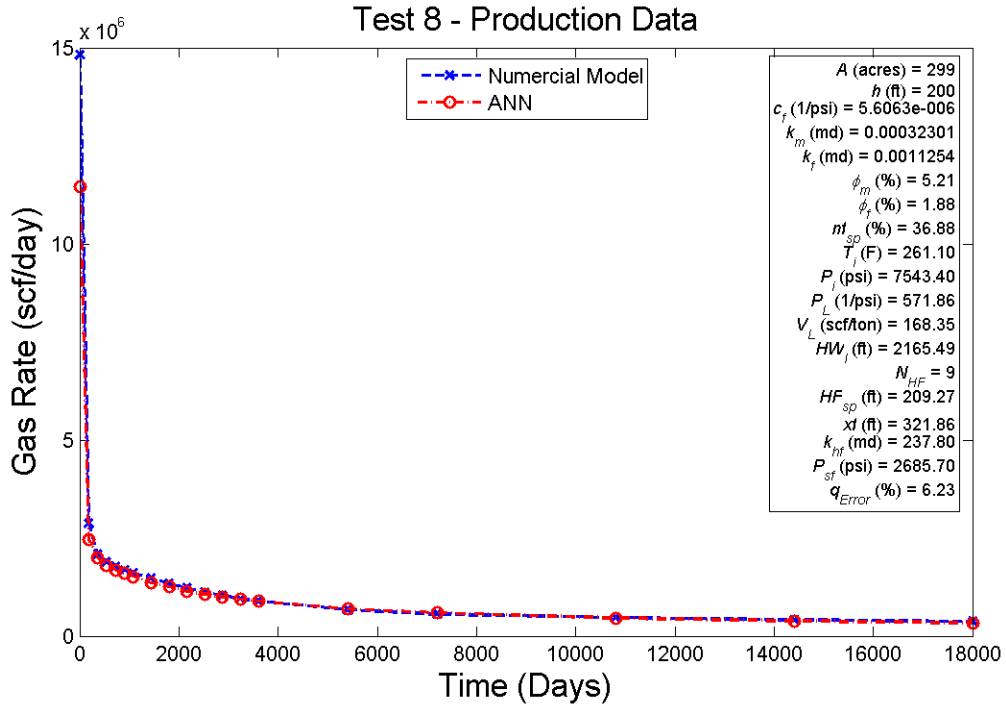

Figure 7-2: Prediction of Production Performance for Data Set 8

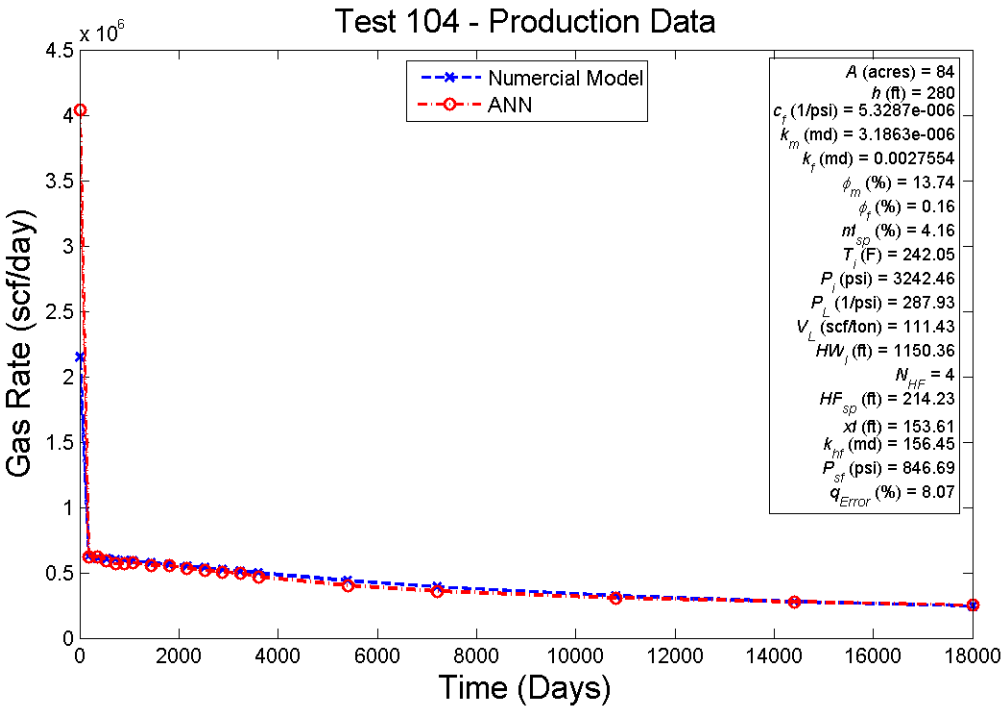

Figure 7-3: Prediction of Production Performance for Data Set 104

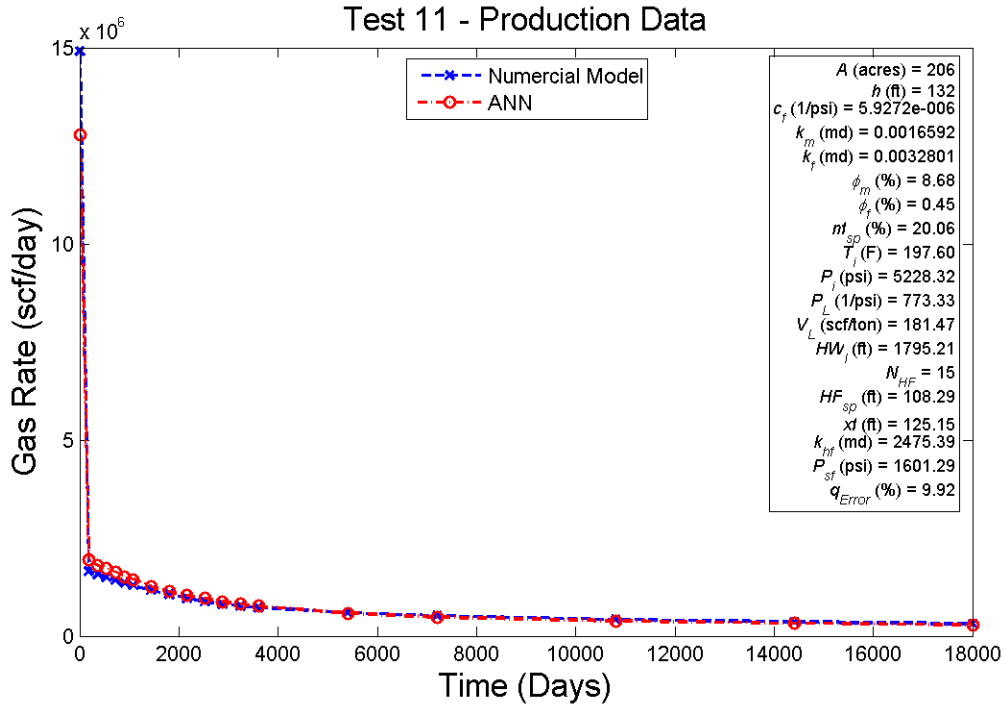

Figure 7-4: Prediction of Production Performance for Data Set 11

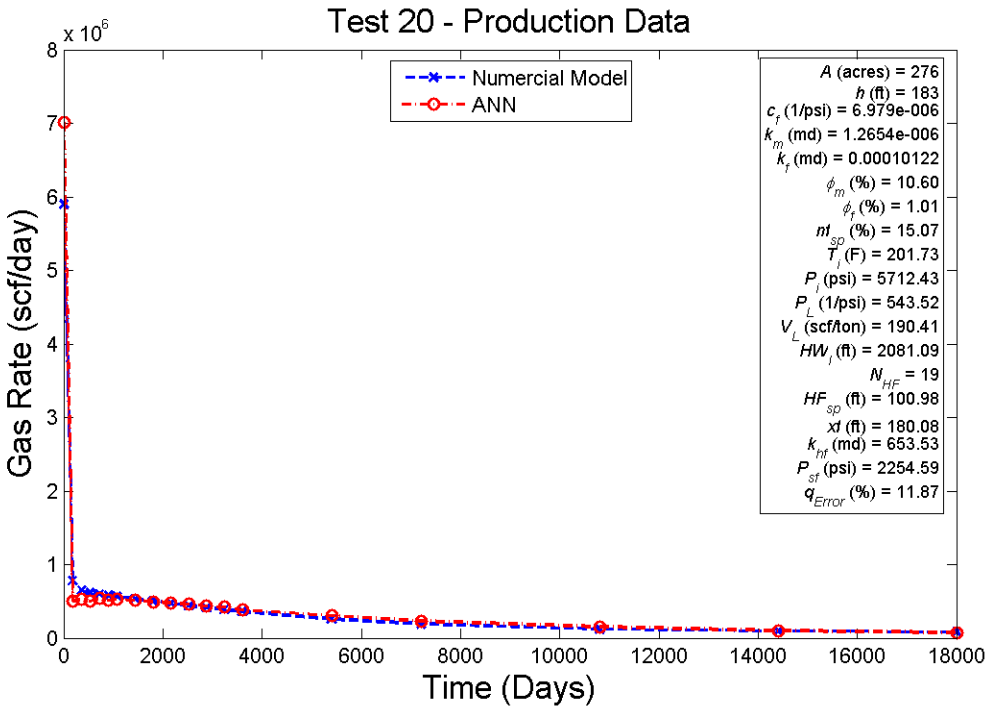

Figure 7-5: Prediction of Production Performance for Data Set 20

For the system shown in Figure 7-1, q_1 is 2.5 times greater than q_{180}, and the gas rate error at day 1 is 24.49% which is higher than the desired tolerance (10%). Similar network's responses can be observed in Figure 7-2 and Figure 7-3 where largest error occurs in the gas rate at day 1. The gas rate errors at day 1 ($q_{1,error}$) for these testing sets are 22.59% and 88.06%, respectively. Most of the time, the network is able to capture a significant drop in gas rate between q_1 and q_{180}. However, as shown in Figure 7-5, the network under predicts gas rate at day 180 with an error of 35.33%. For the tests shown in Figure 7-2 and Figure 7-4, the network slightly under-predicts and over-predicts gas rates in the early life of the reservoir, respectively. In both tests, the largest errors occur during the first 2,000 days. After that, the network starts to catch up the declined trend, and the prediction is significantly improved. In most cases, the network has a near-perfect late-time prediction.

From these figures, it can be seen that the network has a hard time identifying initial gas rate (q_1) and sometimes gas rates in the early life of the reservoir (q_{180}, q_{360}, and q_{540}). This large variation in gas rates impacts the predictive ability and overall performance of the network. There are 36 testing sets out of 520 sets (6.92%) that initial gas rate error significantly impacts the overall performance of the prediction. In other words, average error of gas rates excluding the initial gas rate are below 10%, but large error in initial gas rate when included in the analysis results in an overall average error of 10% or higher.

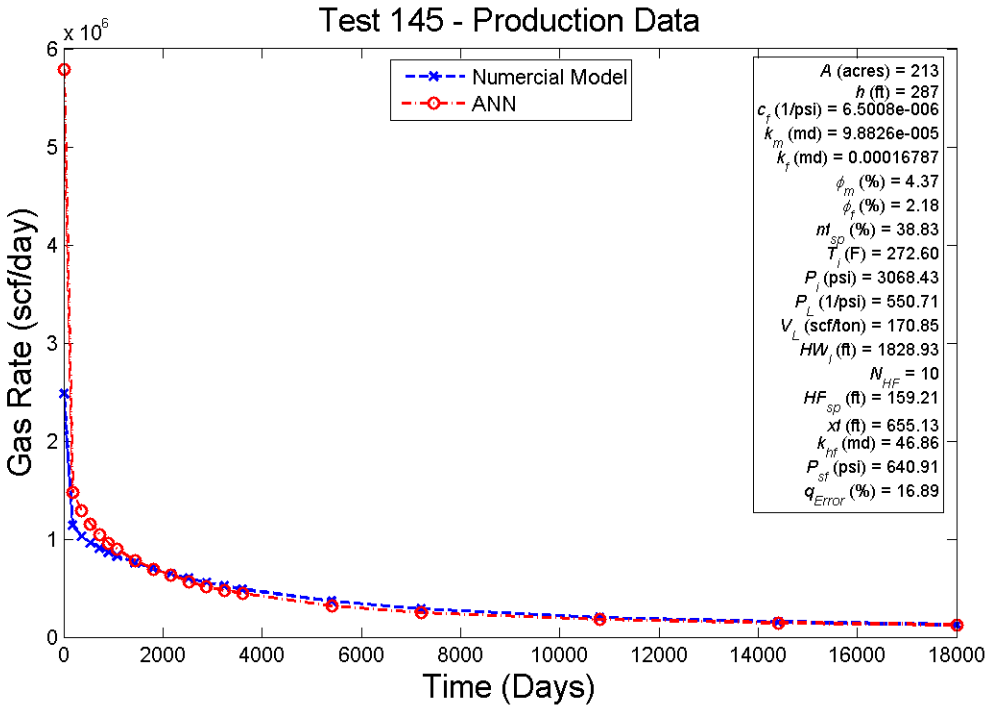

Figure 7-6: Prediction of Production Performance for Data Set 145

Figure 7-6 shows an example of ANN's early over-prediction and late-time under-prediction. In the first 900 days of production, ANN over predicts the gas rates with the largest error occurring on the first day (133.35%). The over-prediction continues until approximately day 2,000 where a "crossover" in gas production rates occurs. ANN starts to under-predict after approximately 2,000th day. The over-predicted and under-predicted gas rates are close to the

actual values enough to yield an overall average error of 16.89%. This gas rate crossover can be misleading in the calculation of cumulative production as over-prediction at the beginning can compensate the under-prediction in later time. This results in a possible misleading cumulative production at the end of 50 years.

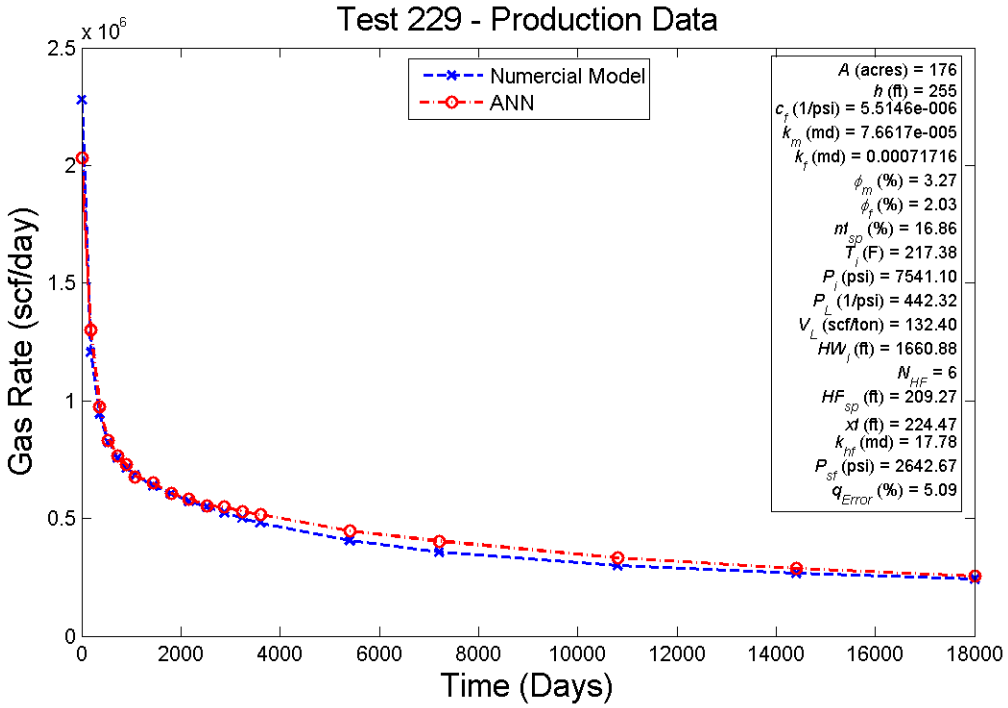

Figure 7-7: Prediction of Production Performance for Data Set 229

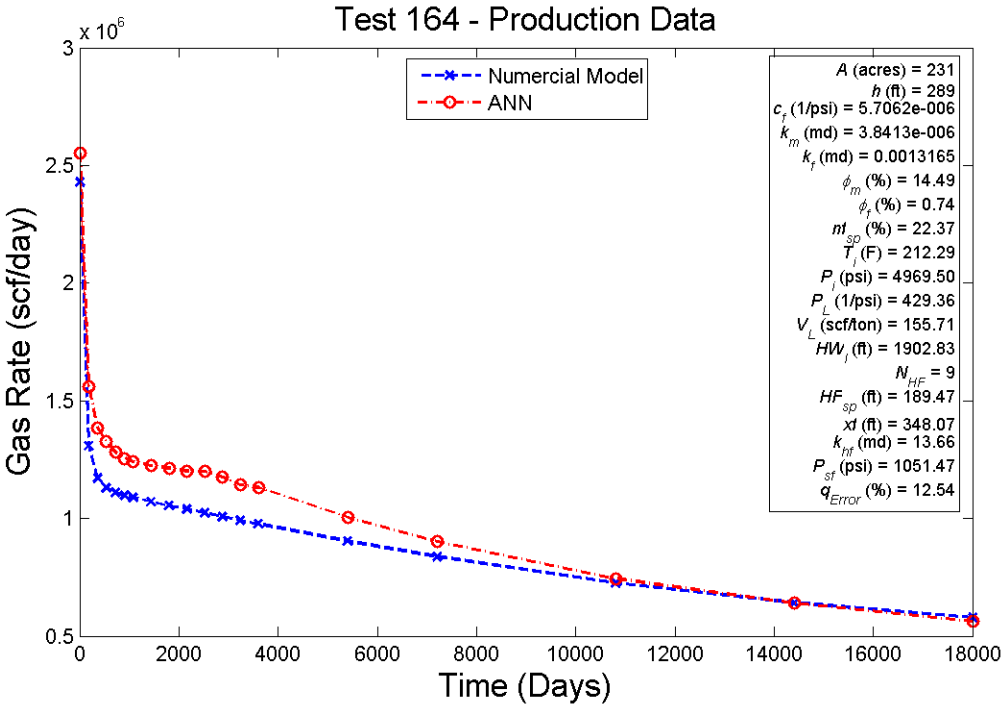

Figure 7-8: Prediction of Production Performance for Data Set 164

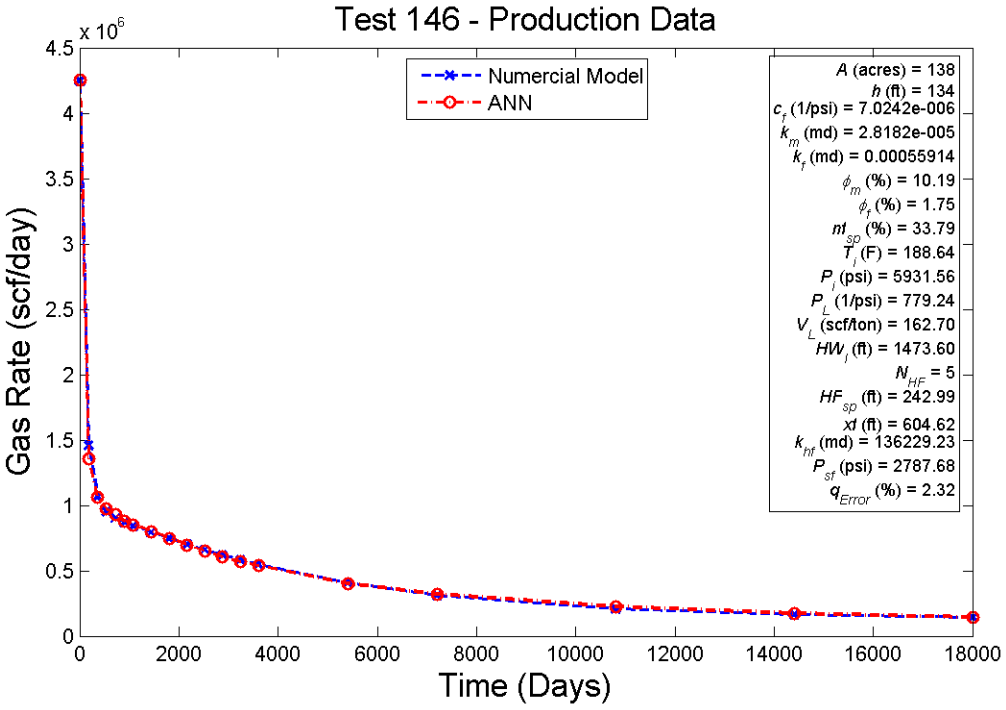

Figure 7-9: Prediction of Production Performance for Data Set 146

In Figure 7-7, the network predicts gas rate with errors less than 5% for the first 2,500 days of production. An over-prediction occurs after approximately 2,500 days of production. Figure 7-8 shows a testing set with low initial gas rate. The network over predicts the gas rates almost the entire production period. As frequently encountered, the largest error (18.28%) occurs at the initial gas rate. A near-perfect match is shown in Figure 7-9. For this testing set, the network is able to capture the gas rates accurately. This includes the first three gas rates which are normally difficult to predict accurately. The overall error for this set is 2.32%.

An observation drawn from these results is that the first three data points are important to the decline curve and are influential outputs in the overall accuracy of the network. Careful consideration should be given to the prediction of initial gas rate (q_1) as the network may not accurately predict the initial gas rate. However, a near-perfect late-time prediction can be expected from the network. The network is likely to accurately predict gas rates if the first three data points are matched. The stabilized gas rates also dictate how the decline curves look like i.e. how much gas rate drops before it reaches stabilized rate. Overall gas rate errors from the 520 testing sets are shown as histogram in Figure 7-10. It can be seen that 55.38% of testing sets are within the desired 10% error, and 75.18% of testing sets are within 15% error.

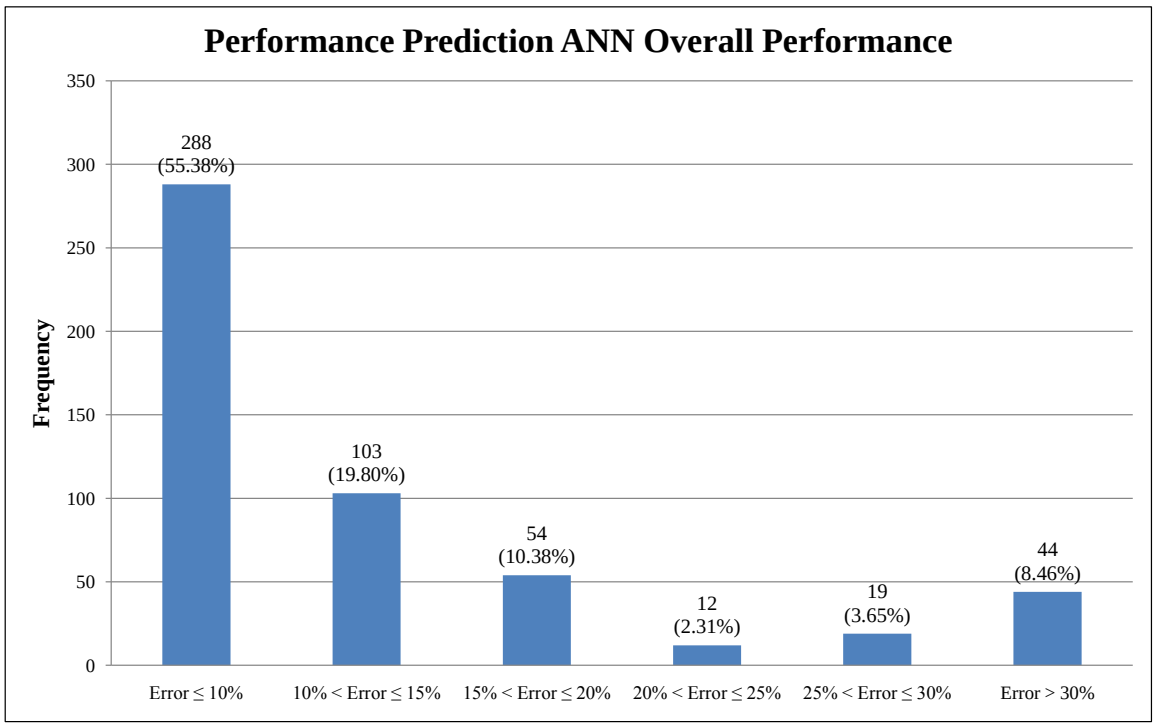

Figure 7-10: Overall Performance of the Performance Prediction ANN

7.1.2 Original Gas In-Place and Cumulative Gas Production

Original Gas In-Place (OGIP) is calculated based on initial conditions and properties of the reservoir. Since shale is a dual-porosity system with adsorbed gas, the OGIP is the sum of free gas in matrix system, free gas in fracture system, and adsorbed gas. OGIP can be calculated with the following equation (Thararoop, 2010).

$$OGIP = 43{,}560\frac{A \cdot h \cdot \phi_m}{B_g} + 43{,}560\frac{A \cdot h \cdot \phi_f}{B_g} + \frac{43{,}560 \cdot A \cdot h \cdot \rho \cdot V_L}{2{,}204.62}$$

where OGIP is original gas in-place in scf, A is area in acres, h is thickness in ft, ϕ_m and ϕ_f are matrix and fracture porosity, B_g is formation volume factor in ft^3/scf, ρ is shale density specified to be 89.58 lb/ft^3, and V_L is Langmuir volume in scf/ton. Formation volume factor is calculated using the following equation along with Dranchuk-Abou-Kassem formulation to calculate gas

compressibility factor Z (Ertekin et al, 2001; Dranchuk and Abou-Kassem, 1975). OGIP is used in calculation of percentage recovery.

$$B_g = \frac{P_{sc} \cdot T_i \cdot Z}{P_i \cdot T_{sc}}$$

Cumulative gas production can be calculated from the area under gas rate vs. time curve. Trapezoidal rule is applied to approximate the area under the curve. It should also be noted that even though gas rates from the ANN are within 10% error, cumulative production calculated from 10% error of gas rates over the 50 year period can accumulate and yield larger cumulative production error at the end of 50^{th} year when compared to the cumulative production from numerical model. The error in cumulative production should be taken into consideration in decision making.

7.2 Equivalency ANN

7.2.1 Non-Unique Equivalent Representation

Utilizing the methodology shown in Figure 5-7, multiple matching sets having reasonable agreement with the production profile from transverse hydraulic fracture representation can be expected in some data sets. This indicates a non-uniqueness of the equivalent representation. As an example, for a certain reservoir with transverse hydraulic fracture representation, an equivalent crushed zone representation can be larger with lower permeability or it can have smaller area with larger permeability.

Figure 7-11 shows matched production profiles of 3 crushed zone representations. Figure 7-12 displays reservoir models of transverse hydraulic fracture representation (a) and three matched crushed zone representations (b), (c), and (d).

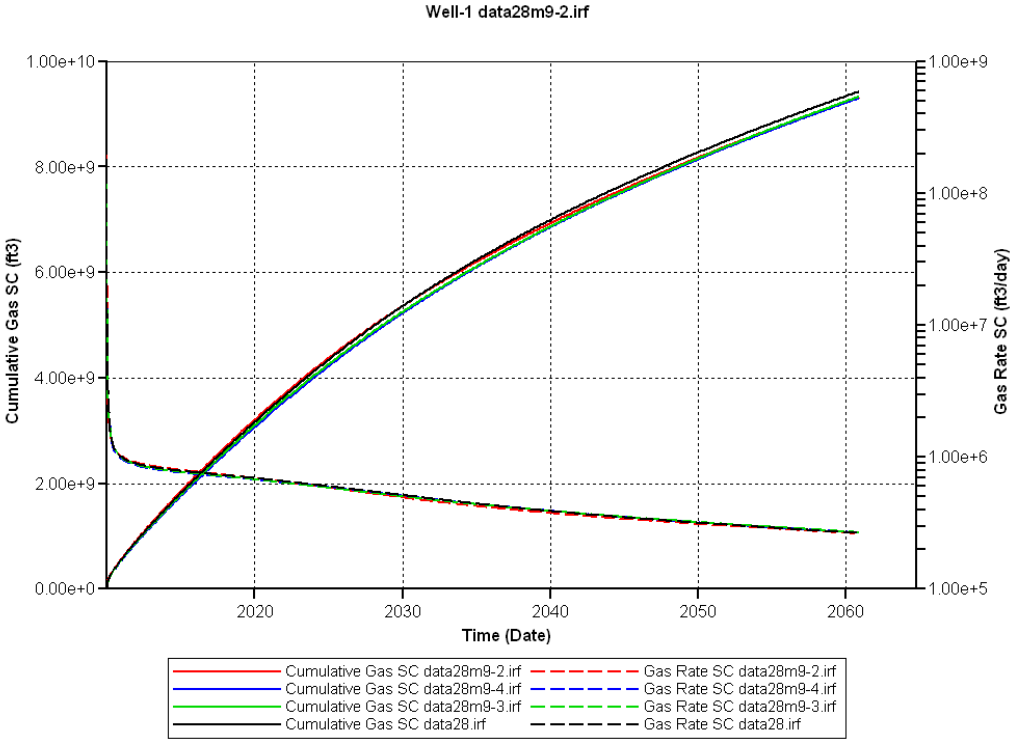

Figure 7-11: Multiple Matched Performance for Equivalent Representations

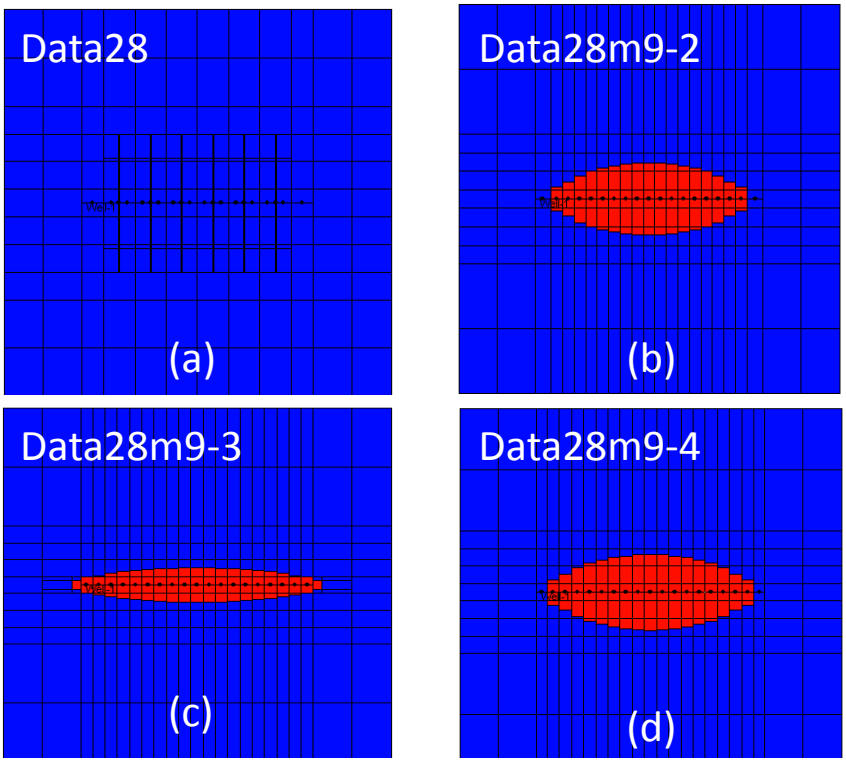

Figure 7-12: Non-Unique Equivalent Representations

From Figure 7-11, the productions profiles are in good agreement with the production profile from transverse hydraulic fracture representation (black line). However, it can be seen from Figure 7-12 that 3 different crushed zone design characteristics (b, c, and d) can create production profiles that are in good agreement with the production profile from the transverse hydraulic fracture model (a). Model (b) and (d) have similar minor axis length. Model (b) has crushed zone permeability of 0.494 mD which is roughly 7.7 times of the crushed zone permeability of model (d). However, model (d) can be considered as more "crushed" than the top right model as the crushed zone fracture spacing is only one third of model (b). Model (c) has smaller crushed zone, but the zone has quite large crushed zone permeability and very small crushed zone fracture spacing. The list of crushed zone design characteristics for the multiple matches is shown in Table 7-1. The case with smallest error (case (c)) is recorded and used in the training of the network.

Table 7-1: Example of Multiple Equivalent Representation Matches

Plot Name	a_{major} (ft)	a_{minor} (ft)	$k_{f,cz}$ (md)	$nf_{sp,cz}$ (ft)	Maximum Gas Rate Error (%)
data28m9-2 (b)	1228.29	444.95	0.494	15.16	4.08
data28m9-3 (c)	1541.01	234.43	0.346	1.235	2.31
data28m9-4 (d)	1292.88	495.2	0.0641	5.526	2.64

There is a difficulty in characterizing hydraulic fracture representation as several factors such as direction of in-situ stress of formation can affect the crushed zone parameters. Nevertheless, the expected outcome of this work is to establish equivalent crushed zone representation that yields production profile within 10% cumulative production error when compared with transverse hydraulic fracture representation.

7.2.2 Establishing Equivalency Performance Analysis

From the observation discussed in previous section regarding the possible multiple matches and attempts in establishing equivalency, the crushed zone parameters can be ranked in order of its sensitivity on gas production as follows:

$$k_{f,cz} > a_{minor} > a_{major} > nf_{sp,cz}$$

The sensitivity ranking of parameters serves as a guideline for matching the transverse hydraulic fracture representation, and it helps in establishing equivalency for some data sets that are difficult to match. Following the protocol in Figure 6-3, the proposed network is tested with additional 124 sets. Some typical comparison plots will be shown and discussed. The desired accuracy of the network is 15% cumulative production error where the error can be calculated from the following equation:

$$CGP_{error} = \frac{|CGP - CGP_{ANN}|}{CGP} \times 100$$

where CGP_{error} is cumulative gas production error in percentage, CGP is cumulative gas production from actual equivalent crushed zone representation, and CGP_{ANN} is cumulative gas production generated from ANN's predicted crushed zone parameters. The matched performances based on ANN predicted crushed zone parameters are plotted in red, and the actual matched performances from numerical model are plotted in blue.

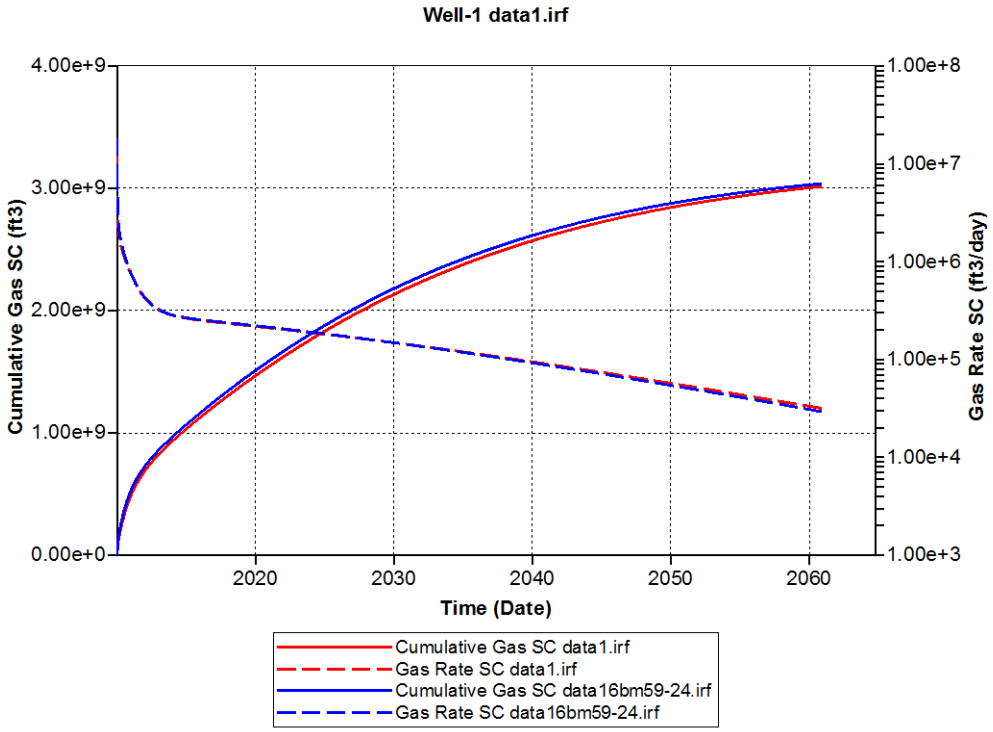

Figure 7-13: Matched Performance for Data 1

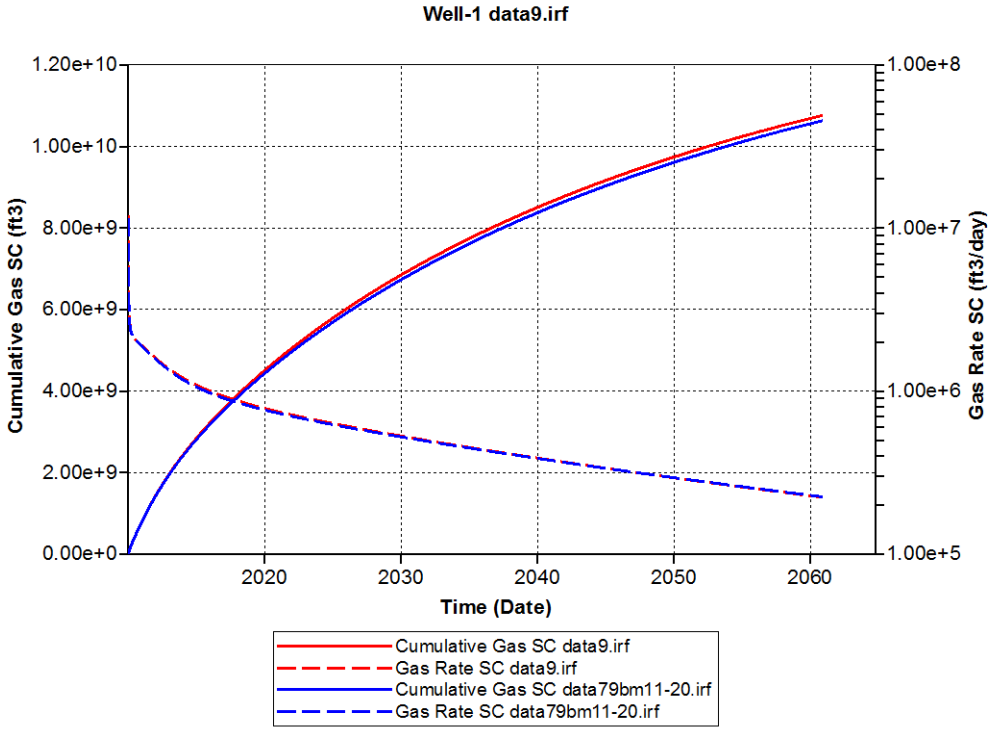

Figure 7-14: Matched Performance for Data 9

Figure 7-13 and Figure 7-14 show examples of good match from ANN. Gas rates are plotted on logarithmic scale for ease of visualization for matching purpose. In Figure 7-13, ANN under predicts the crushed zone design characteristics e.g. too small crushed zone and/or crushed zone permeability. On the other hand, ANN over predicts the crushed zone design characteristics in Figure 7-14. The cumulative production errors are recorded at the end of 50 years for both cases. The errors for both cases are -0.7% and 1.21%, respectively. The plus and minus signs indicates over-prediction and under-prediction, respectively.

Occasionally, gas rates in the early time can be very challenging in matching. As shown in Figure 7-15, large gas rate error is observed during the first 5 years. In this case, the gas rate error is approximately 14.31%. After that, the system is approaching stabilized state where insignificant change in gas rate is observed. The cumulative production error is recorded to be -4.92% at the end of 50 years.

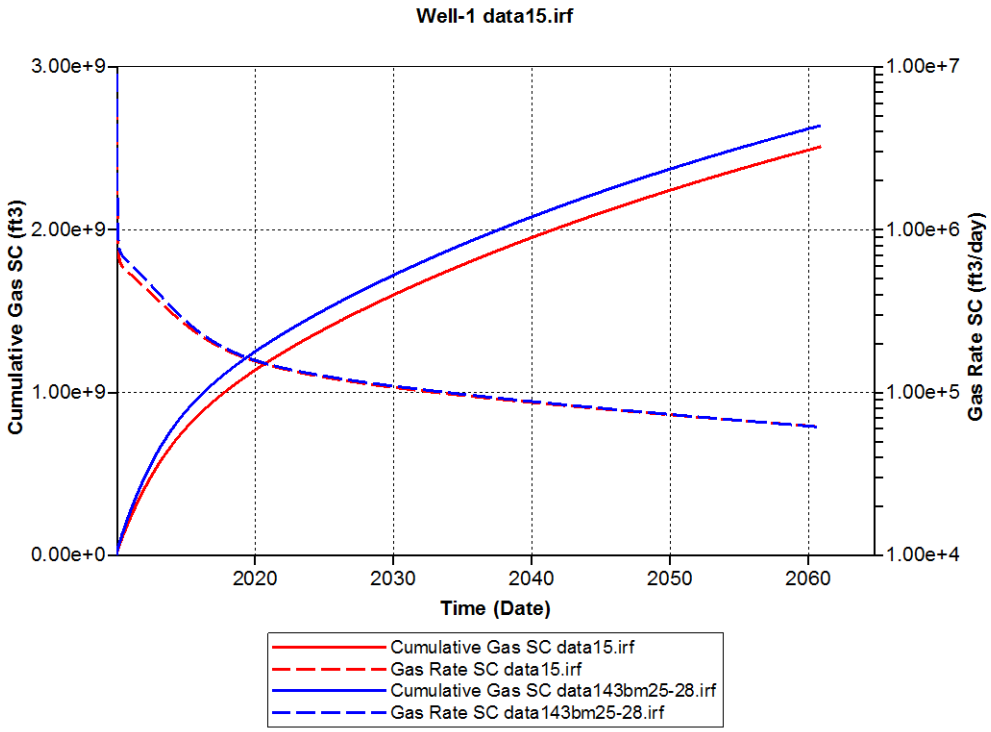

Figure 7-15: Matched Performance for Data 15

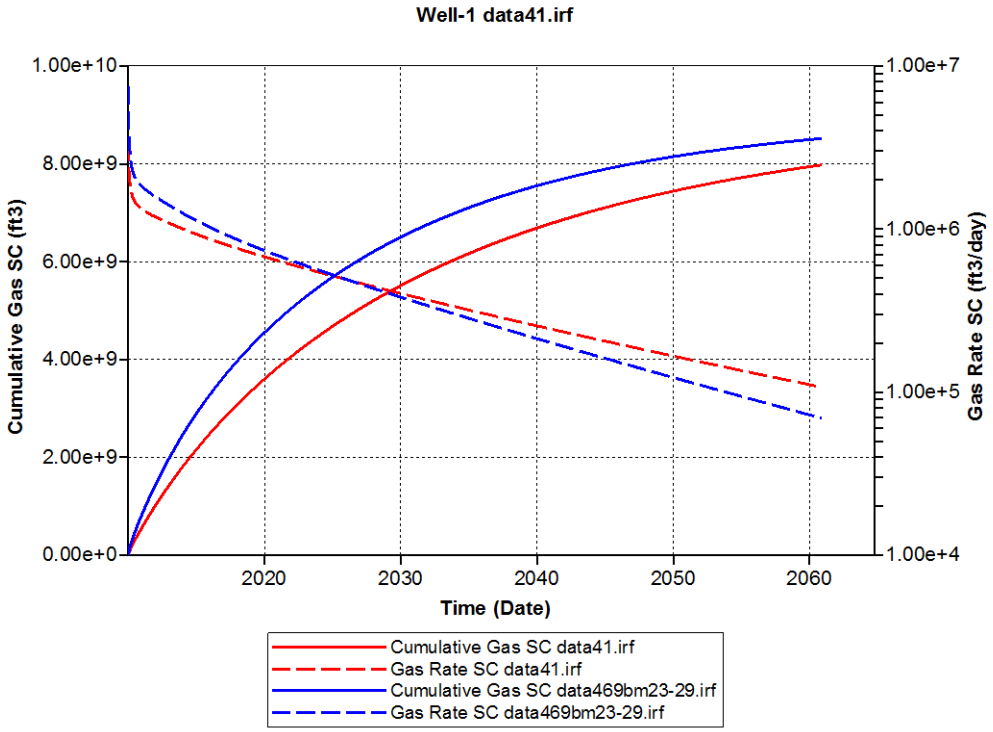

Figure 7-16: Matched Performance for Data 41

Similar to the production profile in Figure 7-15, Figure 7-16 shows a similar system behavior but with under prediction at the beginning and over prediction at late time. After the gas rates crossover, cumulative production using network's predicted crushed zone parameters starts to catch up with the actual cumulative production. The cumulative production curve shows an error of 6.34% at the end of simulation.

Figure 7-17 shows an example of a closer match in gas rate for the first 8 years of production. The network slightly over-predicts gas rates after year 2018 until the end of production. As a result of this small over-prediction for long period, the error in cumulative production slightly increases over time as the production continues. The cumulative production error at the end of the simulation is 4.92%.

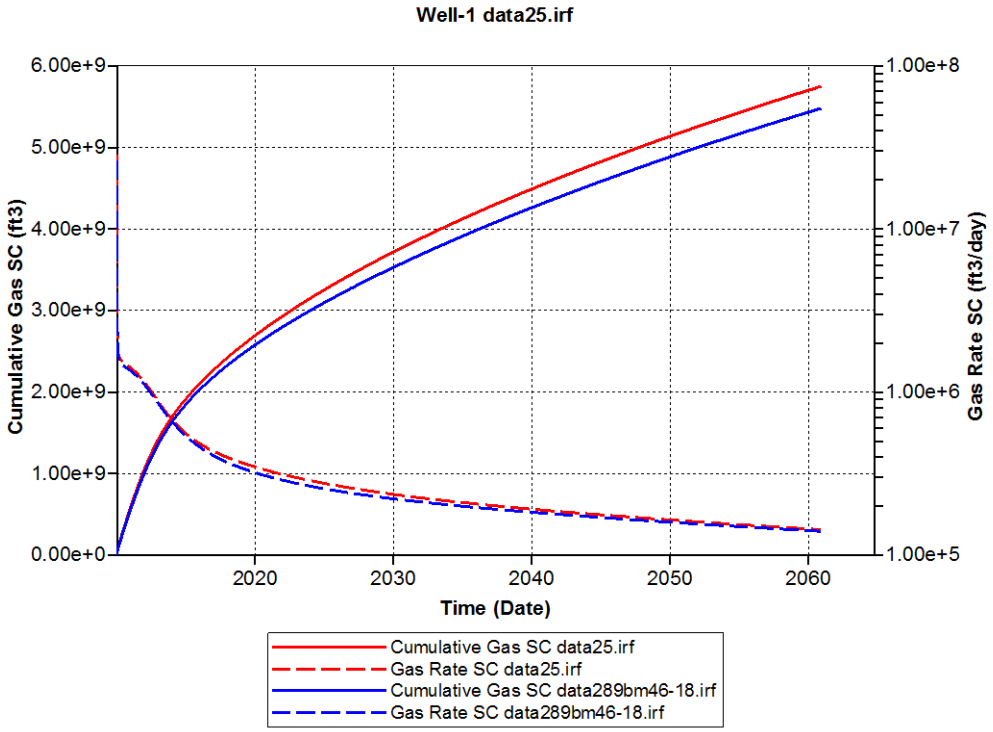

Figure 7-17: Matched Performance for Data 25

The overall errors in cumulative production for the 124 testing sets are grouped based on their errors. It can be seen from Figure 7-18 that approximately 78.22% of the testing sets are within the desired 15% error, and the total of 117 testing sets (94.35%) has cumulative production error less than 30%. It is important to note that the network may predict illogical parameters, and therefore, should be removed from consideration in decision making.

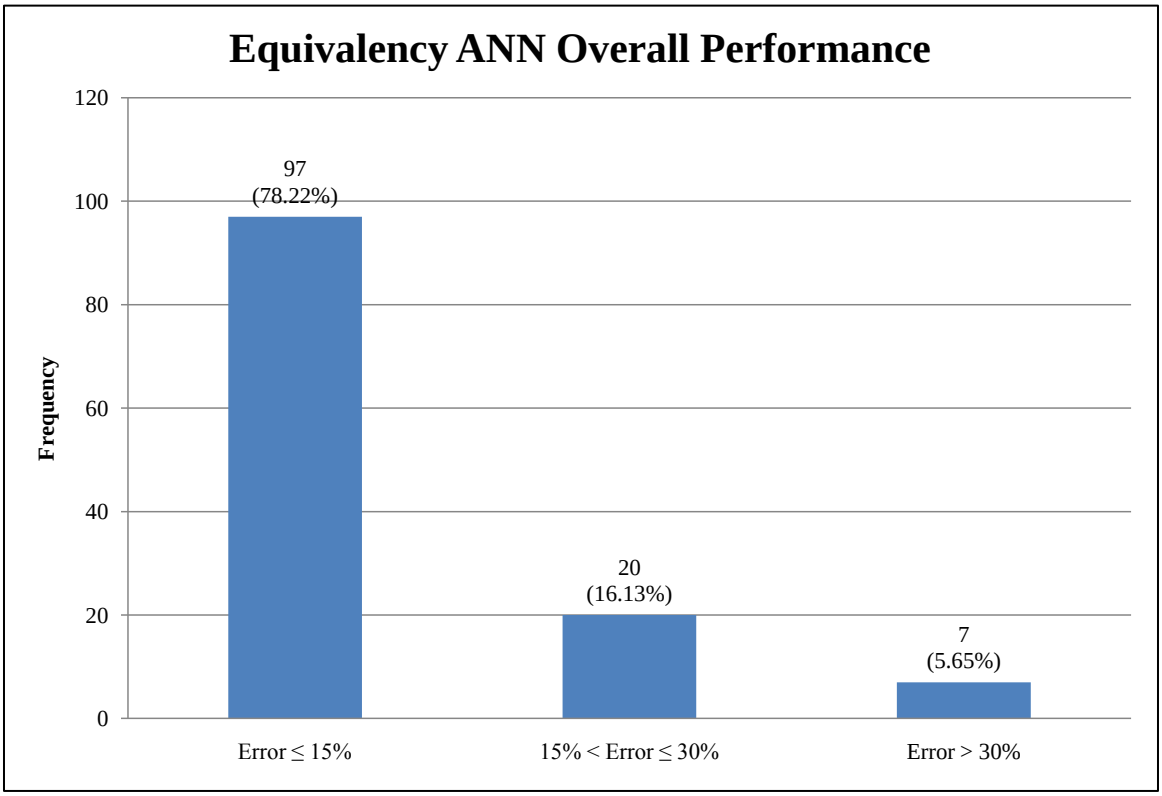

Figure 7-18: Overall Performance of the Equivalency ANN

7.2.3 Bottom-hole Pressure from Equivalent Systems

Further investigation is done for pressure responses from selected equivalent systems. The production profiles of the selected equivalent systems are shown in Figure 7-19 through Figure 7-23. The matched performances based on ANN predicted crushed zone parameters are plotted in red, and the actual matched performances from numerical model are plotted in blue. The cumulative production errors for the selected equivalent systems are -0.1%, 10.68%, 19.19%, 31.7%, and 82.98%, respectively.

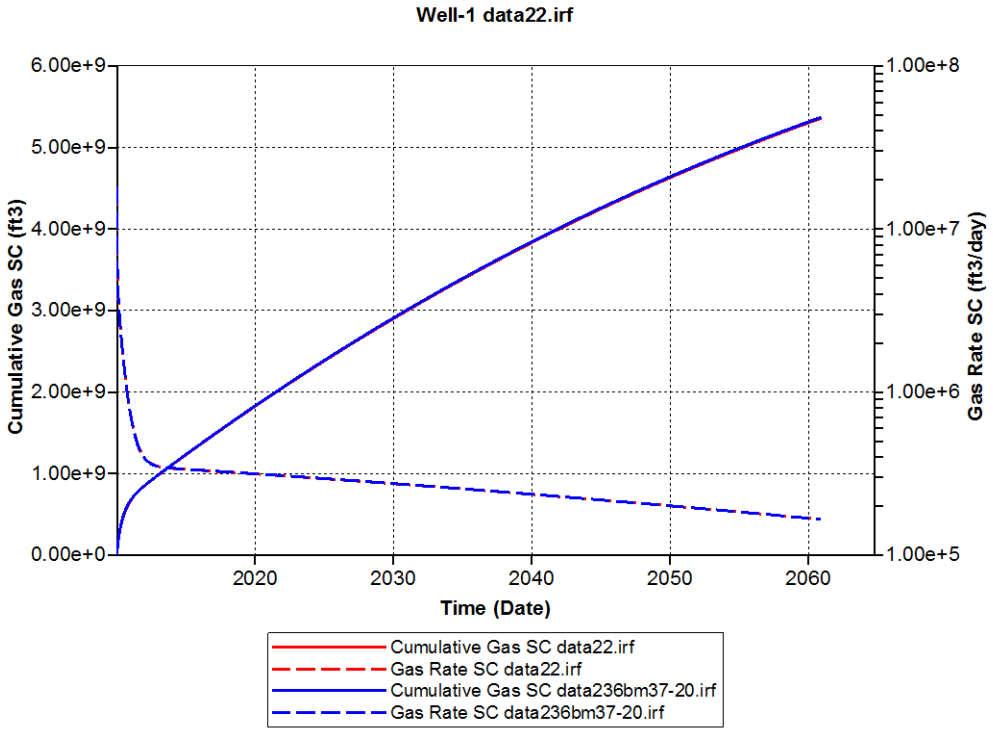

Figure 7-19: Matched Performance for Data 22

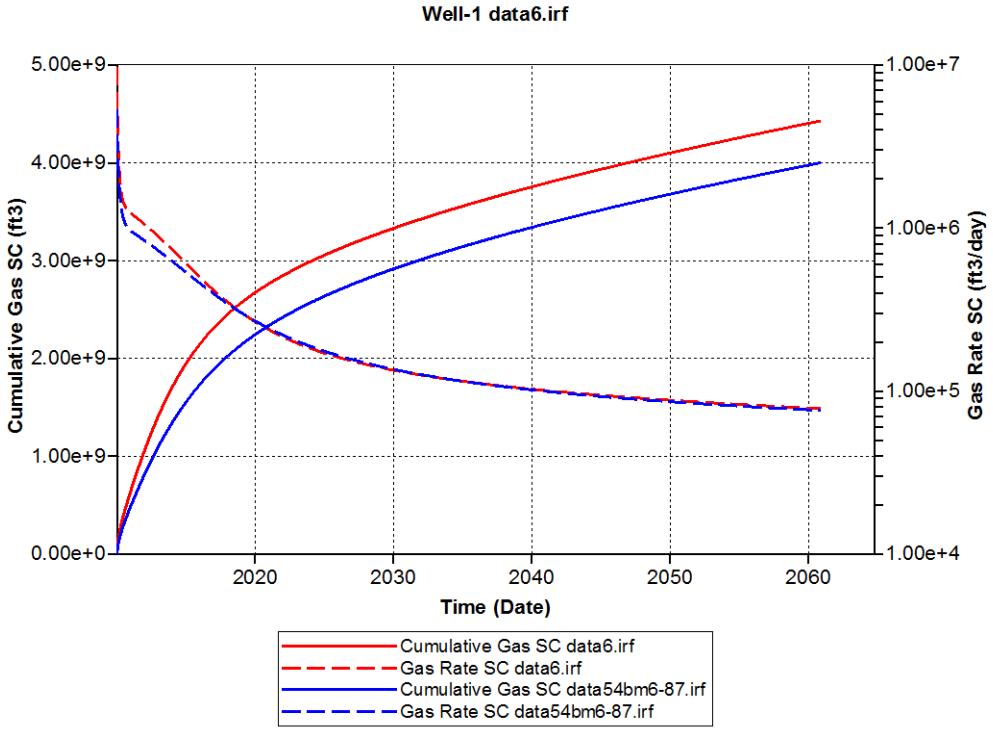

Figure 7-20: Matched Performance for Data 6

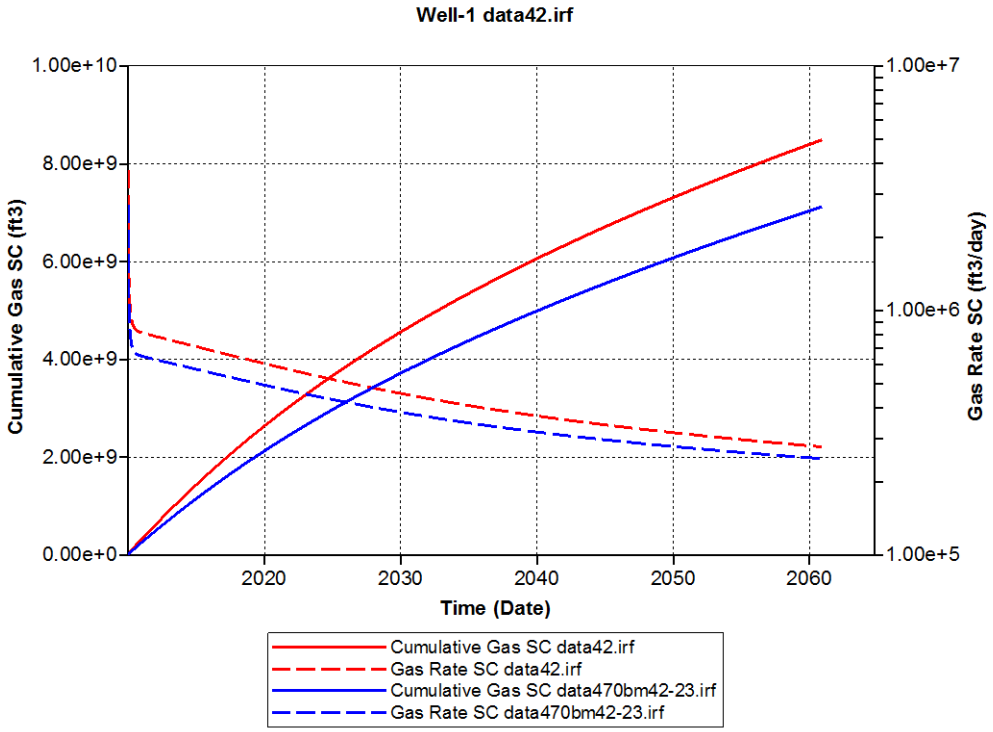

Figure 7-21: Matched Performance for Data 42

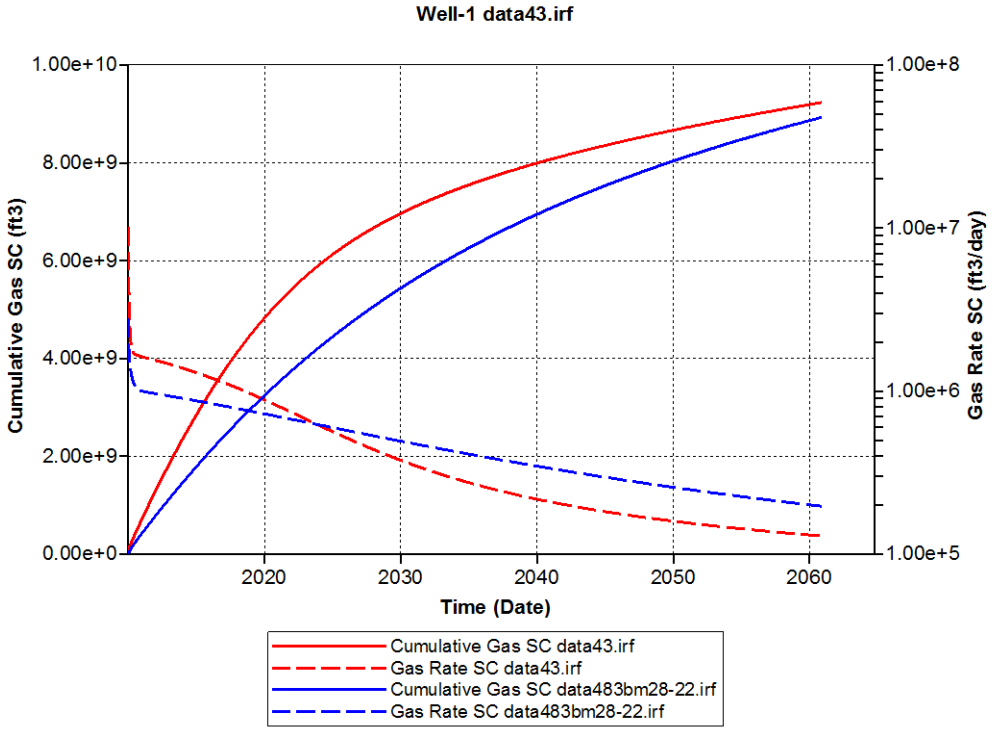

Figure 7-22: Matched Performance for Data 43

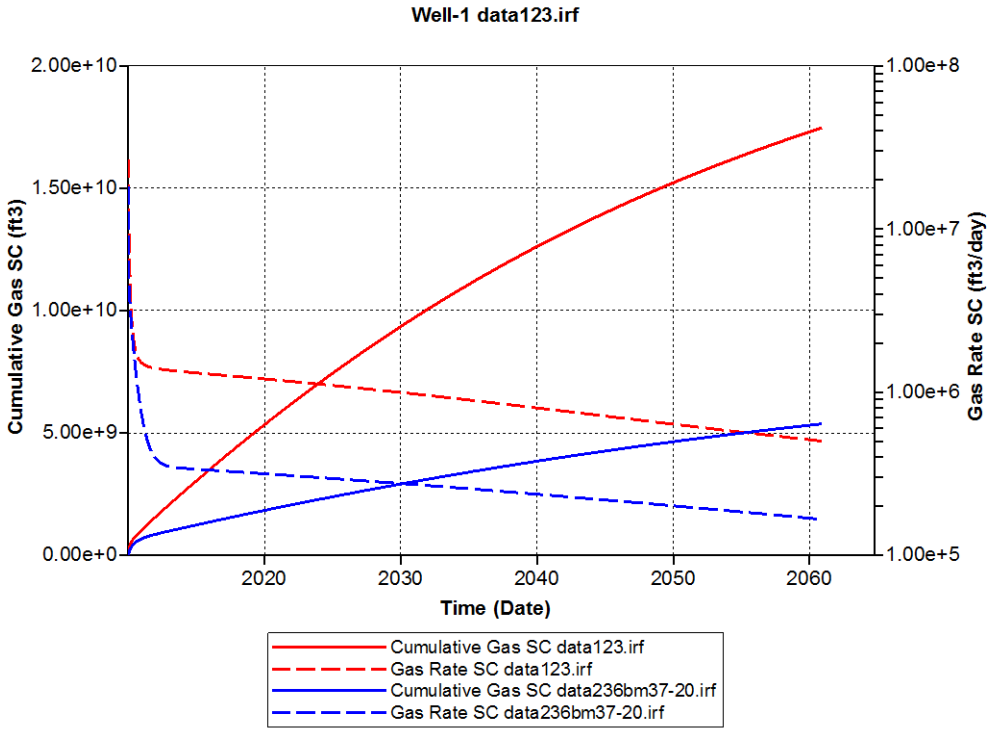

Figure 7-23: Matched Performance for Data 123

In this test, data sets in Figure 7-19, Figure 7-21, and Figure 7-23 and their equivalent transverse hydraulic fracture representations are simulated under constant production rate of 500,000 scf/day. As for data in Figure 7-20 and Figure 7-22 and their equivalent transverse fracture hydraulic fracture representations, a production rate of 100,000 scf/day is used instead. The well bottom-hole pressure response from the reservoir is observed and compared. Figure 7-24 to Figure 7-28 show the bottom-hole pressure responses for the selected cases. The red line and blue line show bottom-hole pressure from crushed zone hydraulic fracture representation and transverse hydraulic fracture representation, respectively. Figure 7-24 shows the best matched case where well bottom-hole pressure for both transverse hydraulic fracture representation and crushed zone representation are in good agreement. The bottom-hole pressure difference is approximately 3.22%. This error is the result of -0.1% cumulative production error. It can be seen

that bottom-hole pressure decreases at a faster rate during the first 10 years of production as a result of high production rate during that period.

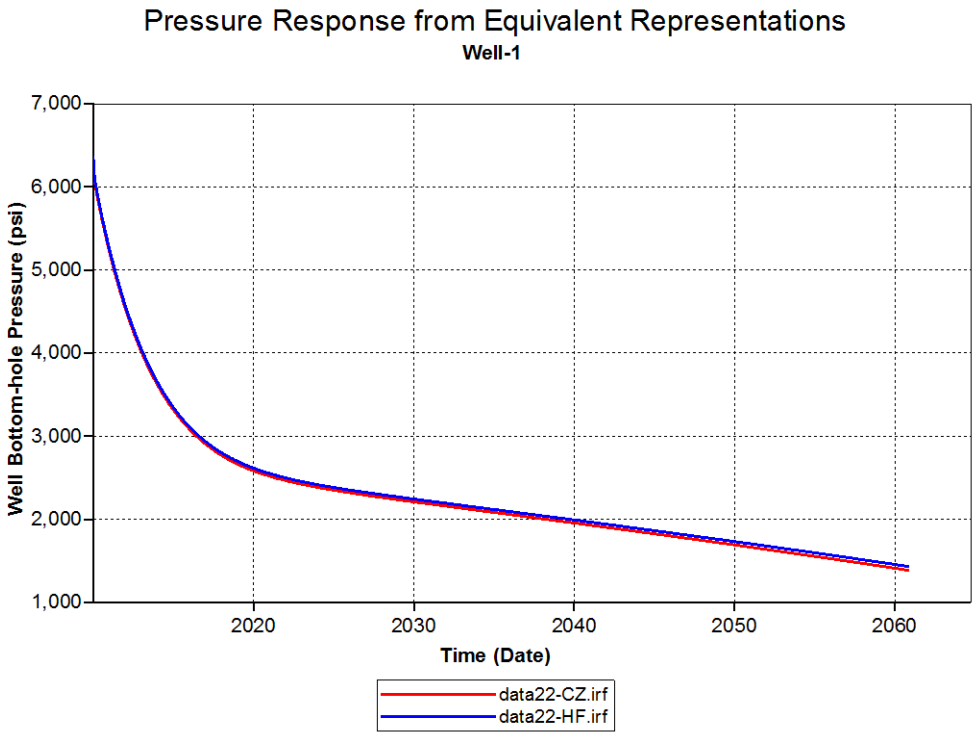

Figure 7-24: Bottom-hole Pressure Comparison for Data 22

For the case shown in Figure 7-25, bottom-hole pressures for both representations are parallel. This constant difference in pressure is a result of difference in production rates during the first 10 years. After that, production rates become almost equal, therefore, the same amount of pressure drop is observed. On the other hand, Figure 7-26 demonstrates an increasing bottom-hole pressure difference as production continues. This corresponds to the growing cumulative production error shown in Figure 7-21.

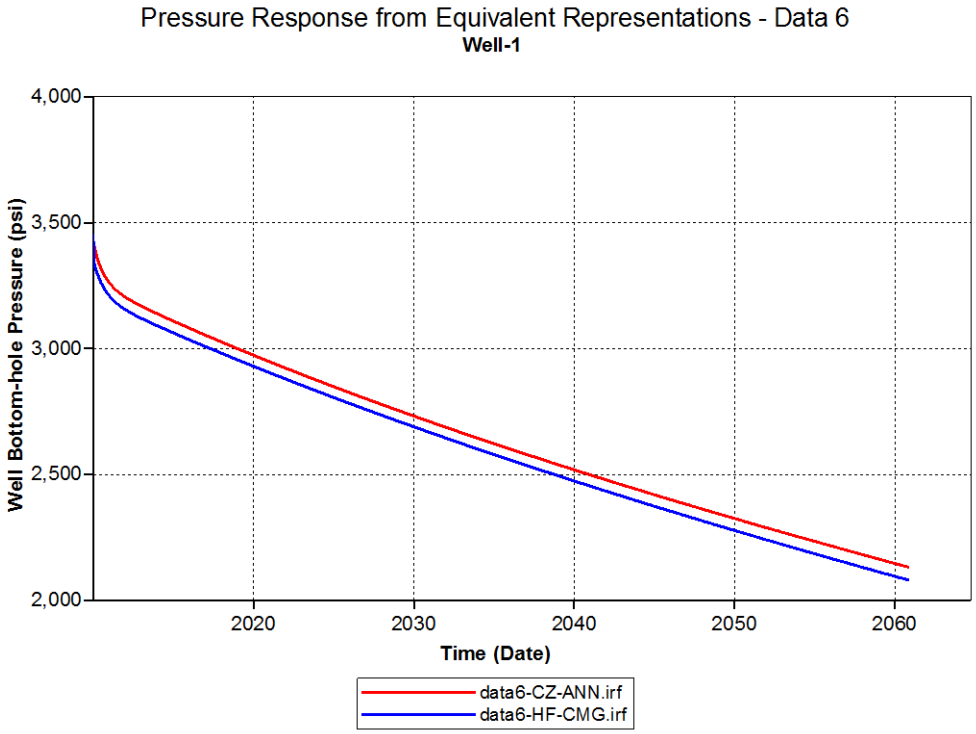

Figure 7-25: Bottom-hole Pressure Comparison for Data 6

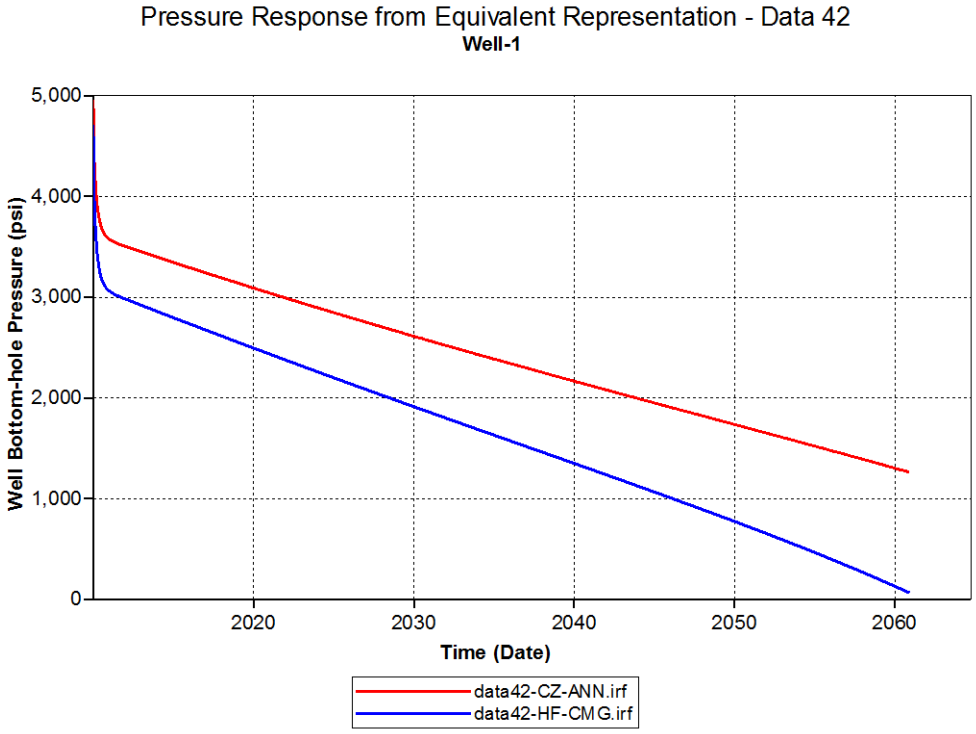

Figure 7-26: Bottom-hole Pressure Comparison for Data 42

As can be seen in Figure 7-22, there is a catch up in cumulative production. Cumulative production error increases until 2025 and decreases since then until the end of the simulation. In Figure 7-27, the bottom-hole pressure for the transverse hydraulic fracture representation is lower until year 2025. Since the production for the crushed zone representation after that year is higher, its bottom-hole pressure decreases at a faster rate than that of transverse hydraulic fracture representation, and it drops to 2559.99 psi which is 2.2% lower than that of transverse hydraulic fracture representation.

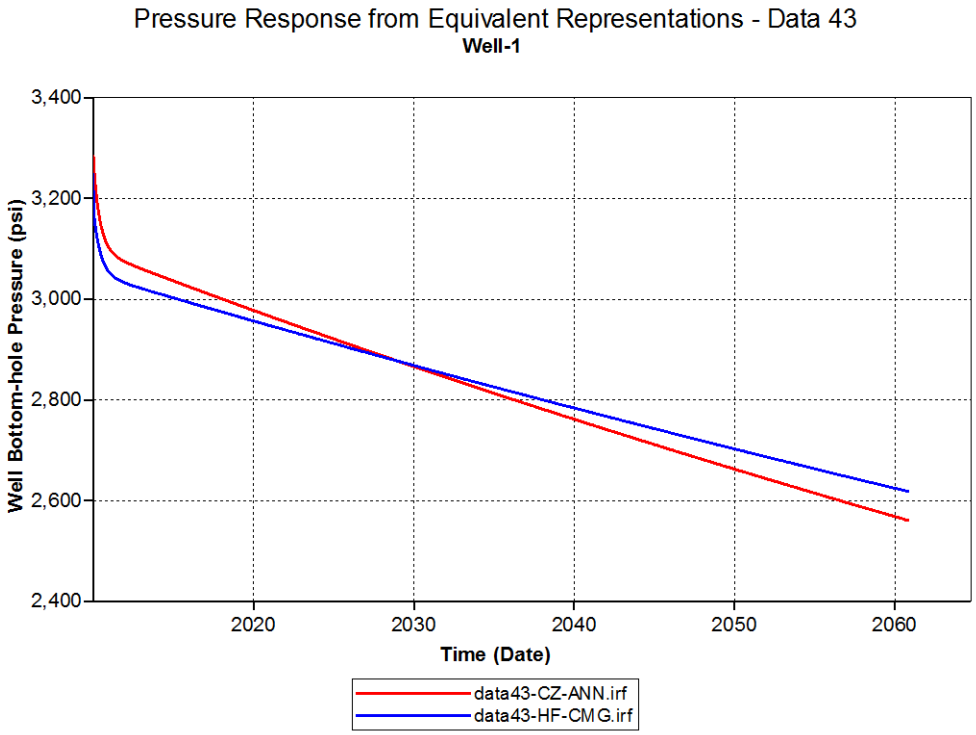

Figure 7-27: Bottom-hole Pressure Comparison for Data 43

Figure 7-28 shows bottom-hole pressure comparison for the case of the equivalent crushed zone representation with 82.98% cumulative production error. The bottom-hole pressure difference is 129.77% as we can expect from the error in cumulative production.

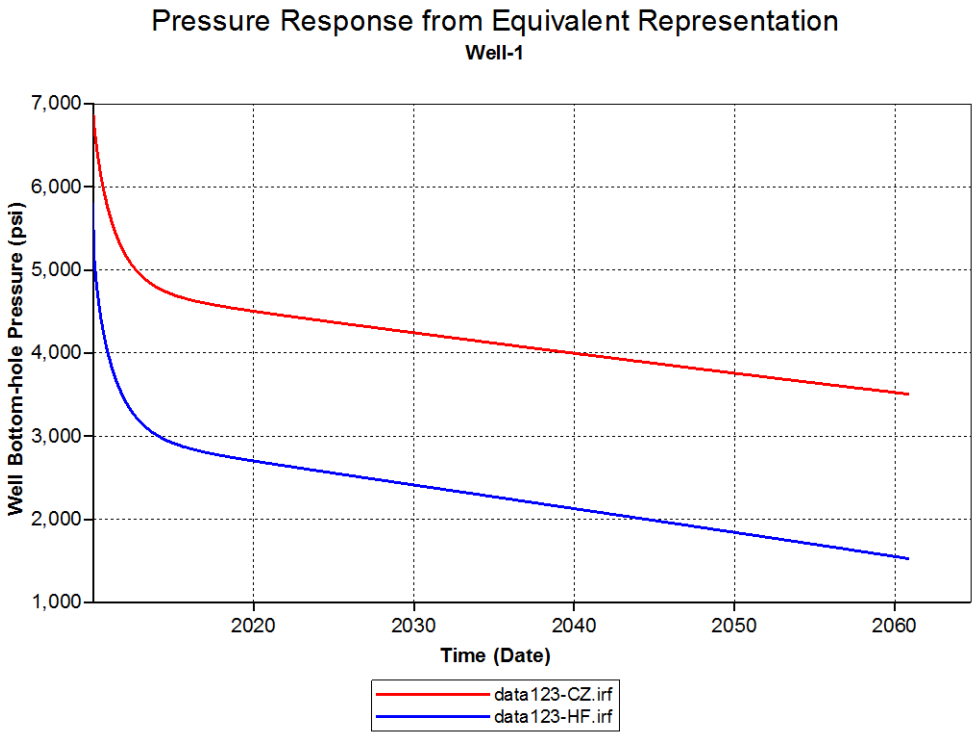

Figure 7-28: Bottom-hole Pressure Comparison for Data 123

The pressure response from equivalent systems indicates that if the production profiles are in good agreement, a good agreement in bottom-hole pressure comparison between the two hydraulic fracture representations can be expected.

Chapter 8

Summary and Conclusions

Horizontal wells coupled with hydraulic fracturing are important in production of natural gas from shale gas reservoirs. As reservoir modeling and simulation can be time-consuming, artificial intelligence technology is enjoying an increased popularity in oil and gas industry due to its widely accepted ability to compute highly non-linear relationships. Two ANNs are developed in this work. The first ANN called "Performance Prediction ANN" is developed to overcome the challenge in field optimization. It can instantly predict production profile from hydraulically fractured horizontal wells in shale gas reservoirs. The second ANN called "Equivalency ANN" is developed to establish equivalent hydraulic fracture representations between transverse fracture model and crushed zone model.

In the development of this work, MATLAB is employed in various steps. Uniformly distributed data sets are generated over the specified ranges of parameters. A MATLAB code is used to generate data sets for the numerical model using transverse hydraulic fracture representation along with a batch file. Numerical model is utilized to generate production profile for each data set. Curve fitting and gas rate selection techniques are employed to characterize the production profile. It is found that curve fitting may not be able to capture a significant drop in gas rates at the beginning of production even though the regression coefficient is close to 1. Therefore, gas rate selection technique is used in this work. Nineteen gas rates at various times are extracted from simulation results and used as outputs in the training of the Performance Prediction ANN. The overall errors in gas rates from the ANN are analyzed to determine the quality of the network.

Similar process is done for the development of the Equivalency ANN. A MATLAB code is written to randomly generate crushed zone parameters and automatically generate data sets for numerical model using crushed zone hydraulic fracture representation. Numerical model is used to simulate the production profile for the data sets in attempt to match the production profile of a hydraulically fractured horizontal well represented with transverse fracture model. The equivalent crushed zone parameters are recorded for the cases with cumulative production error less than 10%. The crushed zone parameters are used in the training of the network. The error in cumulative production between actual matched data set and data set generated from ANN's predicted crushed zone parameters are used as the sole criterion in determining the performance of the network.

The proposed Performance Prediction Network is a four-hidden layer cascade feed-forward backpropagation network with 20 neurons in each hidden layer. Hyperbolic tangent sigmoid transfer function ('*tansig*') is used in all the hidden layers. This network takes 21 inputs and returns 26 outputs, including functional links. The developed network can instantly predict gas rates over a 50-year production period from a hydraulically fractured horizontal well using transverse hydraulic fracture representation (within 10% error from the values obtained from numerical reservoir simulator). The Equivalency ANN is a six-hidden layer feed-forward backpropagation network with 40, 35, 30, 25, 20, 15 neurons in each hidden layer. '*tansig*' transfer functions are used in the hidden layers, except the first and last hidden layer where '*logsig*' transfer functions are used instead. The network takes 23 inputs and returns 13 outputs. The proposed ANN can establish equivalent representations between transverse fracture model and crushed zone model with cumulative production error less than 15%. Finally, graphical user interface is build to assist users and help in visualization of the production profile and the two hydraulic fracture representations.

The following observations and conclusions are drawn from the study:

- Curve fitting may not be the best technique to characterize production profile as the significant decrease in gas rates during the first 10 years of production may not be accurately captured even though the regression coefficient is close to 1. When such a problem occurs, use of gas rates at various times is recommended.
- Adding functional links is found to be of paramount importance in training the network as they help the network establish relationships between inputs and outputs. Eigenvalues of different sets of parameters can also be used as functional links.
- Large error in initial gas rate can be expected from the Performance Prediction ANN, and this large error can affect the overall performance of the network (average gas rate error).
- Among the four crushed zone parameters, crushed zone permeability is the most influential parameters affecting the gas production rates. The parameters can be ranked based on their influences on gas production rates as follows:

$$k_{f,cz} > a_{minor} > a_{major} > nf_{sp,cz}$$

- Non-uniqueness in equivalent representations can be expected and further study is required to determine the most accurate representation. Eliminating major axis length of the crushed zone (a_{major}) by fixing it to the length of the horizontal well is recommended.
- The developed ANNs can be effectively used as tools in reservoir modeling and simulation. Significant amount of time can be saved, especially in establishing equivalent representations.

References

Artun, E.F.: "Optimized Design of Cyclic Pressure Pulsing in Naturally Fractured Reservoirs Using Neural-Network Based Proxy Models." Ph.D. Dissertation, The Pennsylvania State University, 2008.

Beale, M.H., Hagan, M.T., and Demuth, H.B.: *Neural Network Toolbox™ 7: User's Guide*. MathWorks, Inc. 2010.

Dranchuk, P.M. and Abou-Kassem, J.H.: "Calculation of Z Factors for Natural Gases Using Equations of State," *J. Cdn. Pet. Tech*. March 1975.

Ertekin, T., Abou-Kassem, J.H., and King, G.R.: *Basic Applied Reservoir Simulation*, SPE Textbook Series Volume 7, Henry L. Doherty Memorial Fund of AIME, Richardson, TX, ISBN 1-55563-089-8, 2001.

Fausett, L.: *Fundamentals of Neural Networks: Architectures, Algorithms, and Applications*. Prentice-Hall, Englewood Cliffs, NJ, 1994.

Hagan, M. T., Demuth, H. B., and Beale, M.: *Neural Network Design*. PWS Publishing, Boston, MA, 1996.

Hart Energy Exploration and Production.: "DFN modeling unlocks the potential of shale gas reservoirs," http://www.epmag.com/Magazine/2010/2/item52453.php, 2010.

Ingrain Digital Rock Physics Lab. http://www.ingrainrocks.com, 2011.

Kulga, I. B.: "Development of an Artificial Neural Network for Hydraulically Fractured Horizontal Wells in Tight Gas Sands." Master's Thesis, The Pennsylvania State University, 2010.

Marren, A. Harston, C. and Pap, R.: *Handbook of Neural Computing Applications*. Academic Press, Inc., San Diego, CA, ISBN 0-12-471260-6, 1990.

National Energy Board.: "A Primer for Understanding Canadian Shale Gas – Energy Briefing Note." http://www.neb-one.gc.ca, 2011.

National Petroleum Council.: "Topic paper #29 Unconventional Gas." http://www.npc.org/Study_Topic_Papers/29-TTG-Unconventional-Gas.pdf, July 2007.

Neuroshell. *Neuroshell 2 Tutorial*. Ward Systems, Inc., Federick, Maryland. 1998.

Parada, C.H.: "An Artificial Neural Network Based Tool-Box for Screening and Designing Improved Oil Recovery Methods." Ph.D. Dissertation, The Pennsylvania State University, 2008.

Ramgulam et al.: "Utilization of Artificial Neural Networks in the Optimization of History Matching." SPE 107468. Buenos Aires, Argentina. 15-18 April 2007.

Remner, D.J., Ertekin, T., Sung, W. and King, G. R.: "A Parametric Study of the Effects of Coal Seam Properties on Gas Drainage Efficiency", SPE Reservoir Engineering, November 1986, p.633-646.

Sumi, L.: "Shale Gas: Focus on the Marcellus Shale." Oil & Gas Accountability Project/Earthworks, 2008.

Thararoop et al.: "Integration of Seismic Attributes and Production Data for Infill Drilling Strategies – A Virtual Intelligence Approach." Journal of Petroleum Science and Engineering, 2008.

Thararoop, P.: "Development of a Multi-Mechanistic, Dual-Porosity, Dual-Permeability Numerical Flow Model for Coalbed Methane Reservoirs Accounting for Coal Shrinkage and Swelling Effects." Ph.D. Dissertation, The Pennsylvania State University, 2010.

U.S. Energy Information Administration.: "Annual Energy Outlook 2011 with Projections to 2035." U.S. Department of Energy. Washington, DC. 2011.

U.S. Energy Information Administration.: "Drilling Sideways – A Review of Horizontal Well Technology and Its Domestic Application." U.S. Department of Energy. Washington, DC. 1993.

U.S. Environmental Protection Agency.: "Hydraulic Fracturing Research Study." June 2010.

Warpinski et al.: "Stimulating Unconventional Reservoirs: Maximizing Network Growth while Optimizing Fracture Conductivity." SPE 114173. Colorado, U.S.A. 10-12 February 2008.

Appendix A

Graphical User Interface

A Graphical User Interface (GUI) is developed to provide an ease of use of the developed ANNs. This GUI is developed based on MATLAB R2010b (MATLAB 7.11.0).

User Manual

A step-by-step implementation of GUI is discussed in detail in this paragraph.

1. Start MATLAB by double clicking the MATLAB executable file.
2. Browse and change the Current Directory to the location where the ANN toolbox is stored.
3. To start the ANN Toolbox, open the file names Run_ANN_ToolBox.m and run it by pressing F5 or the run button. An alternative way to start the ANN toolbox is to simply type Run_ANN_ToolBox on MATLAB command window. The main GUI window as shown in Figure A-1 will pop up.

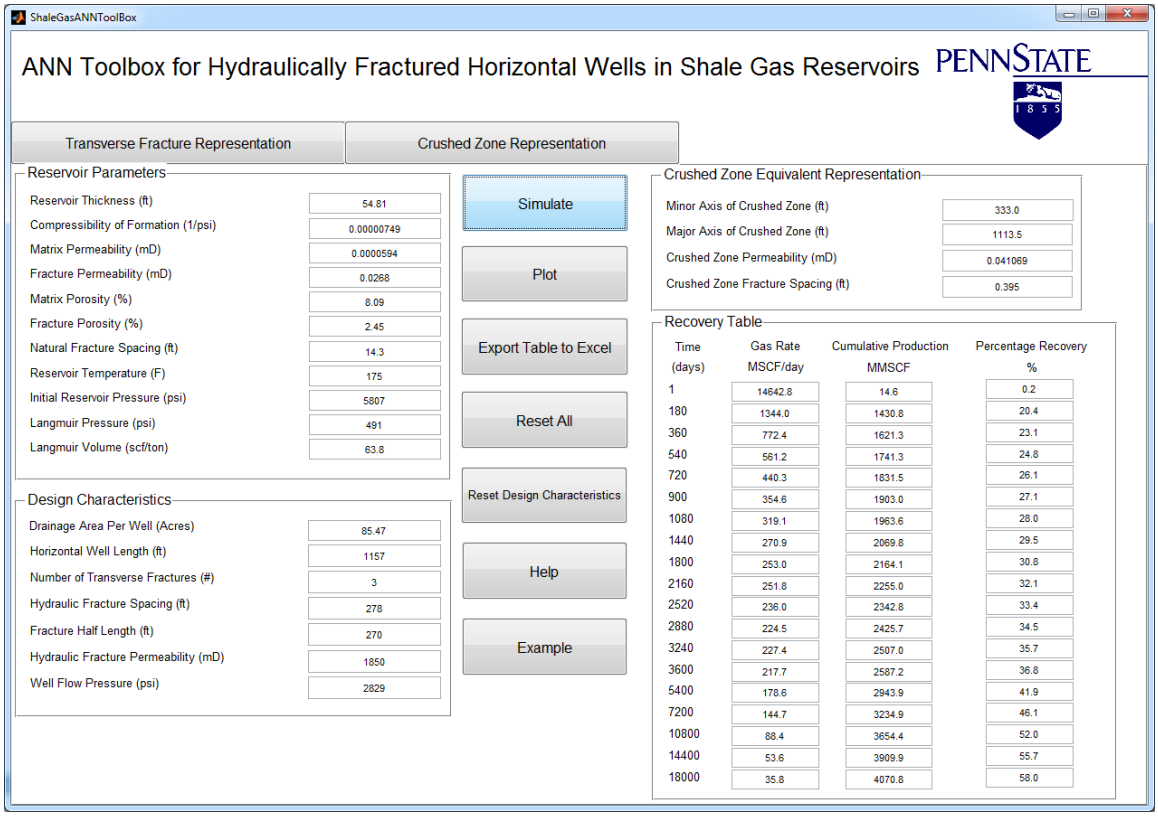

Figure A-1: Main GUI Window

4. Insert reservoir parameters such as reservoir thickness and design characteristics into the provided space or click on Example button to see an example of inputs. A predetermined set of input is filled in the input section.
5. Once all the required parameters are filled, click on the Simulate button. The gas production rate, cumulative production, and percentage recovery are shown in the Recovery Table panel, and the parameters for equivalent crushed zone representation are shown in the Crushed Zone Equivalent Representation panel.
6. To extract the data to Excel, simply click on Extract To Excel button. An Excel spreadsheet will automatically open showing all the inputs and outputs for the simulated run.
7. To plot the gas production rates, cumulative production, and to see the graphical representation of the equivalent systems, click on Plot button. Another window will pop

up as shown in Figure A-2. Gas rate and cumulative production plots are shown in top left and right graphs, respectively. The bottom two figures show a model of transverse hydraulic fracturing planes (red stripes) and its equivalent crushed zone representation (red elliptical shaped area). In this example, three hydraulic fracturing stages are implemented.

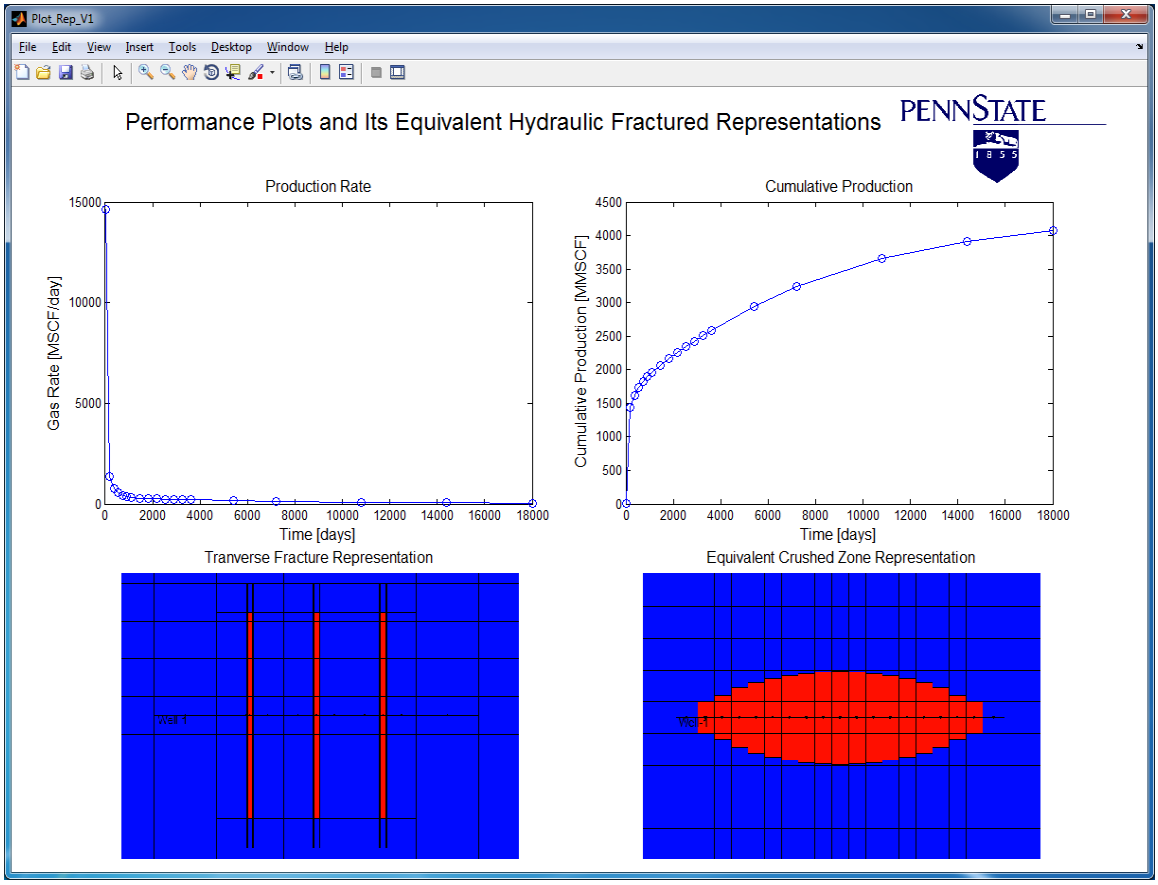

Figure A-2: GUI Plot and Graphical Representations Window

8. Click on Reset button to reset all the parameters. To keep the same reservoir parameters and optimize production, click on Reset Design Characteristics button to clear the design characteristics while keeping the same reservoir parameters.
9. Click on Help button for User Manual and more information about this GUI.

Appendix B

Procedure

MATLAB code is employed in various steps of the procedure. This appendix includes MATLAB codes for generating uniformly distributed data and for training the ANNs.

MATLAB code for Generating Uniformly Distributed Data

```
% ********* Data Input Generation for Numerical Model *********
clear
clc

%% Number of Cases for Numerical Model
n = 1200;

%% 1) edge_l = Edge Length of the reservoir
A = unifrnd(50,300,[1,n]);
A_feet = A*43560;           % Drainage area in square ft
edge_l = (A_feet).^0.5;     % Each side of the square reservoir, L (ft)

%% 2) h = Reservoir Thickness (ft)
h = unifrnd(50,300,[1,n]);

%% 3) depth = Depth (Grid Top) (ft)
depth = unifrnd(1000,15000,[1,n]);

%% 4) cf = Compressibility of Formation (psi-1)
Max = log10(0.000008);
Min = log10(0.000005);
cf = unifrnd (Min,Max,[1,n]);
cf = 10.^cf;

%% 5) km = Matrix Permeability (mD)
Max = log10(0.01);
Min = log10(0.0000001);
km = unifrnd(Min,Max,[1,n]);
km = 10.^km;

%% 6) kf = Fracture Permeability (mD)
Max = log10(1);
Min = log10(0.0001);
kf = unifrnd(Min,Max,[1,n]);
kf = 10.^kf;

%% Input check -- km < kf
```

```
for i = 1:length(km(1,:))
    while km(i) > kf(i)
        km(i) = unifrnd(log10(0.0000001),log10(0.01),1);
        kf(i) = unifrnd(log10(0.0001),log10(1),1);
        km(i) = 10^km(i);
        kf(i) = 10^kf(i);
    end
end

%% 7) phi_m = Matrix Porosity (fraction)
phi_m = unifrnd(0.02,0.16,[1,n]);

%% 8) phi_f = Fracture Porosity (fraction)
phi_f = unifrnd(0.001,0.03,[1,n]);

%% Input check -- phi_m > phi_f
for i = 1:length(km(1,:))
    while phi_m(i) < phi_f(i)
        phi_m(i) = unifrnd(0.02,0.16,1);
        phi_f(i) = unifrnd(0.001,0.03,1);
    end
end

%% 9) nf_spacing = Natural Fracture Spacing (ft)
nf_spacing = unifrnd(1,40,[1,n]);

%% 10) Ti = Initial Temperature (F)
Ti = unifrnd(130,300,[1,n]);

%% 11) Pi = Initial Pressure (psi)
Pi = unifrnd(3000,8000,[1,n]);

%% 12) PL = Langmuir Pressure (psi)
PL1 = unifrnd(200,800,[1,n]);
PL = 1 ./ PL1;           % Convert to the unit of [psi^-1]

%% 13) VL = Langmuir Volume or Gas Content (SCF/ton)
VL1 = unifrnd(50,200,[1,n]);
VL = VL1*(5.97516662*10^(-4));   % Convert to the unit of [gmol/lb]

%% 14) HW_l = Length of Horizontal Well
% The length of a horizontal well is 60% of the edge length
HW_l = edge_l * 0.6;

%% 15) DI = First and Last Two Grid Length on X Direction
DI = (edge_l - HW_l)/4;

%% 16) Wx = Hydraulic Fracture Spacing
% Hydraulic Fracture Spacing = Width of Well Block = Wx
% num_xf = number of blocks for maximum hydraulic fracture length
Wx = unifrnd(100,300,[1,n]);
```

```
%% 17) nfrac = number of hydraulic fracture
nfrac = ( HW_l./Wx ) - 2;
nfrac = ceil(nfrac);

%% 18) HW_l_rem = width of the FIRST and LAST block of the well
HW_l_rem = HW_l - (nfrac.*Wx);
HW_l_rem = HW_l_rem/2;

%% 19) frac_l = Length of Hydraulic Fracture
% Note: frac_l is not always equal to edge_l/4
frac_l = unifrnd(100,3615/4,[1,n]);
for i = 1:length(km(1,:))
%     frac_l(i) = unifrnd(100,(edge_l(i)*0.25),1);
    while frac_l(i) > edge_l(i)*0.248
        frac_l(i) = unifrnd(100,(edge_l(i)*0.25),1);
    end
end

%% 20) Wy = width of each block for hydraulic fracture
% Always have 7 blocks for maximum hydraulic fracture (1 block for
well)
num_xf = ones(1,n);
num_xf = num_xf*7;
Wy = (edge_l/2) ./ num_xf;

%% Block Size Check
% Due to round off in number of blocks, control fracture half length to
be less than L/4
for i = 1:length(frac_l(1,:))
    if (frac_l(i)*2) > Wy(i)*num_xf(i)
        frac_l(i) = (Wy(i)*num_xf(i))/2;
    end
end

%% 21) Number of Grids for Hydraulic Fracture
fracGrid = floor( (frac_l-(Wy/2) )./Wy );        % fracGrid (m) =
number of blocks for HF, excluding well block and last block

%% 22) Number of Grids on X Direction
xGrid = nfrac + 6;

%% 23) Number of Grids on Y Direction
yGrid = num_xf + 4;

%% 24) First and Last Two Grid Length on Y Direction
DJ = edge_l/8;

%% 25) frac_k = Permeability of Fracture
Min = log10(10);
Max = log10(1000000);
frac_k = unifrnd(Min,Max,[1,n]);
frac_k = 10.^frac_k;
```

```
Cd = ones(1,n);
for i = 1:length(Cd(1,:))
    Cd(i) = (0.05*frac_k(i))/(frac_l(i)*km(i));
end

%% 27) Psf = Pressure Specified
Psf = unifrnd(0 , 0.5 , [1,n]);
Psf = Psf .* Pi + 14.7;

%% data = Compilation of All Parameters
indata = [edge_l; h; depth; cf; km; kf; phi_m; phi_f; nf_spacing; Ti;
Pi; PL; VL; HW_l; DI; Wx; nfrac; HW_l_rem; ...
    frac_l; Wy; fracGrid; xGrid; yGrid; DJ; frac_k; gamma; Psf; Cd];
input = [A; h; cf; km; kf; phi_m; phi_f; nf_spacing; Ti; Pi; PL1; VL1;
HW_l; nfrac; Wx; frac_l; frac_k; Psf];

%% Exporting Files
save input.txt input -ASCII
save indata.txt indata -ASCII
```

MATLAB Code for Training ANNs

```
clear
clc
format long
%% Import Cleaned Inputs
load ANNdata.txt
load time.txt

data = ANNdata;
gasrate = data(19:38,:);
r = length(data(1,:));

%% Eigenvalue Calculations
lambda3 = zeros(length(ANNdata(1,:)),1);
lambda6 = zeros(length(ANNdata(1,:)),1);
lambda7 = zeros(length(ANNdata(1,:)),1);
for i=1:length(ANNdata(1,:));
    A3 = [ANNdata(9,i) ANNdata(10,i); ANNdata(11,i) ANNdata(12,i)];

    A6 = [ANNdata(19,i) ANNdata(38,i); ANNdata(10,i)
log10(ANNdata(5,i))];
    A7 = [ANNdata(19,i) ANNdata(16,i); log10(ANNdata(17,i))
ANNdata(38,i)];
    lambda3(i) = max(eig(A3));
    lambda6(i) = max(eig(A6));
    lambda7(i) = max(eig(A7));
end
lambda3 = transpose(lambda3);
lambda6 = transpose(lambda6);
lambda7 = transpose(lambda7);
```

```
%% Combine Input, Output(coefficients), and Functional Links
% *** Take Log10 to Data: km, kf, frac_k ***
input = [data(1:3,1:r); log10(data(4:5,1:r)); data(6:16,1:r);
log10(data(17,1:r)); data(18,1:r); ...
    lambda1; data(6,1:r).*data(2,1:r);
data(6,1:r).*log10(data(4,1:r))];

% Output
output = [data(19:38,1:r); lambda6; lambda7; lambda3;
data(10,1:r)./data(18,1:r); ...
    0.05*log10(data(17,1:r))./log10(data(4,1:r))./data(16,1:r);
data(13,1:r).*data(16,1:r)];

%% Train Artificial Neural Network
P = input;
T = output;
% ***** Normalising the Data *****
% Pn stands for normalized input, and Tn stands for normalized output
[Pn,ps] = mapminmax(P,-1,1);   % Gives all values between -1 & 1
[Tn,ts] = mapminmax(T,-1,1);   % Gives all values between -1 & 1

[mi,ni] = size(Pn);
[mo,no] = size(Tn);

% ***** Defining some variables required in the network *****
N_in = mi;    % # of inputs in the network
N_out = mo;   % # of outputs in the network
Tot_in = ni;  % total no. of simulations

% ***** Seperating Training, Testing, & Validation data *****
% When random selection command is available through higher version,
use "dividerand"
% command
[Pn_train,Pn_val,Pn_test,trainInd,valInd,testInd] =
dividerand(Pn,0.9,0.05,0.05);
[Tn_train,Tn_val,Tn_test] = divideind(Tn,trainInd,valInd,testInd);

val.T = Tn_val;
val.P = Pn_val;
test.T = Tn_test;
test.P = Pn_test;

% ***** Initiating Network Parameters *****
NNeu1 = 20;
NNeu2 = 20;
NNeu3 = 20;
NNeu4 = 20;

% ***** TRANSFER FUNCTIONS *****
% tansig, logsig, purelin, newcf, newff, newpr, newrb, 'logsig',
'tansig'

% *** 4 Hidden Layers ***
```

```
net = newcf(Pn,Tn,[NNeu1,NNeu2,NNeu3,NNeu4,mo]...
    ,{'tansig','tansig','tansig','tansig',...
    'purelin'},'traincgf','learngdm','msereg');

% ***** TRAINING FUNCTIONS *****
% Conjugate gradient: traincgf, traincgp, traincgb, trainscg, traingdm
% Quasi-Newton: trainbfg, trainoss
% Levenberg-Marquardt: trainlm
% traingda traingdm traingdx trainr trainrp trains trainb trainbfgc
trainbr trainbuwb trainc traingd

% ***** LEARNING FUNCTIONS *****
% learncon learngdm learngd  learnh learnhd learnis learnk learnlv1
learnlv2 learnos learnp learnpn learnsom learnsomb learnwh

% ***** Setting Training Parameters for the Network *****
net.trainParam.goal = 0.0001;    % Accuracy within this range
net.trainParam.epochs = 15000;   % Number of iteration sets
net.trainParam.show = 1;
net.trainParam.max_fail = 100000;
net.trainParam.mem_reduc = 60;   % To reduce memory requirements

% ***** Starting Training the Network *****
[net,tr] = train(net,Pn_train,Tn_train,[],[],test,val);
plotperf(tr)

beep

% -------------------------------------------------
% ***** getting data from the trained network *****
% -------------------------------------------------
Tn_train_ann = sim(net,Pn_train);
Tn_test_ann = sim(net,Pn_test);

% ***** Denormalizing the Obtained Data Sets *****
% Output Reversal
T_train = mapminmax('reverse',Tn_train,ts);
T_test = mapminmax('reverse',Tn_test,ts);
T_train_ann = mapminmax('reverse',Tn_train_ann,ts);
T_test_ann = mapminmax('reverse',Tn_test_ann,ts);

% Input Reversal
P_train = mapminmax('reverse',Pn_train,ps);
P_val = mapminmax('reverse',Pn_val,ps);
P_test = mapminmax('reverse',Pn_test,ps);

%% Gas Rate and Cumulative Production Error Errors
% *** Gas Rate Error at Various Times ***
error_q1 = abs((T_test(1,:) - T_test_ann(1,:))./T_test(1,:))*100;
error_mean_q1 = mean(error_q1);
error_q2 = abs((T_test(2,:) - T_test_ann(2,:))./T_test(2,:))*100;
error_mean_q2 = mean(error_q2);
error_q3 = abs((T_test(3,:) - T_test_ann(3,:))./T_test(3,:))*100;
```

```
error_mean_q3 = mean(error_q3);
error_q4 = abs((T_test(4,:) - T_test_ann(4,:))./T_test(4,:))*100;
error_mean_q4 = mean(error_q4);
error_q5 = abs((T_test(5,:) - T_test_ann(5,:))./T_test(5,:))*100;
error_mean_q5 = mean(error_q5);
error_q6 = abs((T_test(6,:) - T_test_ann(6,:))./T_test(6,:))*100;
error_mean_q6 = mean(error_q6);
error_q7 = abs((T_test(7,:) - T_test_ann(7,:))./T_test(7,:))*100;
error_mean_q7 = mean(error_q7);
error_q8 = abs((T_test(8,:) - T_test_ann(8,:))./T_test(8,:))*100;
error_mean_q8 = mean(error_q8);
error_q9 = abs((T_test(9,:) - T_test_ann(9,:))./T_test(9,:))*100;
error_mean_q9 = mean(error_q9);
error_q10 = abs((T_test(10,:) - T_test_ann(10,:))./T_test(10,:))*100;
error_mean_q10 = mean(error_q10);
error_q11 = abs((T_test(11,:) - T_test_ann(11,:))./T_test(11,:))*100;
error_mean_q11 = mean(error_q11);
error_q12 = abs((T_test(12,:) - T_test_ann(12,:))./T_test(12,:))*100;
error_mean_q12 = mean(error_q12);
error_q13 = abs((T_test(13,:) - T_test_ann(13,:))./T_test(13,:))*100;
error_mean_q13 = mean(error_q13);
error_q14 = abs((T_test(14,:) - T_test_ann(14,:))./T_test(14,:))*100;
error_mean_q14 = mean(error_q14);
error_q15 = abs((T_test(15,:) - T_test_ann(15,:))./T_test(15,:))*100;
error_mean_q15 = mean(error_q15);
error_q16 = abs((T_test(16,:) - T_test_ann(16,:))./T_test(16,:))*100;
error_mean_q16 = mean(error_q16);
error_q17 = abs((T_test(17,:) - T_test_ann(17,:))./T_test(17,:))*100;
error_mean_q17 = mean(error_q17);
error_q18 = abs((T_test(18,:) - T_test_ann(18,:))./T_test(18,:))*100;
error_mean_q18 = mean(error_q18);
error_q19 = abs((T_test(19,:) - T_test_ann(19,:))./T_test(19,:))*100;
error_mean_q19 = mean(error_q19);

% *** Cumulative Production Error ***
Error_GPC = abs((T_test(20,:) - T_test_ann(20,:))./T_test(20,:))*100;
Error_mean_GPC = mean(Error_GPC);

%% Error Analysis
% *** Error for Each Test at Various Times ***
Error_each_test = [error_q1; error_q2; error_q3; error_q4; error_q5;
error_q6; error_q7; error_q8; error_q9; error_q10; error_q11;
error_q12; error_q13; error_q14; error_q15; error_q16; error_q17;
error_q18; error_q19];

% *** Overall Error for Each Test ***
Error_overall = mean(Error_each_test);
Error_mean_overall = mean(Error_overall);

%% Saves the ANN Toolbox
save ANNToolBox.mat
```

Appendix C

Parameter Distributions

This appendix includes the histograms of parameters for the first model which are generated by the method described in Figure 5-1. In training of ANNs, it is important to have well-distributed data, and it can be seen that the parameters have good distributions.

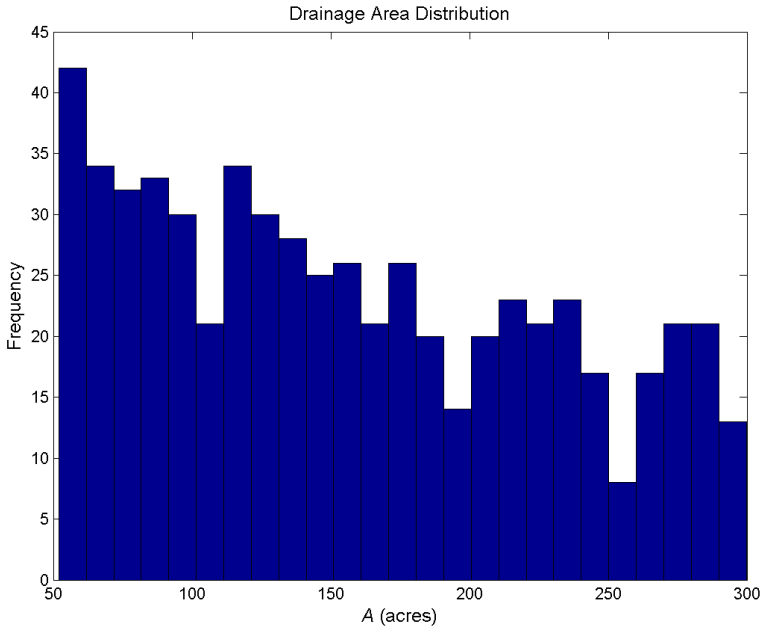

Figure C-1: Drainage Area Distribution

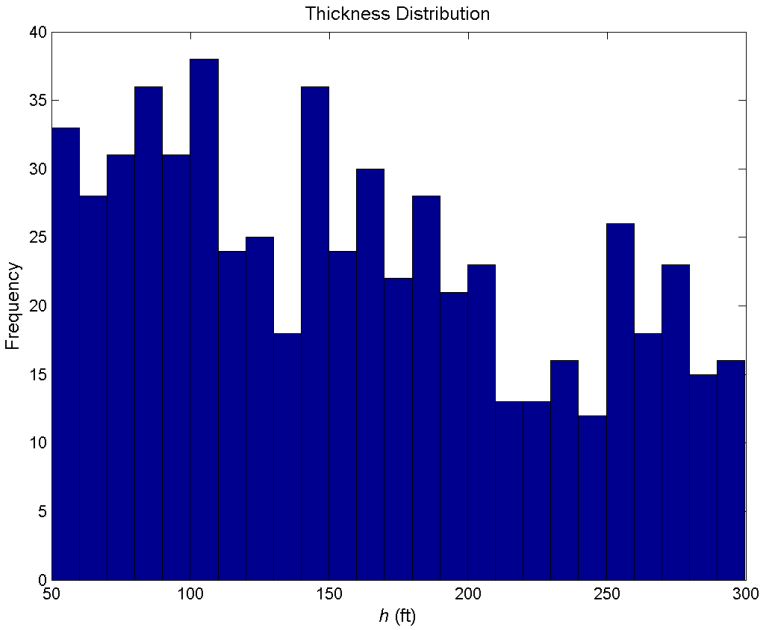

Figure C-2: Thickness Distribution

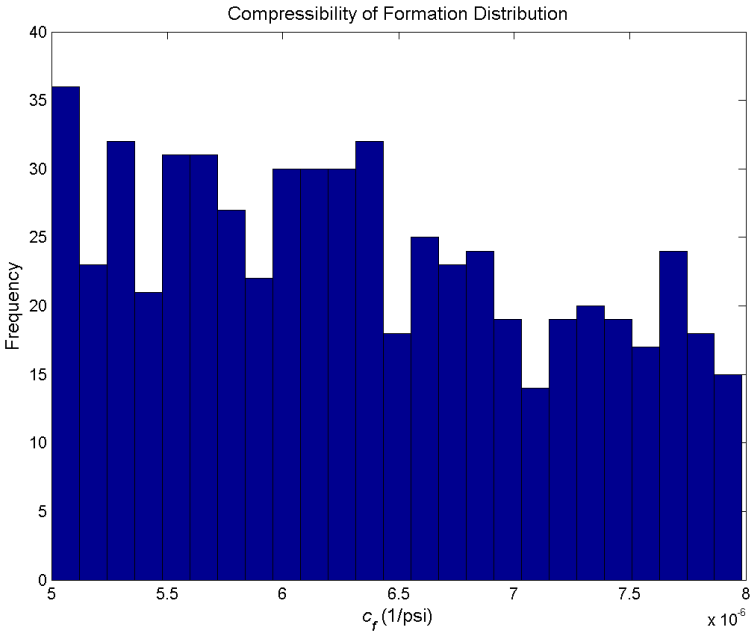

Figure C-3: Compressibility of Formation Distribution

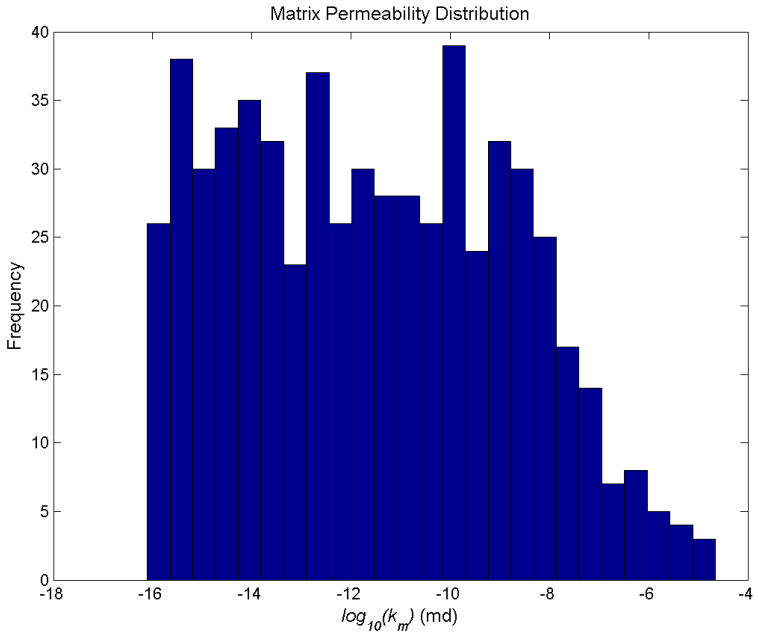

Figure C-4: Log-scaled Matrix Permeability Distribution

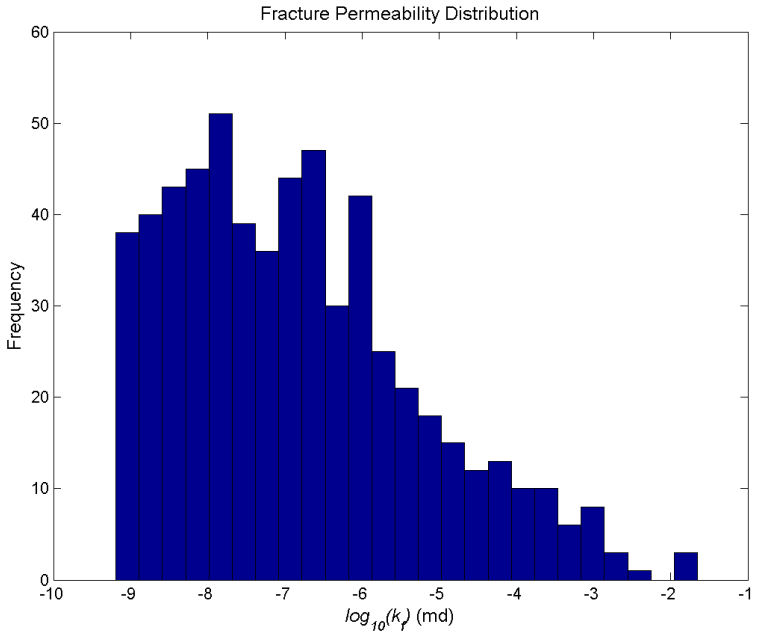

Figure C-5: Log-scaled Fracture Permeability Distribution

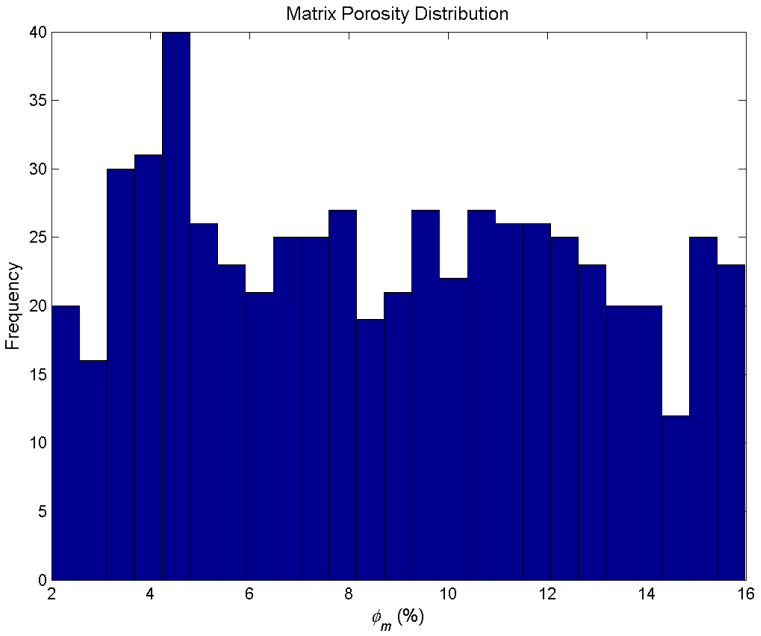

Figure C-6: Matrix Porosity Distribution

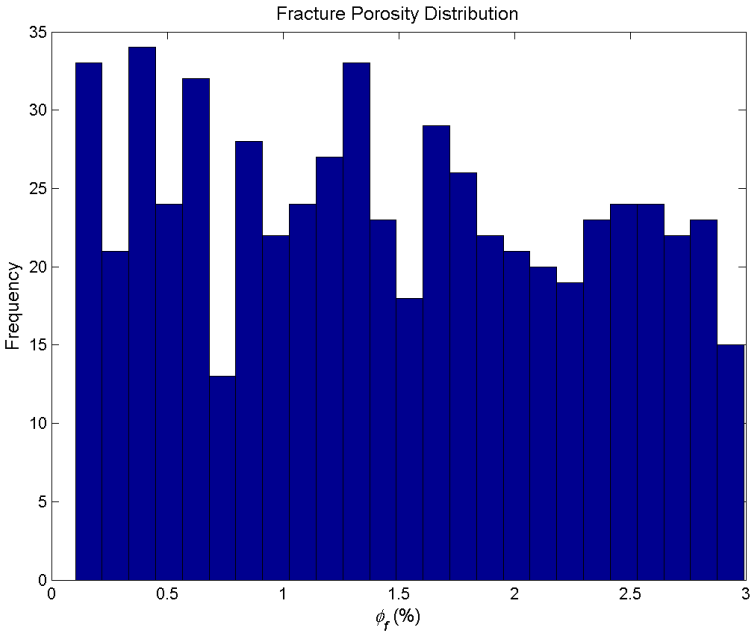

Figure C-7: Fracture Porosity Distribution

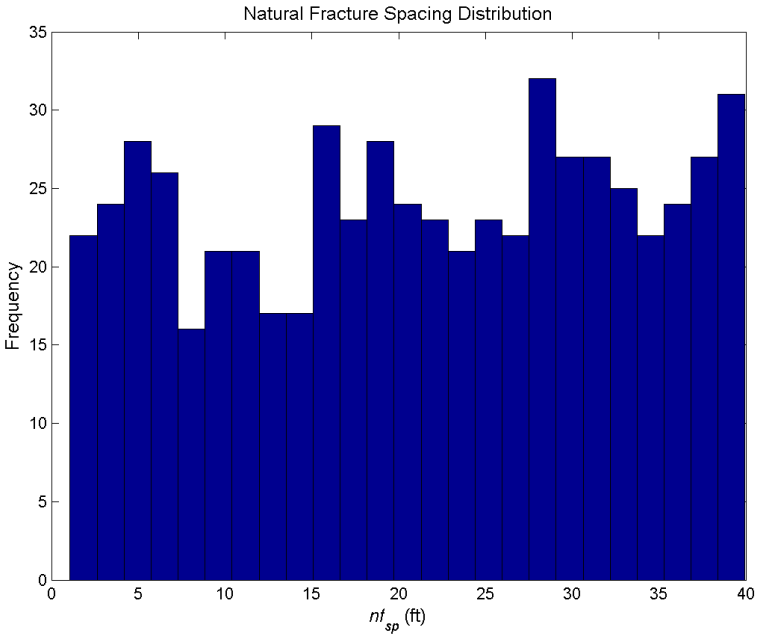

Figure C-8: Natural Fracture Spacing Distribution

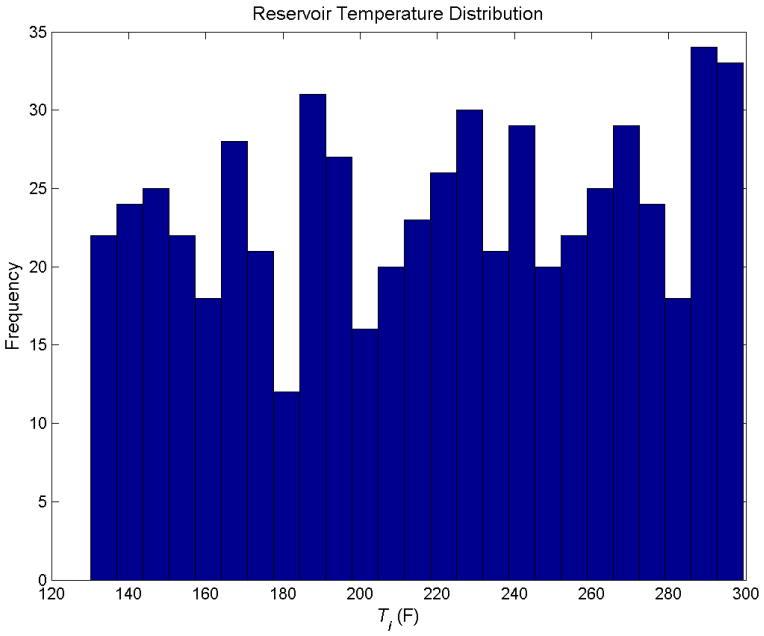

Figure C-9: Reservoir Temperature Distribution

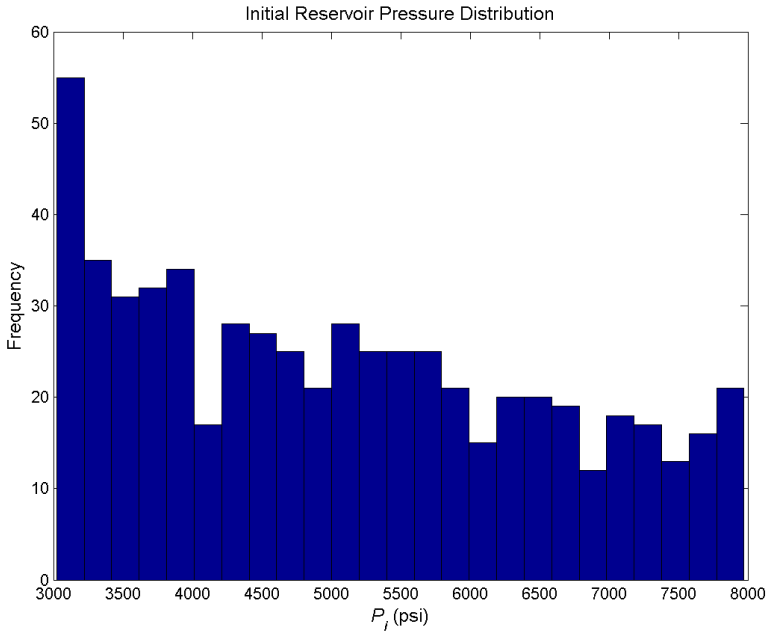

Figure C-10: Initial Reservoir Pressure Distribution

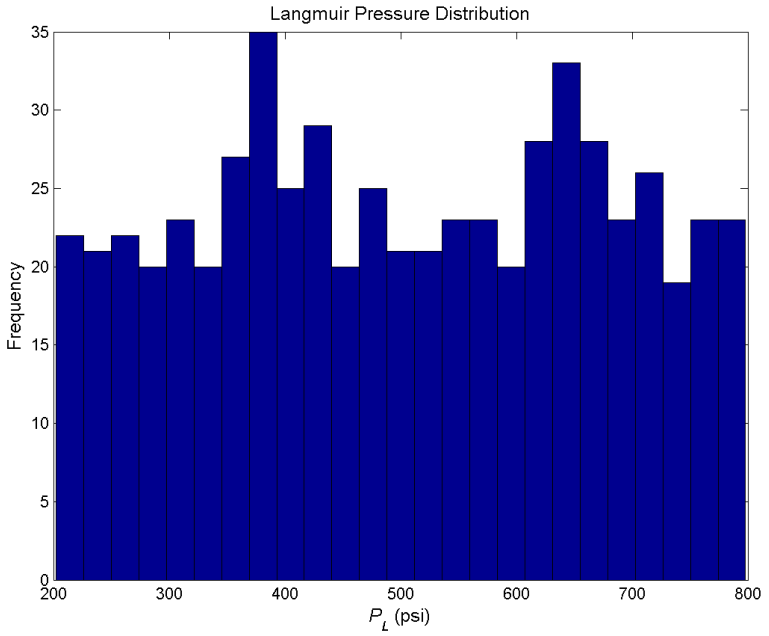

Figure C-11: Langmuir Pressure Distribution

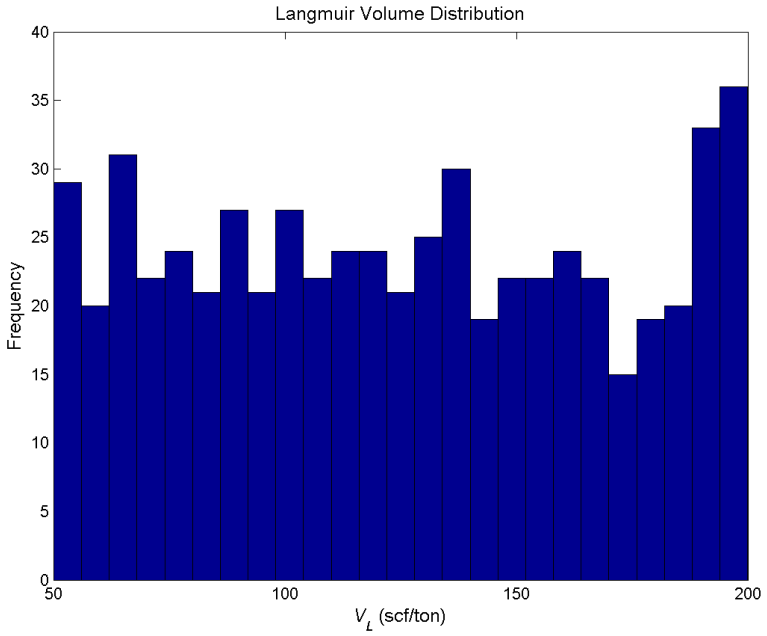

Figure C-12: Langmuir Volume Distribution

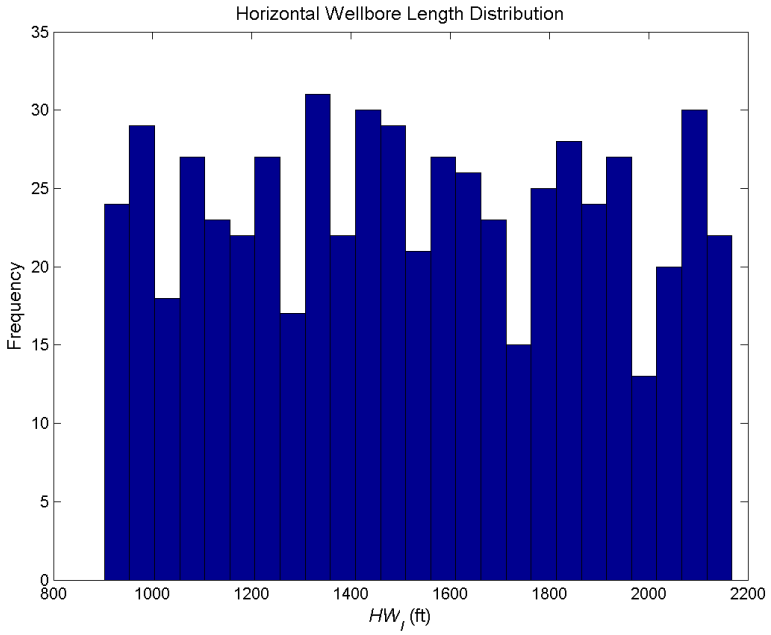

Figure C-13: Horizontal Well Length Distribution

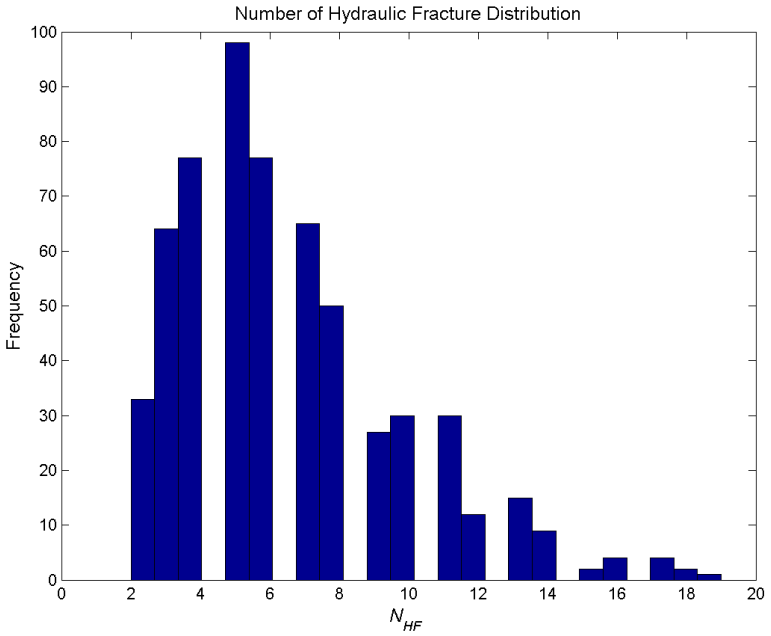

Figure C-14: Number of Hydraulic Fracture Distribution

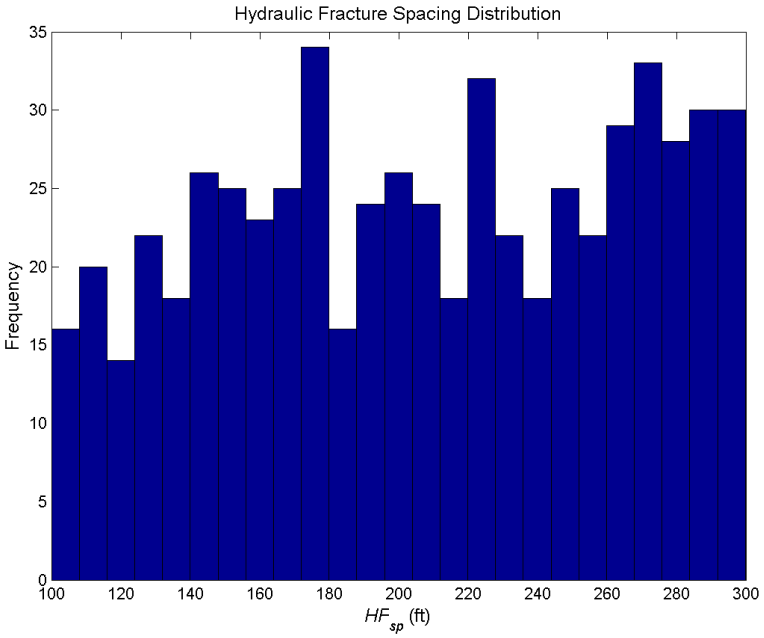

Figure C-15: Hydraulic Fracture Spacing Distribution

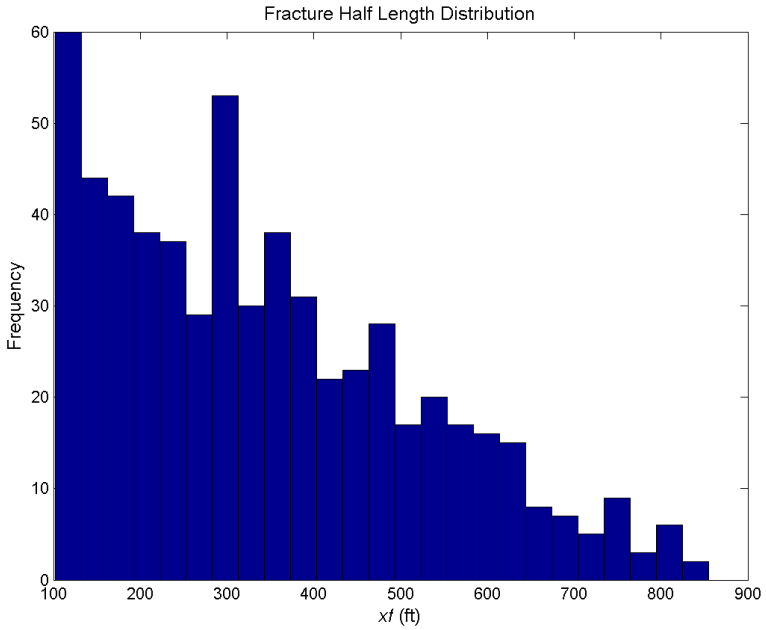

Figure C-16: Fracture Half Length Distribution

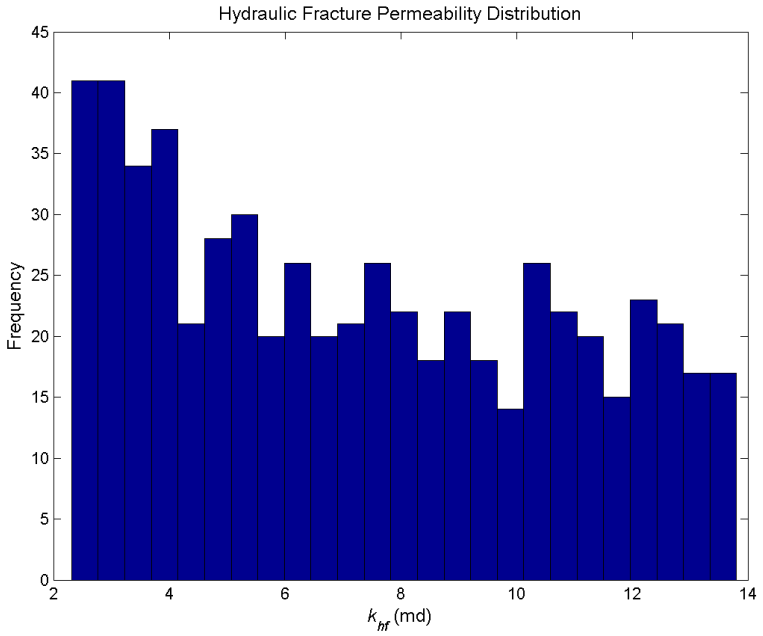

Figure C-17: Hydraulic Fracture Permeability Distribution

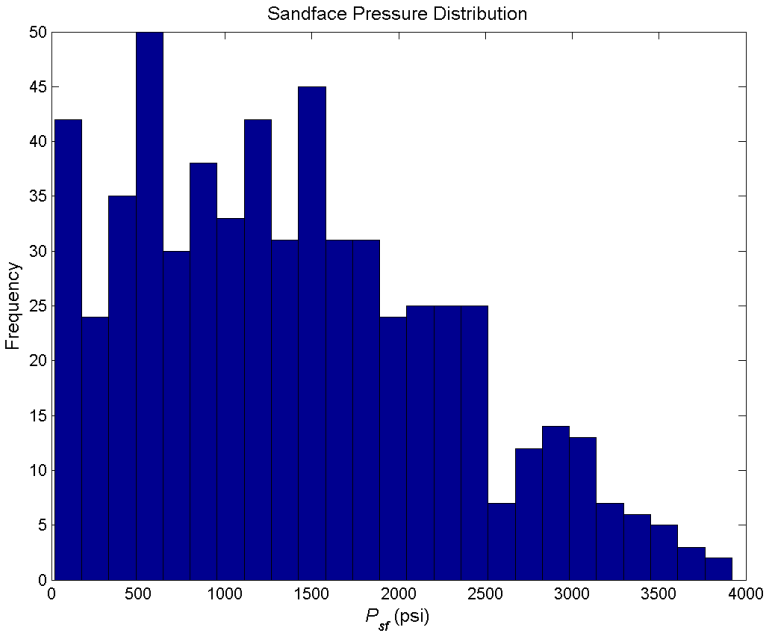

Figure C-18: Specified Pressure Distribution

Appendix D

Training and Testing Data Sets

This appendix includes some sample training and testing data sets generated by MATLAB. These data sets are used in training and testing of the Performance Prediction ANN and Equivalency ANN.

D.1 Performance Prediction ANN

Table D-1: Sample Reservoir Parameters Used for Training the Performance Prediction ANN

Data	h	c_f	k_m	k_f	ϕ_m	ϕ_f	nf_{sp}	T_i	P_i	P_L	V_L
1	256.4	6.7E-06	1.8E-07	0.001915	0.103	0.029	14.8	286.6	4394.3	629.1	121.0
8	76.0	5.1E-06	6.9E-07	0.004686	0.160	0.016	32.9	152.4	5968.8	709.9	80.6
11	81.3	6.2E-06	1.1E-05	0.000647	0.095	0.012	7.3	188.6	3995.7	279.7	172.3
20	161.1	5.4E-06	1.8E-06	0.000109	0.021	0.008	21.1	195.6	6519.5	595.4	116.0
41	237.5	6.2E-06	0.00137	0.045137	0.033	0.002	6.1	287.0	6715.3	663.7	137.7
49	259.3	5.1E-06	7E-07	0.000881	0.052	0.020	36.5	172.6	5577.5	435.2	65.5
51	124.8	5.9E-06	3.4E-05	0.000244	0.129	0.014	36.4	170.4	4191.0	493.8	86.1
52	176.8	5.2E-06	4E-06	0.003971	0.042	0.005	38.0	201.4	6964.9	622.7	122.5
63	160.0	7.6E-06	2.7E-07	0.001508	0.057	0.016	23.9	286.4	4306.9	202.3	123.7
64	279.6	6.9E-06	2.4E-07	0.000567	0.084	0.011	38.1	143.4	3532.0	684.2	86.6
65	285.3	7.9E-06	4.3E-05	0.0008	0.047	0.006	29.6	242.2	7076.1	477.4	195.3
70	121.1	6.7E-06	2.2E-07	0.000243	0.042	0.021	32.6	264.1	3653.7	245.4	146.1
78	214.1	6.1E-06	4.8E-05	0.000102	0.132	0.025	38.6	269.5	7512.4	468.0	104.4
80	109.9	7.3E-06	7.1E-06	0.000169	0.049	0.027	36.9	187.2	6358.0	555.5	98.7
96	183.0	5.2E-06	9.1E-07	0.004225	0.077	0.004	4.7	275.3	3198.3	781.7	59.6
97	163.5	6.6E-06	0.00349	0.008362	0.084	0.023	9.3	172.0	4171.5	766.3	169.7
104	78.1	6.4E-06	3.9E-07	0.000424	0.100	0.025	39.3	207.1	7774.4	742.2	93.7
115	50.6	8E-06	1.5E-06	0.000331	0.036	0.015	7.2	232.6	4366.1	382.8	172.6
125	161.2	5.8E-06	3E-05	0.000173	0.093	0.007	6.6	192.4	5178.5	607.2	142.2
126	161.0	6.2E-06	2E-06	0.001366	0.126	0.010	3.5	272.5	7195.2	466.9	101.8

Data	h	c_f	k_m	k_f	ϕ_m	ϕ_f	nf_{sp}	T_i	P_i	P_L	V_L
127	173.7	5.6E-06	0.00014	0.000549	0.077	0.016	27.6	203.0	5293.9	777.4	60.4
145	80.7	6.3E-06	9E-07	0.008017	0.044	0.018	20.5	283.0	5879.4	218.9	137.0
146	65.8	5.7E-06	8.1E-06	0.003863	0.033	0.020	17.4	187.5	7704.7	307.5	194.8
170	88.4	6.5E-06	9.1E-07	0.00036	0.093	0.019	3.4	185.6	6288.2	269.6	120.7
185	172.6	5.7E-06	0.00041	0.008246	0.136	0.024	11.3	134.6	3223.5	430.3	73.0
186	87.1	5.2E-06	1.3E-07	0.000189	0.093	0.002	30.2	198.9	5508.6	425.0	164.9
187	262.1	6E-06	7.3E-06	0.000259	0.078	0.008	10.0	295.4	3885.4	523.0	175.1
205	200.5	7.4E-06	2.2E-05	0.000164	0.141	0.025	33.1	219.5	3955.6	538.2	156.4
206	55.5	5.3E-06	0.00367	0.016861	0.124	0.002	37.8	135.9	3402.6	664.2	98.9
207	115.7	5.7E-06	4E-07	0.015483	0.045	0.020	20.7	287.2	3087.6	725.1	60.3
221	65.4	7.8E-06	0.00034	0.008463	0.150	0.017	15.7	273.7	5822.6	599.5	153.8
222	179.3	7.4E-06	0.00044	0.001947	0.086	0.017	26.4	252.2	3423.8	747.4	64.9
230	293.3	6.4E-06	8E-05	0.000898	0.094	0.024	3.5	269.3	6278.2	508.2	187.9
232	74.8	6.4E-06	0.00025	0.000869	0.152	0.024	2.4	288.2	6756.1	264.7	165.5
234	188.5	5.2E-06	2E-05	0.002075	0.117	0.008	6.4	145.0	4805.0	404.4	129.6
239	83.7	6.5E-06	1.3E-05	0.01999	0.038	0.027	30.4	217.1	3076.1	368.8	187.2
240	247.5	6E-06	9.6E-07	0.000146	0.159	0.018	34.7	239.9	3575.3	502.0	71.0
241	197.3	5.6E-06	0.00014	0.000158	0.076	0.015	12.5	268.2	7763.6	434.4	142.3
243	247.7	5.1E-06	7.6E-05	0.000197	0.031	0.020	33.0	154.1	3329.9	393.4	153.7
249	96.3	6.7E-06	0.0009	0.00859	0.099	0.002	33.1	208.6	6703.0	545.3	91.6
257	102.6	5.8E-06	3.4E-06	0.000474	0.152	0.010	36.1	274.1	5775.3	301.0	137.4
269	156.5	5.6E-06	1.7E-05	0.000176	0.101	0.012	31.8	220.5	5423.8	371.6	71.6
277	188.0	5.9E-06	1.6E-07	0.000508	0.024	0.004	39.3	229.2	7418.5	556.4	107.5
286	59.6	6.2E-06	0.00035	0.001448	0.129	0.012	30.3	150.3	3404.6	656.2	64.6
295	97.4	5.2E-06	2.5E-06	0.005572	0.134	0.012	27.8	214.7	3101.4	645.2	195.8
300	149.8	7.9E-06	3E-05	0.001322	0.133	0.012	17.2	291.1	5747.8	512.0	132.8
301	153.6	5E-06	1E-06	0.000191	0.157	0.006	29.7	290.1	5771.6	565.8	112.4
311	274.6	7.8E-06	6.1E-05	0.002462	0.045	0.011	17.9	132.0	5406.4	378.6	83.5
318	151.6	7.2E-06	2.4E-07	0.002124	0.115	0.005	11.3	208.8	3690.1	642.7	82.1
319	84.0	6.2E-06	7.1E-07	0.000164	0.115	0.010	18.4	140.2	5317.1	485.3	190.5
328	269.4	5.2E-06	2.6E-07	0.001199	0.068	0.006	32.5	279.2	3426.7	681.0	114.3
337	62.7	5.1E-06	8.4E-06	0.002254	0.140	0.003	24.6	226.8	6035.8	434.8	66.2
355	72.2	5.1E-06	3.3E-06	0.001303	0.125	0.029	11.5	242.5	4278.1	447.2	63.8
356	182.7	6.7E-06	7.9E-07	0.001249	0.117	0.007	25.8	153.2	6034.4	348.5	54.7
364	81.0	6.5E-06	6.3E-06	0.001168	0.038	0.015	13.6	226.5	3104.3	474.0	199.9
368	154.3	6.2E-06	6.2E-07	0.001184	0.062	0.017	12.8	268.9	5415.6	667.6	96.4
379	67.8	6.1E-06	0.00056	0.005007	0.096	0.004	1.4	149.3	4418.6	412.4	133.2
394	212.7	5.7E-06	4.6E-07	0.008536	0.048	0.027	1.6	297.3	5189.3	376.4	128.1
401	86.4	6.4E-06	0.00013	0.001582	0.034	0.003	36.9	141.0	4682.4	707.1	195.9

Data	h	c_f	k_m	k_f	ϕ_m	ϕ_f	nf_{sp}	T_i	P_i	P_L	V_L
409	74.0	6E-06	6.9E-07	0.003107	0.108	0.021	39.1	144.9	6148.5	507.8	87.3
426	67.3	6.5E-06	1.7E-06	0.002488	0.054	0.010	19.8	140.0	7009.3	323.8	95.9
427	147.3	5.8E-06	1.5E-07	0.000914	0.053	0.010	19.9	225.8	4611.7	658.9	190.3
433	178.9	5.9E-06	1.8E-06	0.000354	0.123	0.001	24.8	216.3	7739.5	363.0	196.2
442	264.8	7.7E-06	1.2E-06	0.000133	0.036	0.020	30.1	256.1	3668.8	563.0	79.9
447	166.9	5E-06	2.6E-06	0.00057	0.041	0.005	27.5	245.2	5890.8	424.3	104.7
458	186.6	7.3E-06	1.8E-05	0.002032	0.150	0.006	13.6	222.5	7912.8	452.8	148.9
463	78.5	6.7E-06	0.00035	0.00182	0.057	0.025	4.1	282.4	5269.4	516.7	192.3
473	68.3	7.2E-06	3.3E-07	0.005598	0.147	0.017	23.0	221.0	4426.0	398.6	124.6
478	271.0	5.3E-06	0.00078	0.001	0.026	0.018	18.2	140.9	5031.9	277.6	121.4
491	198.5	7.9E-06	2.3E-05	0.000115	0.127	0.018	4.1	208.5	5619.8	365.7	181.9
499	187.8	6.9E-06	6.2E-07	0.000112	0.053	0.019	2.0	181.2	6399.7	616.7	196.8
504	285.5	6.3E-06	0.00062	0.002934	0.051	0.013	20.2	216.4	4553.4	533.4	66.2
516	80.7	5.4E-06	0.00016	0.00017	0.100	0.004	20.9	191.2	3873.2	233.0	75.9
523	123.2	7.7E-06	1.1E-07	0.000487	0.143	0.015	33.5	238.4	5301.3	428.9	73.6
528	101.4	7E-06	0.00018	0.000947	0.125	0.009	21.7	278.5	7937.1	580.4	182.4
537	205.6	6.5E-06	4.1E-05	0.001007	0.070	0.023	38.8	177.2	3813.2	763.3	112.1
541	117.7	6E-06	4.6E-05	0.012784	0.094	0.022	2.7	292.9	4412.8	764.2	68.7
550	154.7	7.6E-06	5.7E-07	0.000173	0.094	0.002	39.7	152.5	3831.0	609.9	108.9
561	254.0	7E-06	0.00038	0.003285	0.063	0.016	38.6	294.9	5650.7	507.2	163.6
564	103.1	5.1E-06	6.6E-07	0.000905	0.094	0.017	21.6	144.4	5409.5	326.2	176.6
568	67.1	6.7E-06	0.00017	0.000356	0.131	0.006	1.8	191.9	5131.1	394.9	55.4
569	99.6	5.3E-06	3.3E-06	0.002165	0.150	0.027	37.8	181.9	4639.5	738.5	89.3
570	162.8	6E-06	2.2E-07	0.000114	0.046	0.018	2.6	281.2	5217.0	421.3	71.7
571	185.0	6.2E-06	2.8E-05	0.0002	0.140	0.006	38.0	213.7	5065.8	657.0	69.7
572	289.0	6.3E-06	1.1E-07	0.000947	0.104	0.014	34.9	215.2	3600.9	434.1	130.3
575	174.6	7.1E-06	7E-07	0.000614	0.049	0.026	15.5	293.3	4729.5	214.6	99.1
578	54.4	7.3E-06	1.7E-06	0.097266	0.157	0.009	33.5	143.3	5521.9	783.0	141.7
581	82.9	5.6E-06	3.8E-06	0.191474	0.142	0.002	23.3	243.1	3623.3	238.6	76.7
582	258.5	5.5E-06	2.3E-06	0.000107	0.114	0.027	28.2	255.6	6628.5	669.7	197.4
584	115.1	6.5E-06	1.5E-06	0.001033	0.107	0.028	20.5	286.9	7235.0	396.5	193.3
588	153.4	7.8E-06	1.9E-05	0.007688	0.031	0.025	13.1	276.7	3662.0	309.4	176.7
590	107.8	5.6E-06	0.00028	0.001539	0.072	0.028	2.6	274.6	5093.8	460.1	54.6
591	196.2	7.4E-06	1.7E-07	0.001409	0.076	0.023	18.4	152.4	5785.6	351.6	60.8
593	132.9	6.8E-06	1.4E-07	0.00097	0.087	0.014	26.1	143.1	3097.9	453.0	96.1
594	108.4	6.5E-06	2.1E-06	0.000557	0.050	0.018	39.7	246.5	4303.7	735.3	160.1
597	165.1	6.3E-06	5.7E-05	0.001026	0.021	0.012	2.9	237.3	6949.5	595.5	182.6
599	142.7	5.5E-06	1.3E-05	0.001516	0.065	0.006	27.8	156.2	6543.4	298.4	54.4
600	148.6	6.7E-06	2.7E-05	0.000872	0.116	0.013	30.5	190.7	3557.3	509.5	84.2

Table D-2: Sample Design Characteristics Used for Training the Performance Prediction ANN

Data	A	HW_l	N_{HF}	HF_{sp}	xf	k_{hf}	P_{sf}
1	79.1	1113.9	3	234.23	242.99	25058.58	2186.71
8	297.9	2161.5	6	294.03	238.18	2166.70	2219.42
11	213.8	1831.1	6	244.01	741.16	262318.16	74.88
20	68.5	1036.4	4	189.41	317.83	40013.22	2576.05
41	122.3	1385.0	7	172.33	371.02	12.76	2990.76
49	157.2	1570.3	4	278.55	478.19	23.56	2453.40
51	91.7	1198.9	3	242.32	186.00	94153.66	960.07
52	129.7	1426.1	5	214.66	186.85	7249.90	3300.04
63	170.7	1636.2	9	163.48	165.47	97.36	1714.02
64	108.4	1304.1	4	252.79	193.62	110664.00	482.69
65	113.6	1334.4	8	134.68	323.27	12.64	2203.73
70	242.8	1951.2	11	156.11	444.53	10.49	22.10
78	235.5	1921.6	5	280.02	508.17	297544.93	2450.49
80	84.5	1150.8	6	158.84	150.19	43.27	3021.13
96	244.9	1959.8	7	222.49	668.11	25.77	1284.37
97	129.1	1422.9	5	230.47	142.18	477.18	1812.15
104	61.2	979.9	4	184.33	329.92	1344.85	479.28
115	245.6	1962.3	10	165.95	245.71	6099.22	22.87
125	164.1	1604.0	12	116.39	444.77	1338.11	2242.67
126	69.7	1045.3	4	188.06	326.83	3045.85	3196.99
127	181.5	1687.1	7	190.78	675.88	39.06	1627.57
145	123.6	1392.2	8	143.70	437.52	10.49	1320.63
146	240.8	1943.2	6	256.66	527.14	383666.74	3861.41
170	268.2	2050.7	7	234.38	667.90	18.15	2883.46
185	86.7	1165.9	2	293.80	305.67	180546.26	95.27
186	112.5	1328.3	5	191.26	160.91	296.11	666.53
187	71.5	1058.6	2	286.92	352.76	325953.39	481.38
205	108.6	1305.0	6	172.09	250.97	183592.05	310.97
206	194.0	1744.2	11	143.71	435.11	11623.91	1218.27
207	287.5	2123.4	9	201.40	243.16	32.68	1074.12
221	189.9	1725.5	10	155.06	583.01	12.42	2771.67
222	65.4	1012.8	5	164.46	123.83	17.78	1320.36
230	62.9	993.5	8	108.87	118.71	16.28	1967.08
232	129.4	1424.6	4	269.27	127.57	8204.31	3274.00
234	274.4	2074.5	7	231.81	710.48	23.00	1720.91
239	128.7	1420.5	3	293.12	126.65	787.61	1539.94

Data	A	HW_l	N_{HF}	HF_{sp}	xf	k_{hf}	P_{sf}
240	153.1	1549.5	6	204.13	164.91	28355.67	1444.66
241	211.2	1819.7	8	200.38	343.07	13131.70	2496.11
243	87.9	1174.2	4	221.42	464.63	117.90	912.18
249	181.4	1686.8	8	173.77	270.47	793.04	2970.46
257	266.3	2043.5	6	257.74	644.74	20923.71	2275.80
269	246.7	1967.0	14	129.01	318.24	850296.58	435.12
277	207.6	1804.3	13	125.68	201.48	27507.23	1069.00
286	199.4	1768.5	11	138.83	642.63	293.43	1349.70
295	295.9	2153.9	8	238.05	393.18	38047.56	1491.35
300	58.0	953.4	2	289.59	380.44	230324.47	2745.70
301	68.2	1034.3	8	106.45	324.03	128123.22	497.86
311	74.8	1082.9	5	178.31	173.21	31029.89	2424.02
318	96.0	1227.3	4	226.29	476.64	4110.26	676.62
319	153.4	1550.8	9	151.70	297.73	38828.19	1704.49
328	129.4	1424.3	5	234.08	382.90	2439.38	1376.53
337	255.9	2003.2	15	118.59	814.06	69.54	111.23
355	203.4	1785.8	10	153.86	587.70	5591.74	627.01
356	151.7	1542.6	9	142.82	204.24	13.99	2975.71
364	94.4	1216.7	5	175.37	226.67	2052.13	1258.88
368	115.7	1347.2	3	270.75	346.72	1644.23	1535.16
379	272.7	2067.9	16	115.20	292.71	100.04	1751.05
394	63.7	999.1	2	265.51	155.44	65904.85	270.13
401	297.3	2159.1	8	239.10	612.82	230.04	544.99
409	245.3	1961.5	6	249.82	454.66	386.53	414.07
426	163.7	1602.1	11	128.69	242.18	2070.81	3257.77
427	162.9	1598.5	10	140.29	147.22	93674.54	380.35
433	171.4	1639.5	7	199.20	520.40	313.50	1835.88
442	232.9	1911.2	5	295.72	545.38	180277.55	914.52
447	205.9	1797.0	7	201.72	379.59	3201.12	2676.57
458	134.4	1451.9	4	260.42	128.76	273.67	1190.85
463	138.6	1474.4	13	103.54	228.60	55.74	2429.58
473	284.8	2113.5	6	276.55	377.17	15.01	329.57
478	168.3	1624.7	5	237.05	315.74	236249.85	1355.49
491	101.4	1260.8	6	171.17	191.36	3798.41	1395.38
499	181.3	1686.0	7	203.65	214.65	311816.80	3083.87
504	57.6	950.7	5	152.01	181.16	59.72	620.46
516	115.0	1342.7	4	266.61	205.13	93861.87	1443.66
523	264.0	2034.9	7	234.32	737.57	12855.47	2426.09
528	290.5	2134.3	16	120.02	790.41	17.85	3920.25

Data	A	HW_l	N_{HF}	HF_{sp}	xf	k_{hf}	P_{sf}
537	81.3	1129.4	2	294.33	393.41	1330.46	1889.02
541	136.9	1465.0	12	109.34	356.99	23.47	1212.89
550	161.5	1591.4	4	284.97	377.86	11.83	1847.24
561	73.5	1073.7	2	288.15	305.80	4006.96	342.66
564	86.1	1161.9	4	193.98	153.81	955885.94	1771.98
568	282.6	2105.1	13	142.68	474.64	335.74	956.84
569	262.7	2029.6	8	224.84	816.70	44.12	983.12
570	243.0	1952.1	7	223.40	762.87	207982.38	1754.78
571	53.9	918.9	3	224.97	363.11	53.22	559.64
572	208.1	1806.4	6	232.51	115.22	13755.58	771.46
575	140.6	1484.9	5	244.60	359.58	243410.83	725.06
578	71.5	1059.1	2	288.08	184.78	330.76	2037.24
581	136.8	1464.9	7	180.34	465.70	295.11	1136.56
582	124.2	1395.4	7	163.16	131.65	84140.78	2126.77
584	296.5	2156.4	8	223.94	187.05	22.85	1891.35
588	230.4	1900.7	9	176.03	339.98	10.67	958.69
590	289.9	2132.1	8	225.09	296.65	22939.41	2463.10
591	185.2	1704.1	4	290.88	583.05	11629.76	2212.72
593	219.7	1856.1	14	123.72	633.30	18.18	1521.61
594	195.8	1752.3	6	249.17	701.31	10.46	1252.96
597	172.3	1643.6	6	211.05	370.85	533.77	21.89
599	187.0	1712.3	6	223.60	202.67	247.24	2901.07
600	143.5	1499.9	8	166.62	215.51	203.41	978.68

Table D-3: Sample Reservoir Parameters Used for Testing the Performance Prediction ANN

Data	h	c_f	k_m	k_f	ϕ_m	ϕ_f	nf_{sp}	T_i	P_i	P_L	V_L
1	256.4	6.7E-06	1.8E-07	0.001915	0.103	0.029	14.8	286.6	4394.3	629.1	121.0
8	76.0	5.1E-06	6.9E-07	0.004686	0.160	0.016	32.9	152.4	5968.8	709.9	80.6
11	81.3	6.2E-06	1.1E-05	0.000647	0.095	0.012	7.3	188.6	3995.7	279.7	172.3
20	161.1	5.4E-06	1.8E-06	0.000109	0.021	0.008	21.1	195.6	6519.5	595.4	116.0
41	237.5	6.2E-06	0.00137	0.045137	0.033	0.002	6.1	287.0	6715.3	663.7	137.7
49	259.3	5.1E-06	7E-07	0.000881	0.052	0.020	36.5	172.6	5577.5	435.2	65.5
51	124.8	5.9E-06	3.4E-05	0.000244	0.129	0.014	36.4	170.4	4191.0	493.8	86.1
52	176.8	5.2E-06	4E-06	0.003971	0.042	0.005	38.0	201.4	6964.9	622.7	122.5
63	160.0	7.6E-06	2.7E-07	0.001508	0.057	0.016	23.9	286.4	4306.9	202.3	123.7
64	279.6	6.9E-06	2.4E-07	0.000567	0.084	0.011	38.1	143.4	3532.0	684.2	86.6
65	285.3	7.9E-06	4.3E-05	0.0008	0.047	0.006	29.6	242.2	7076.1	477.4	195.3
70	121.1	6.7E-06	2.2E-07	0.000243	0.042	0.021	32.6	264.1	3653.7	245.4	146.1
78	214.1	6.1E-06	4.8E-05	0.000102	0.132	0.025	38.6	269.5	7512.4	468.0	104.4
80	109.9	7.3E-06	7.1E-06	0.000169	0.049	0.027	36.9	187.2	6358.0	555.5	98.7
96	183.0	5.2E-06	9.1E-07	0.004225	0.077	0.004	4.7	275.3	3198.3	781.7	59.6

Table D-4: Sample Design Characteristics Used for Testing the Performance Prediction ANN

Data	A	HW_l	N_{HF}	HF_{sp}	xf	k_{hf}	P_{sf}
1	79.1	1113.9	3	234.23	242.99	25058.58	2186.71
8	297.9	2161.5	6	294.03	238.18	2166.70	2219.42
11	213.8	1831.1	6	244.01	741.16	262318.16	74.88
20	68.5	1036.4	4	189.41	317.83	40013.22	2576.05
41	122.3	1385.0	7	172.33	371.02	12.76	2990.76
49	157.2	1570.3	4	278.55	478.19	23.56	2453.40
51	91.7	1198.9	3	242.32	186.00	94153.66	960.07
52	129.7	1426.1	5	214.66	186.85	7249.90	3300.04
63	170.7	1636.2	9	163.48	165.47	97.36	1714.02
64	108.4	1304.1	4	252.79	193.62	110664.00	482.69
65	113.6	1334.4	8	134.68	323.27	12.64	2203.73
70	242.8	1951.2	11	156.11	444.53	10.49	22.10
78	235.5	1921.6	5	280.02	508.17	297544.93	2450.49
80	84.5	1150.8	6	158.84	150.19	43.27	3021.13
96	244.9	1959.8	7	222.49	668.11	25.77	1284.37

D.2 Equivalency ANN

Table D-5: Sample Reservoir Parameters Used for Training the Equivalency ANN

Data	h	c_f	k_m	k_f	ϕ_m	ϕ_f	nf_{sp}	T_i	P_i	P_L	V_L
1	256.4	6.7E-06	1.84E-07	0.001915	0.103	0.029	14.8	286.6	4394.3	629.1	121.0
5	115.8	6.5E-06	0.000222	0.003209	0.106	0.023	35.0	283.0	4001.4	618.6	191.6
10	193.7	6.91E-06	1.01E-07	0.000205	0.104	0.001	39.6	243.7	6553.0	743.5	62.4
18	189.5	7.91E-06	2.88E-06	0.003204	0.048	0.004	10.0	264.3	3685.0	284.7	137.8
23	121.6	6.19E-06	0.000185	0.000991	0.146	0.005	12.5	166.9	3305.5	263.0	123.7
30	83.1	5.32E-06	7.66E-06	0.000292	0.075	0.015	23.2	186.6	4573.0	342.1	78.0
36	166.9	6.46E-06	5.61E-06	0.000118	0.152	0.026	21.2	236.6	4470.2	226.1	71.3
41	237.5	6.2E-06	0.001375	0.045137	0.033	0.002	6.1	287.0	6715.3	663.7	137.7
49	178.3	5.61E-06	0.00048	0.001662	0.069	0.004	35.6	293.5	4211.7	202.8	165.5
55	52.6	5.24E-06	0.000154	0.001526	0.081	0.018	32.1	281.0	5654.1	652.4	119.3
62	160.0	7.62E-06	2.66E-07	0.001508	0.057	0.016	23.9	286.4	4306.9	202.3	123.7
69	121.1	6.67E-06	2.25E-07	0.000243	0.042	0.021	32.6	264.1	3653.7	245.4	146.1
70	153.0	5.88E-06	0.000194	0.000469	0.112	0.011	36.8	272.9	6686.6	607.1	143.3
77	214.1	6.06E-06	4.8E-05	0.000102	0.132	0.025	38.6	269.5	7512.4	468.0	104.4
83	162.4	6.91E-06	2.82E-06	0.000369	0.087	0.013	5.5	247.2	6023.3	737.2	94.8
88	226.9	6.1E-06	3.48E-06	0.000149	0.069	0.017	34.4	263.6	7358.4	469.8	187.6
97	141.6	7.26E-06	1.08E-05	0.003199	0.092	0.011	28.3	269.4	6841.5	456.2	109.5
102	113.7	6.28E-06	1.1E-07	0.002138	0.126	0.008	11.7	231.6	4863.6	391.5	173.9
110	96.1	7.6E-06	0.000153	0.000254	0.075	0.010	7.9	240.5	3547.3	479.1	195.0
119	191.0	6.58E-06	1.48E-07	0.000107	0.058	0.009	24.0	287.8	5768.6	338.4	114.2
128	180.8	5.73E-06	0.000242	0.000259	0.043	0.016	29.8	155.9	3262.2	572.5	55.7
134	255.7	5.83E-06	6.63E-05	0.000707	0.022	0.008	8.7	225.4	5644.0	674.1	131.1
143	80.7	6.34E-06	9E-07	0.008017	0.044	0.018	20.5	283.0	5879.4	218.9	137.0
147	134.7	5.64E-06	3.34E-06	0.002175	0.129	0.017	37.5	261.5	5875.6	269.6	131.3
158	252.8	5.14E-06	0.00012	0.004999	0.060	0.020	29.9	258.9	3179.8	270.0	96.5
169	122.0	6.48E-06	1.62E-06	0.000217	0.067	0.014	29.0	208.6	3569.1	790.6	171.9
175	90.6	5.06E-06	1.49E-05	0.001839	0.145	0.013	26.0	183.1	7036.1	780.6	187.8
186	173.7	6.82E-06	4.25E-06	0.023839	0.076	0.010	19.7	295.1	4141.0	428.8	189.2
194	98.8	5.74E-06	2.27E-06	0.001972	0.082	0.012	22.1	141.2	5444.9	459.8	188.2
206	151.4	6.74E-06	5.89E-05	0.000518	0.153	0.019	7.0	235.6	5355.4	376.0	94.7
211	140.1	6.93E-06	8.92E-07	0.001043	0.096	0.028	15.9	298.6	3799.9	268.4	191.0
220	73.1	7.9E-06	1.29E-06	0.000396	0.107	0.017	29.6	144.6	7880.5	568.7	58.5
229	74.8	6.42E-06	0.000253	0.000869	0.152	0.024	2.4	288.2	6756.1	264.7	165.5
234	112.0	6.45E-06	2.53E-05	0.000586	0.114	0.013	21.5	290.5	3473.9	513.3	86.9

Data	h	c_f	k_m	k_f	ϕ_m	ϕ_f	nf_{sp}	T_i	P_i	P_L	V_L
243	205.0	5.8E-06	5.39E-07	0.000372	0.102	0.019	36.1	158.8	7121.0	787.6	193.2
244	167.2	5.61E-06	3.64E-06	0.001411	0.107	0.027	1.7	191.8	4593.1	362.6	144.9
251	175.7	6.43E-06	4.42E-07	0.000206	0.114	0.013	38.8	168.8	4799.3	737.2	193.4
256	141.9	5.05E-06	0.001196	0.00124	0.044	0.025	28.3	294.0	7553.9	255.2	66.9
263	107.9	6.72E-06	0.00071	0.00804	0.054	0.013	28.9	286.9	3385.0	358.7	70.9
275	253.2	7.4E-06	1.37E-05	0.000511	0.042	0.029	16.7	186.6	4307.5	313.9	113.6
281	111.9	5E-06	1.15E-05	0.000111	0.123	0.027	35.7	168.1	3091.7	644.7	150.7
282	109.6	5.92E-06	3.19E-07	0.000292	0.094	0.004	39.6	291.1	4762.1	438.4	143.1
292	97.4	5.21E-06	2.53E-06	0.005572	0.134	0.012	27.8	214.7	3101.4	645.2	195.8
299	262.6	5.48E-06	0.000458	0.000462	0.036	0.008	6.3	199.2	7624.3	433.3	51.0
305	107.9	5.76E-06	4.85E-07	0.000617	0.123	0.004	19.0	270.9	6987.7	504.3	82.6
308	185.8	5.97E-06	0.000205	0.000278	0.071	0.001	22.2	222.5	6278.1	669.5	116.7
316	190.5	7.52E-06	8.31E-06	0.000247	0.134	0.017	4.5	130.4	4307.3	404.2	94.1
317	290.5	6.8E-06	1.37E-07	0.000206	0.144	0.005	2.5	281.9	5011.2	520.5	64.2
323	127.8	5.11E-06	5.34E-05	0.00015	0.090	0.019	17.6	244.3	6291.7	374.9	123.9
332	266.2	7.43E-06	9.27E-05	0.000118	0.069	0.025	4.9	238.4	7865.1	724.6	103.4
340	238.8	6.28E-06	1.17E-05	0.00051	0.100	0.024	34.4	188.4	3806.7	288.3	129.7
344	250.2	5.63E-06	0.000826	0.000866	0.104	0.014	18.3	259.4	4454.7	701.2	151.3
353	146.6	5.39E-06	1.04E-07	0.000175	0.071	0.013	10.3	153.1	4373.5	313.3	112.1
359	121.7	5.31E-06	3.82E-06	0.020562	0.076	0.014	15.5	252.8	3727.7	770.6	75.7
367	56.3	5.95E-06	1.83E-06	0.00034	0.141	0.029	18.1	263.0	3179.2	347.7	197.3
374	189.1	5.56E-06	7.28E-05	0.000475	0.125	0.013	10.0	163.1	7745.4	543.6	152.6
385	144.0	7.57E-06	4.11E-07	0.001011	0.093	0.016	26.4	271.2	5983.7	635.5	118.1
390	85.1	7.5E-06	4.5E-07	0.00077	0.078	0.027	10.3	245.0	5804.2	203.3	166.9
400	226.6	5.12E-06	0.00093	0.002299	0.085	0.026	12.9	272.5	3474.6	300.3	190.6

Table D-6: Sample Design Characteristics Used for Training the Equivalency ANN

Data	Transverse Fracture Design Characteristics							Equivalent Crushed Zone Parameters			
	A	HW_l	N_{HF}	HF_{sp}	xf	k_{hf}	P_{sf}	a_{major}	a_{minor}	$k_{f,cz}$	$nf_{sp,cz}$
1	79.1	1113.9	3	234.23	242.99	25058.58	2186.7	103.6	1163.5	0.03462	3.24
5	102.4	1267.2	3	287.30	172.58	99062.61	1772.1	329.2	1285.4	0.00765	21.22
10	282.9	2106.2	8	213.60	479.05	33126.62	1824.6	937.5	1882.1	0.00942	1.08
18	100.7	1256.4	3	269.03	159.85	471062.14	1427.3	279.0	1608.1	0.00974	1.25
23	284.3	2111.3	11	173.08	480.35	44016.91	822.8	1092.2	2016.2	0.04226	11.24
30	227.9	1890.3	6	246.30	687.50	11169.22	2233.7	1046.4	2311.9	0.00491	0.15
36	227.0	1886.8	6	260.42	300.05	34977.72	931.5	627.9	2180.0	0.00130	17.73
41	122.3	1385.0	7	172.33	371.02	12.76	2990.8	510.6	1353.9	0.04775	3.82
49	279.6	2093.9	18	107.78	218.94	148.94	970.8	492.1	2090.8	0.02972	9.35
55	277.7	2087.0	11	163.73	148.08	10867.80	1687.4	189.2	1987.9	0.02814	0.41
62	170.7	1636.2	9	163.48	165.47	97.36	1714.0	805.3	1904.5	0.00316	10.95
69	242.8	1951.2	11	156.11	444.53	10.49	22.1	915.4	1849.7	0.00419	31.33
70	252.6	1990.2	5	291.15	287.02	23.06	1739.5	87.0	2373.6	0.00410	15.06
77	235.5	1921.6	5	280.02	508.17	297544.93	2450.5	990.6	2052.2	0.00164	30.53
83	67.6	1029.9	2	268.59	303.77	149470.44	2321.1	156.1	1024.4	0.00707	4.75
88	156.5	1566.8	4	278.23	625.05	9014.11	1983.1	778.5	2035.6	0.00477	2.51
97	269.1	2054.2	5	299.71	354.25	29.45	1484.4	663.9	1605.5	0.01089	19.00
102	214.5	1834.1	8	191.80	348.79	885.29	2276.3	379.7	2079.2	0.04098	1.28
110	179.2	1676.5	5	270.59	623.45	578.47	960.8	854.8	2074.2	0.00467	1.22
119	161.1	1589.2	6	217.51	456.80	10983.96	2828.5	826.3	1368.7	0.00709	3.63
128	187.8	1716.0	7	206.16	191.73	3431.32	22.4	179.8	1990.4	0.00444	28.71
134	69.7	1045.3	3	235.84	179.39	45097.21	952.5	156.7	795.3	0.04747	6.74
143	123.6	1392.2	8	143.70	437.52	10.49	1320.6	149.4	1660.1	0.01271	16.49
147	82.9	1140.3	5	189.19	107.51	39420.28	2256.7	199.3	1322.5	0.00626	25.07
158	143.4	1499.4	5	226.68	282.37	479.66	328.5	464.5	1476.1	0.02919	10.06
169	181.1	1685.3	5	248.42	562.94	33148.57	1049.4	859.3	2063.5	0.00417	4.26
175	168.2	1624.1	10	145.76	641.94	94.22	2465.6	803.3	2106.8	0.03439	23.69
186	106.7	1293.7	5	203.89	303.49	15.11	1818.6	635.7	1040.1	0.03069	15.12
194	94.8	1219.4	7	143.47	178.42	747.96	1753.9	495.9	1006.4	0.01672	12.86
206	57.9	952.9	5	140.52	236.57	1023.61	753.6	403.3	722.9	0.03528	3.08
211	177.4	1668.0	5	276.55	581.20	584315.41	1365.5	856.9	1967.7	0.03439	9.59
220	120.1	1372.2	6	171.62	343.82	43919.66	580.6	625.4	1363.3	0.00933	7.33
229	129.4	1424.6	4	269.27	127.57	8204.31	3274.0	201.7	1119.3	0.00447	0.23
234	153.2	1549.7	11	124.92	380.96	34.22	948.5	533.2	1767.2	0.01293	10.11
243	175.5	1658.9	7	205.77	290.00	205991.47	270.1	544.3	1570.8	0.00785	31.37
244	104.9	1282.4	3	268.76	201.61	968431.91	567.1	159.1	978.3	0.02415	1.05
251	142.2	1493.3	10	128.74	390.33	71407.66	1183.6	492.4	1988.3	0.01445	8.69

Data	Transverse Fracture Design Characteristics							Equivalent Crushed Zone Parameters			
	A	HW_l	N_{HF}	HF_{sp}	xf	k_{hf}	P_{sf}	a_{major}	a_{minor}	$k_{f,cz}$	$nf_{sp,cz}$
256	53.8	918.5	2	241.18	351.59	9347.63	527.8	227.7	946.9	0.04620	9.58
263	127.4	1413.5	4	242.33	302.71	9196.93	911.1	716.6	1487.1	0.02802	20.46
275	273.1	2069.4	6	291.52	294.64	41818.82	957.7	418.9	2034.5	0.00980	3.86
281	224.5	1876.4	16	109.92	574.40	36005.23	1499.3	1020.3	2470.0	0.01471	28.61
282	288.5	2126.9	7	261.57	854.74	109196.39	512.0	1177.9	2627.1	0.01370	5.36
292	295.9	2153.9	8	238.05	393.18	38047.56	1491.4	1181.0	2189.0	0.03970	7.52
299	154.0	1554.2	10	140.08	120.67	38.67	3047.1	797.0	1486.0	0.00211	4.92
305	131.9	1438.1	6	182.55	122.82	19.75	2679.6	253.0	1385.7	0.00167	6.62
308	295.7	2153.3	9	197.08	161.32	26.45	834.7	135.2	1919.8	0.00362	5.09
316	98.7	1244.0	4	244.12	111.19	26866.16	2013.8	87.8	1461.6	0.00143	0.94
317	155.7	1562.4	6	202.10	474.69	86.04	2093.8	756.6	1523.3	0.00782	0.90
323	232.4	1909.2	8	201.36	658.85	103.83	2103.0	1018.2	2422.9	0.00510	10.83
332	266.7	2045.0	10	184.64	300.93	52.60	2047.8	383.7	2415.3	0.00474	4.09
340	226.7	1885.6	7	226.76	171.04	927.57	1853.2	618.0	1674.7	0.00382	30.61
344	99.1	1246.9	4	230.85	419.28	159.44	2241.5	543.1	1450.0	0.01357	1.62
353	157.6	1571.8	5	259.76	543.51	109.38	971.0	732.5	2083.7	0.00311	0.54
359	137.5	1468.4	4	269.90	577.10	77.06	1347.4	270.3	1877.1	0.03601	4.19
367	62.8	992.6	3	206.22	353.51	215319.66	579.8	469.9	1247.5	0.00244	5.61
374	211.1	1819.5	10	152.20	210.27	27.52	2689.9	225.3	1815.7	0.00800	5.21
385	154.2	1555.0	5	255.94	150.15	864803.58	2318.1	146.1	1452.7	0.01169	8.96
390	64.9	1008.9	5	164.58	396.34	281256.66	2609.0	541.4	1338.9	0.03016	2.01
400	87.5	1171.2	9	109.14	443.39	22.64	1467.9	436.3	1483.9	0.01154	11.39

Table D-7: Sample Reservoir Parameters Used for Testing the Equivalency ANN

Data	h	c_f	k_m	k_f	ϕ_m	ϕ_f	nf_{sp}	T_i	P_i	P_L	V_L
1	54.8	7.494E-06	5.94E-05	0.0268816	0.081	0.025	14.3	175.0	5807.2	491.5	63.8
6	228.9	6.952E-06	4.089E-05	0.0002661	0.097	0.018	16.1	290.7	3456.1	749.6	156.0
9	199.4	5.483E-06	8.557E-05	0.0063841	0.039	0.005	3.8	162.9	3709.3	759.6	190.3
15	164.1	5.327E-06	0.0005039	0.0012058	0.038	0.003	16.9	273.0	3286.6	694.5	76.7
22	107.2	7.644E-06	6.09E-05	0.0298271	0.130	0.012	2.3	144.1	6437.3	418.3	52.8
25	109.8	5.569E-06	0.0004259	0.0018299	0.053	0.003	36.4	262.6	3812.8	240.2	188.1
32	96.4	7.144E-06	0.0001425	0.0258265	0.155	0.013	5.9	268.8	3867.1	724.1	60.1
41	231.3	7.85E-06	0.0035116	0.0063292	0.034	0.010	35.1	167.2	5577.1	753.9	190.4
42	107.5	5.214E-06	0.0022286	0.0027276	0.131	0.004	24.4	252.9	5344.7	723.3	153.3
43	264.7	7.071E-06	6.897E-05	0.0001057	0.116	0.004	13.6	133.0	3317.4	718.9	91.4
50	226.3	7.701E-06	6.504E-05	0.0003181	0.115	0.004	24.2	158.6	3477.9	611.9	62.9
60	108.1	6.051E-06	1.517E-06	0.0023816	0.119	0.018	39.5	146.4	7388.1	356.5	52.3
75	186.6	5.535E-06	9.123E-07	0.0026821	0.096	0.015	15.6	231.7	5188.4	590.6	167.8
123	193.8	7.359E-06	0.00022	0.0004036	0.158	0.008	23.9	165.8	6968.4	566.9	87.5
124	250.4	5.641E-06	1.976E-07	0.0008917	0.152	0.022	10.1	257.5	3347.5	472.4	88.9

Table D-8: Sample Design Characteristics Used for Testing the Equivalency ANN

Data	Transverse Fracture Design Characteristics							Equivalent Crushed Zone Parameters			
	A	HW_l	N_{HF}	HF_{sp}	xf	k_{hf}	P_{sf}	a_{major}	a_{minor}	$k_{f,cz}$	$nf_{sp,cz}$
1	85.5	1157.7	3	278.37	270.97	1850.68	2829.8	541.8	1187.9	0.04857	12.32
6	90.7	1192.3	6	149.82	410.64	544185.42	775.1	444.3	1416.2	0.02446	9.66
9	204.0	1788.6	9	173.70	106.62	46665.07	1237.2	217.5	1672.7	0.03142	2.31
15	137.7	1469.7	9	137.73	370.13	913.92	1338.0	664.6	1381.1	0.04684	15.64
22	79.4	1115.5	5	166.01	323.44	179.02	3221.4	607.0	1307.3	0.04940	1.16
25	251.4	1985.4	13	140.98	332.64	8866.12	133.3	614.6	1882.0	0.04821	12.10
32	268.8	2053.3	11	165.30	179.98	101.82	1387.9	600.9	2251.3	0.03908	2.51
41	110.7	1317.6	3	266.62	238.06	388.90	2503.1	561.4	969.8	0.02566	11.31
42	279.4	2093.0	7	254.05	518.80	11.16	2464.3	452.5	2775.3	0.00512	4.40
43	208.9	1810.1	14	116.40	478.52	25.59	281.0	976.1	1748.6	0.00614	13.10
50	159.7	1582.3	7	192.68	353.88	4908.18	1054.1	529.7	1956.8	0.01017	7.10
60	63.0	994.1	4	190.39	159.95	2175.65	2345.6	96.1	1068.3	0.01900	33.29
75	76.2	1093.2	3	254.19	338.89	990148.43	1136.7	340.3	1149.5	0.04926	11.86
123	227.8	1890.0	7	224.35	610.98	11.96	2225.6	515.3	1888.8	0.00427	11.11
124	120.4	1373.9	4	272.14	476.04	12191.59	640.7	581.0	1703.0	0.02691	3.55